2007

A root-mean-square reduction of a generic variable-amplitude spectrum to a constant-amplitude equivalent for aluminum 7075-T651

Matthew Adam Adler
Lehigh University

Adler, Matthew Adam

A Root-Mean-Square Reduction of a Generic Variable-Amplitude Spectrum to a...

May 2007

A ROOT-MEAN-SQUARE REDUCTION OF A GENERIC VARIABLE-AMPLITUDE SPECTRUM TO A CONSTANT-AMPLITUDE EQUIVALENT FOR ALUMINUM 7075-T651

b y

Matthew Adam Adler

A Thesis
Presented to the Graduate and Research Committee
of Lehigh University
in Candidacy for the Degree of
Master of Science

in
Mechanical Engineering and Mechanics

Lehigh University

May 21, 2007

This thesis is accepted and approved in partial fulfillment of the requirements for the Master of Science.

April 20, 2007

Date

Dr. Robert P. Wei

Thesis Advisor

Dr. Herman F. Nied

Chairperson of the Department

Acknowledgement

The author wishes to express his gratitude to Professor R.P. Wei for his support and guidance. His unparalleled selflessness and relaxed disposition have motivated and sustained this research. Thanks are also extended to the author's parents, Neal and Lea Adler, for endowing and cultivating within the author the substantial framework of mind and body capable of synthesizing the ubiquitous matters of science.

Acknowledgement is made for the support by the National Science Foundation under the NSF: IGERT "Materials Lifetime Science and Engineering" Fellowship under Subcontract No. OR 1966-01.01 from the University of Tennessee-Knoxville (NSF Grant No. DGE-9987548, CFDA-47.076) as well as by The Defense Advanced Research Projects Agency (DARPA) under Contract HR0011-04C-0003, through a Purchase order #472248 from the Northrop Grumman Corporation. Dr. Leo Christodoulou is the DARPA Program Manager, and Dr. John Papazian is the Principal Investigator for NGC.

The opinions expressed or otherwise implied herein are the sole opinions of the author and are not necessarily those of the National Science Foundation, Northrop Grumman Corporation, or Lehigh University.

***

This thesis is dedicated to every tortured hour of loneliness, denial, frustration, and abuse he was made to spend – and to the battles he won. To Howard Roark.

Table of Contents

List of Tables

List of Figures

Nomenclature

ACPD	=	alternating current potential drop
DCPD	=	direct current potential drop
a_{ι}	=	damage size, [m]
a_o	=	initial pit radius, [m]
a_{tc}	=	depth of damage at the transition from a surface crack to a through-the thickness crack, [m]
C_c	=	coefficient in the power law form for the crack growth rate equation
$F(x)$	=	cdf; $F(x) = \Pr\{X \leq x\}$
F_{tc}	=	geometric relationship for a through-the-thickness crack emanating from a circular hole
I_{po}	=	pre-exponential constant in pitting current relationship, [A]
K_t	=	stress concentration factor due to a circular hole
M	=	molecular weight of the material, [kg]
N	=	cycles
n	=	valence
n_c	=	exponential in the power law form of the crack growth rate equation
PoO	=	probability of occurrence
SIF	=	stress intensity factor, $\left[\text{MPa}\sqrt{\text{m}}\right]$
t	=	Time, [s]
t_{tc}	=	time of transition from a surface crack to a through-the-thickness crack, [s]
ΔK_{sc}	=	driving force for a surface crack, $\left[\text{MPa}\sqrt{\text{m}}\right]$
$\Delta\sigma$	=	far field stress range, [MPa]
ρ	=	density of the material, [kg/m^3]
CFC	=	corrosion fatigue cracking
F	=	Faraday's constant, $\left[\frac{\text{A}\cdot\text{s}}{\text{mol}}\right] = \text{C/mol}$
MHWC	=	multiple-hole-wall crack
cdf	=	cumulative distribution function
a_c	=	radius of cylindrical specimen, [m]
r	=	radial distance from center of conductor, [m]
δ	=	$1/\sqrt{f\pi\sigma\mu}$ = skin depth where $J(r) = J(a)/e$, [m]
f	=	frequency, [1/s] = [Hz]
ρ	=	resistivity, $= \left[\frac{\text{kg}\cdot\text{m}^3}{\text{s}^3\text{A}^2}\right] = \left[\Omega\cdot\text{m}\right]$
σ	=	conductivity = $1/\rho$, $\left[\frac{\text{s}^3\text{A}^2}{\text{kg}\cdot\text{m}^3}\right] = \left[\frac{1}{\Omega\cdot\text{m}}\right]$

μ = absolute magnetic permeability of conductor = $\left[\frac{kg \cdot m}{s^2 A^2}\right] = \left[\frac{H}{m}\right]$

μ_r = relative magnetic permeability of conductor

μ_o = magnetic permeability of free space = $4\pi \times 10^{-7}, \left[\frac{H}{m}\right]$

$J(r)$ = current density in cylindrical specimen as a function of radius r, [A/m^2]

$J(a)$ = surface current density in cylindrical specimen at $r=a$, [A/m^2]

$J(a)_p$ = surface current density for semi-infinite plate, [A/m^2]

$J(z)$ = current density for semi-infinite flat plate as a function of z, [A/m^2]

I = total current passing through conductor, [A]

L = specimen probe spacing, [m]

V_a = instantaneous potential across notch, $\left[\frac{kg \cdot m^2}{s^3 A}\right] = \left[\frac{J}{C}\right] = [V]$

$V_{a,0}$ = initial potential across notch, [V]

V_r = instantaneous reference potential, [V]

$V_{r,0}$ = initial reference potential, [V]

V_n = normalized potential drop, [V]

V = electrical potential drop, [V]

ΔV = relative electrical potential drop associated with a notch, [V]

$J_0(x)$ = Bessel function of the fist kind, order zero, with complex argument x

$J_1(x)$ = Bessel function of the first kind, order one, with complex argument x

a_1 = constant of integration specific to frequency and material

EMF = electromagnetic force, [V]

EDM = electrical discharge machining

DSO = design service objective

CA = constant amplitude

VA = variable amplitude

K = stress-intensity factor, $\left[MPa\sqrt{m}\right]$

ΔK_{rms} = root-mean-square stress intensity factor range, $\left[MPa\sqrt{m}\right]$

P_{max} = maximum load in variable-amplitude spectrum, $\left[\frac{kg \cdot m}{s^2}\right] = [N]$

P_{min} = maximum load in variable-amplitude spectrum, [N]

R = load ratio

R_{rms} = root-mean-square load ratio

R_{eq} = optimal load ratio

n_c = deterministic crack growth exponent

da/dN = crack growth rate per cycle [m/cycle]

da/df = rate of change in crack length per flight [m/flight]

$LEFM$ = linear elastic fracture mechanics

GAG = Ground-Air-Ground cycle or spectrum

SCC	=	stress corrosion cracking
FCG	=	fatigue crack growth
$f(a/W)$	=	function of specimen geometry and loading condition
OWP	=	outer wing panel
NDT	=	non destructive testing
$\Delta P_{max,rms}$	=	root-mean-square range of max load, [N]
$\Delta P_{min,rms}$	=	root-mean-square range of min load, [N]
C	=	normalized K gradient
$SIPS$	=	Structural Integrity Prognosis Systems
T_{dp}	=	dew point, [K]
RH	=	relative humidity

Abstract

Critical structures are subjected to complex loading histories and methodologies to predict their responses are required. The current approach is to conduct spectrum fatigue testing and to invoke complex computer codes in order to estimate crack growth response and structure life. These methods are inadequate for use in probabilistic assessments since they neither reflect long-term operating conditions nor consider the sources or extent of variability.

The objective of this thesis was twofold. The first objective was to develop and upgrade experimental techniques for monitoring crack growth – emphasizing a comparison between direct and alternating current potential drop techniques. The second aim was to conduct a feasibility analysis on the efficacy of variable-amplitude (VA) spectrum reduction to a constant-amplitude (CA) equivalence. This analysis consisted of both numerical and experimental studies.

The goal is to approximate a VA spectrum by an equivalent CA spectrum or some other simpler spectrum. It was postulated that a correlation between VA and CA spectra is achieved when fatigue crack growth is plotted as a function of the root-mean-square (RMS) stress intensity factor range. A numerical study showed that there was promise to this approach. Accordingly, fatigue tests were conducted on the reduced CA spectrum. The load ratio R was then adjusted until the CA fatigue response converged to the VA fatigue response. Equivalence was considered to be that point when congruence was achieved between respective crack length a versus cycle count N curves.

It was thus shown that the reduced CA spectrum can replace the VA spectrum when the load ratio is optimally chosen. The optimal load ratio for a given spectrum depends on the magnitude of the maximum load in the spectrum. Also, it is the high maximum load, low R cycles dominate crack growth.

In addition, the environment was of critical influence on crack growth rates. Accordingly, additional experiments were conducted with rigorous control over environment at the specimen. These tests strongly suggest that there is promise to the hypothesis of this thesis, namely, that a VA spectrum can be reduced to a CA equivalent when both the maximum and minimum loads are defined as their respective root-mean-square value. Semilog plots of the rate of change in crack length with flight da/df versus crack length a for both the VA and reduced CA spectra shows the efficacy of this approach. This plot is more meaningful than a crack length versus cycle count plot because small errors in the initial crack length will generate a large variance in total lifetime since crack growth rates at the onset of testing are low.

This work provides a means of VA spectrum reduction to a CA equivalence. Future work must be to conduct additional experiments to ensure repeatability of this approach.

1. INTRODUCTION

1.1 Structure of Thesis

This thesis is divided into two main sections. The first section, Chapter One through Chapter Three, consists of general background and motivation. This includes development of the experimental techniques that will be used throughout the experimental study. The second section, Chapter Four through Chapter Six consists of a combined numerical and experimental feasibility study intended to simplify the prediction of variable-amplitude fatigue. Each section is self-contained. For the reader not interested in the development of the testing methodologies it is recommended that Chapter Three be passed over.

Chapter One, is an introduction and describes the motivation, fundamental issues, previous work, and objectives for this thesis.

Chapter Two is a review of the technical background that provides the conceptual framework and basis for the current research. This includes a case study on a Boeing 707 as well as data acquisition methodologies.

Chapter Three consists of the development and upgrade of the testing methodology. This includes an introduction to potential drop methods and then a flaw detection study. Since the electromagnetic behavior of fracture specimens is difficult to assess this study was performed on cylindrical specimens. It is noted that upgrades were necessitated due to significant advances in the field since the system at Lehigh has had been last updated some twenty years ago

Chapter Four is a description of the experimental procedures utilized to achieve the objectives stated in Chapter One. This includes a discussion of specimen preparation and equipment.

Chapter Five presents and discusses the experimental results.

Chapter Six provides a summary of the work of this thesis and provides suggestions for future, more extensive work.

1.2 Introduction

The exterior skin on modern aircraft is primarily fabricated from aluminum alloys. This is due to their good strength to weight ratio, formability, high fracture toughness, high resistance to corrosion, and suitable cost. Specifically due to its high strength in tension, aluminum 7075-T651, predominantly alloyed with zinc and copper, is used extensively for the wingskins in many commercial, civilian, and military aircraft.

During flight, dynamic, structural stresses act on the exterior skin of aircrafts. For the lower wingskin, specifically, the dominant mode of loading is tension or what is commonly treated as Mode-I loading. In addition, the load spectrum experienced is variable as a result of flight maneuvers, wind gusts, payload, etc. For constant-amplitude loading crack growth is uniquely dependent on stress intensity range ΔK as the driving force for crack growth. For complex loading sequences, however, including variable-amplitude spectra, the direct application of this expression in life prediction is not clear because of crack closure, overload, and load history effects[1].

Moreover, from the computational perspective, variable amplitude fatigue simulations are exceedingly taxing on system resources[2] since the prediction of crack growth according to a complex spectrum requires numerical integration schemes which involve some form of cycle-by-cycle analysis. Reduction of the variable amplitude loading history to an equivalent constant-amplitude spectrum would facilitate real-time predictions of both single component and total system stability.

Consider that as the outer wing panel (OWP) of an aircraft develops microcracks emanating from the high stress concentration zones of its fastener holes, for example, that real-time data from able, modern sensors can be implemented into crack growth models. Predictions can then be made to provide for the capacity to quantify the air-worthiness of the aircraft at some future date based upon the anticipated missions. This information would provide the fleet commander with a more reliable basis for assessing the availability and mission capabilities of the aircraft under his purview. For this reason, and because aircraft are increasingly being utilized well beyond their original design service objectives (DSO), it is important to develop methodologies to safeguard their structure, as well as the safety of the passengers and crew.

The focus of this effort was therefore to develop a methodology for constructing an equivalent constant-amplitude spectrum to replace an original variable-amplitude spectrum. For fatigue experiments conducted in a controlled environment in which the derived constant-amplitude spectrum is used in proxy of the original variable-amplitude spectrum, the two spectra should yield like results. This comparison will be

on the basis of crack growth rate per flight d*a/df* versus crack length *a*. Thus a convenient, easily verified metric is established for spectra equivalence, namely, a comparison of the respective *da/df* versus *a* plots. An equivalent set of *da/df* versus *a* plots indicates that the constant-amplitude spectrum may be used in proxy of the variable-amplitude spectrum for waveform generation in fatigue tests. What may even be more valuable is that fatigue predictions for the variable-amplitude spectrum can then be extracted from the well-understood crack propagation mechanics inherent to constant-amplitude fatigue.

1.3 Previous Work

Experiments and analysis on various bridge steels conducted by J.M. Barsom[3] have shown that a correlation between variable-amplitude random-sequence[a] and constant-amplitude load spectra is achieved when fatigue crack growth rate *da/dN* is plotted as a function of the root-mean square (*rms*) stress intensity factor range, ΔK_{rms}. Mathematically this is expressed:

$$\frac{da}{dN} = C_C \Delta K_{rms}^{n_r} \tag{1.1}$$

[a] It must be highlighted, that for the Barsom study here referenced, that the variable-amplitude sequences were not entirely random. In fact, the spectra that Barsom considered were a composite of mission profiles with a finite number of types which were strung together in fixed sequences and repeated in a loop. There is, therefore, clearly an aspect of determinism inherent to this random sequence.

where ΔK_{rms} is the root-mean-square stress intensity factory range, n_c the deterministic crack growth exponent which relays the functional dependence of the crack growth on the driving force ΔK, and C_c is a material constant that characterizes the variability in the material. The following relationships are used to obtain the root-mean-square loads:

$$P_{\max_{rms}} = \left[\frac{1}{M} \sum_{i=1}^{m} (P_{\max})^2 \right]^{1/2} \tag{1.2}$$

$$P_{\min_{rms}} = \left[\frac{1}{M} \sum_{i=1}^{m} (P_{\min})^2 \right]^{1/2} \tag{1.3}$$

and the effective load ratio, R_{rms} , based on the rms loads:

$$R_{rms} = \frac{P_{\min_{rms}}}{P_{\max_{rms}}} \tag{1.4}$$

It should be recognized, however, that the Barsom study considered fully random loading on bridge steels. There are at least two reasons to be cautious in applying a like methodology to the present situation. First, the spectra Barsom used for fatigue experiments were a composite of mission profiles with a finite number of types that were strung together in fixed sequences and then repeated in a loop. This approach, therefore, inherently captures a deterministic aspect. Secondly, the present study is on aluminum and not ferrous alloys. These differences induce doubt that a similar methodology may not prove useful. C.M Hudson[4] showed that the Barsom

root-mean-square approach can be applied to the 2xxx series aluminum alloys and to reflect an aircraft spectrum. Additional support for an RMS approach has been offered by Pook[5]. The prior work suggests that a similar approach might be applied to emulate the response of 7xxx series aluminum alloys to a flight spectrum.

Hudson also suggested that the capability for a constant-amplitude spectrum to simulate the effects of a variable-amplitude is affected by the limit loads of the spectrum. The optimal load ratio that is required by the replacement constant-amplitude spectrum is suggested, therefore, to depend on the maximum load P_{max}. It is the intent of this thesis to establish the condition that a root-mean-square approach is also rational for the aluminum 7075-T651 alloy as well as to quantify this relationship for a given variable-amplitude spectrum.

1.4 Statement of Thesis

Analytic models which can account for crack closure, overload, and load-history effects that permit the rapid prediction of crack growth as a basis for life estimation have yet to be developed[6]. This is especially so for variable-amplitude load histories for which load interaction effects impact a significant proportion of overall crack accumulation. It has thus been the effort of computational models to bridge this gap. Computational models, however, are regarded as insufficient for the synthesis of accurate crack growth predictions due to the obstacle of implementing empirical parameters into probabilistic assessments.

Moreover, current methods for predicting fatigue lives are generally based on the use of the *safe-life* and *crack growth* approaches which are highly empirical. These empirically based approaches inherently cannot adequately reflect either long-term operating conditions or identify sources for variability[7]. They are therefore only viable over the extent of available data, most of which were obtained under accelerated testing conditions. It is, therefore, desired to reduce the VA problem to a problem in CA since CA is easier to model than VA.

It is proposed that one may replace a given variable-amplitude (VA) spectrum with an equivalent constant-amplitude (CA) spectrum that is created by setting the maximum and minimum loads equal to the respective RMS values from the original VA spectrum. Fatigue for the constant-amplitude spectrum and variable-amplitude spectra will be the same.

The benefit of this reduction will be that variable-amplitude experiments can be greatly reduced in number. This will reduce the demand on servohydraulic components, as well as operational expenses and training requirements on new technicians. In addition, crack growth computational models such as FASTRAN[8] or AFGROW[9] will be able to abandon cumbersome cycle-by-cycle integration schemes in favor of fast, effective block-type integrations. Circumvention of the variable-amplitude condition in favor of constant-amplitude will effectively reduce the number of identifiable, key random variables in facilitation of probabilistic analyses in support of fleet management.

2. TECHNICAL BACKGROUND

2.1 Function of Fracture Mechanics

The principal engineering problem of concern is that the residual strength of a structure progressively decreases with increasing crack size[10]. Stated alternatively, the crack growth rate in a structure increases with increasing cycle count as endured per its service load. Accordingly, it is the principal task of fracture mechanics to then answer the following questions[11]:

a. A question of integrity: what is the critical crack size for the expected service load?

b. A question of durability: how long does it take for a crack to grow from some initial crack or flaw size to the critical size?

c. A question reliability: how confident are you in these predictions?

Classical theories of fracture such as the von Mises criterion or maximum distortion energy criterion, often used for their simplicity, are generally not valid due to the presence of cracks and crack-like defects and their dominance in the failure process [11]. Fracture mechanics, however, is capable of providing a direct, exacting response to the first of the above questions. It is also capable of providing probative value to the other questions.

2.2 Fatigue

Normal stresses perpendicular to the plane of the crack and parallel to the displacements of the crack surfaces give rise to Opening Mode or Mode I loading, which is technically the most significant since this is the primary mode of both loading and fracture. A fracture mechanics approach to evaluating the stresses at a crack tip presumes both that the stresses at the crack tip are very large and that the crack surfaces are stress-free. It can be shown by a combination of complex variable methods and linear elasticity, i.e. the Westergaard approach and the Airy's stress function, that the in-plane crack tip stresses can be expressed as:

$$\sigma_{ij} = \frac{K_I}{\sqrt{2\pi r}} f_{ij}(\theta) \tag{2.1}$$

where σ_{ij} are the stresses acting on a material element $dxdy$ at a distance r from the crack tip and at an angle of θ from the plane of the crack and $f_{ij}(\theta)$ are known functions of θ, and are universal for Mode I loading *[10]*. The crack-tip coordinate system is shown in Figure 2.1. For a given specimen and loading geometry it is clear that the entire crack tip stress field will be known if K_I is known. K is known as the stress intensity factor with the subscript I indicative of Mode I. Performing a dimensional analysis on Equation 2.1 indicates that K must have the dimensions of

stress times the square root of length, and according to the variable definitions as provided in Figure 2.1 that the stress intensity factor is defined as:

$$K = \sigma\sqrt{\pi a}\, f(a/W) \tag{2.2}$$

with crack length a, applied stress σ, and where $f(a/W)$ is a nondimensional number that varies with specimen geometry and loading condition.

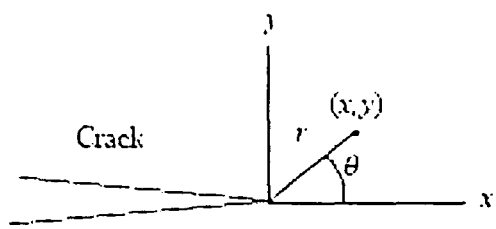

Figure 2.1: Crack-tip coordinate system where σ_{ij} are the stresses acting on a material element $dxdy$ at a distance r from the crack tip.

In order to provide similitude between two cracked bodies of different size and shape, but of the same material, then the stress intensities for the two cases must be equal. If the stress intensities for the two cases are equal then one can expect the two cracks to respond in a similar manner in terms of their respective crack growth rates.

An additional similitude parameter is imposed, however, as to whether the material is in plane strain, plane stress, or an otherwise mixed mode. Complete similitude in crack growth behavior is only possible for the case of plane strain which is necessary

for complete constraint. For situations of incomplete restraint, similitude is achieved only for plates of equal thicknesses with through-the-thickness cracks [10].

For a given fatigue loading cycle in constant-amplitude in which the fatigue varies from between some minimum value to some positive value the stress intensity also cycles over this range:

$$\Delta K = K_{max} - K_{min} \tag{2.3}$$

Paris, Gomez, and Anderson[12] were the first to make this observation and validate it with test data as well as to suggest that crack growth rate *da/dN* versus ΔK often yields a straight line in logarithmic coordinates. In practice, countless experiments have shown that a power-law relationship develops [8, 10]. This yields a sigmoidal curve such as the Paris-type expression as valid only for intermediate ΔK values across what it known as the Region II crack growth regime:

$$\frac{da}{dN} = C_c \Delta K^{n} \tag{2.4}$$

Here, n is a material constant and C_c is a dimensioned constant that changes with n. We reason that deviations at both the lower and upper end of the ΔK range are expected: at high ΔK values (Region III) where unstable crack growth occurs as the crack reaches its critical size for fast-fracture and at low ΔK values (Region I) where the crack length may be on the order of the microstructure, i.e. the grain size, and so

LEFM becomes invalid. The efficacy of this approach is the idealization of similitude and is at the core of LEFM: whether one has a long crack at low stress or a small crack at high stress, that the two cracks will exhibit the same crack growth rate so long ΔK is the same.

It is possible to extract both the threshold stress intensity factor K_{th}, below which cracks will not grow, as well as the critical stress intensity factor K_{IC} (or K_c) required for final fracture from a plot of crack growth rate da/dN versus ΔK. In this investigation both decreasing-K and increasing-K experiments were conducted according to the standards and testing procedures specified by ASTM E-647, Standard Test Method for Measurement of Fatigue Crack Growth Rates[13], and crack growth curves were generated. A detailed discussion of the procedure and results of this research is presented in chapters four and five, respectfully.

General fatigue, as the term is used in this thesis, refers to a cyclic loading condition in an inert environment. It is important to note that subcritical crack propagation can occur, however, by means other than fatigue, most notably by stress corrosion cracking (SCC), which is the effect of a static or sustained load in a deleterious environment, or by corrosion fatigue cracking (CFC), which is the result of cyclic fatigue in deleterious environment. A multitude of experiments have arrived at the consensus that corrosion and corrosion fatigue damage reduce the overall fatigue life of structures[14].

Moreover, it is known that corrosion is strongly dependent on temperature and pH and so that the corrosion of aluminum in various commercial and military aircraft is

kinetically supported while the aircraft are on the ground[15]. During flight, fatigue is the dominant mode of damage evolution since corrosion is not kinetically supported at the low temperatures of high altitudes even though structural components experience powerful and dynamic fatigue loads while in flight. It is the coupled effect of this repetitive ground-air-ground (GAG) flight cycle that is of great structural concern to aircraft aging. A corrosion fatigue model developed by Harlow and Wei is thus presented in the next section. Their model incorporates models for both pitting corrosion and corrosion fatigue and incorporates as set of transition criteria to link these two phenomena. One of the objectives of this thesis is to provide additional data to evaluate the merit of this model.

2.3 Simplified Mechanistically-Based Probability Model

2.3.1 Introduction

Harlow and Wei[16] have demonstrated that the early state of the damage evolution process is dominated by pitting corrosion with the later stages being dominated by fatigue crack growth. Fatigue cracks are likely to nucleate from inhomogeneities such as constituent particles or localized damage and corrosion pits in highly stressed regions, for example, in aircraft wings. More extensive details can be found in reference [16], however, the notable aspects of the model are repeated here for purposes of clarity:

2.3.2 Pitting Corrosion Model

It is assumed that corrosion pits are hemispherical in shape and that they propagate at a constant volumetric rate according to Harlow and Wei [16]:

$$\frac{dV}{dt} = 2\pi a^2 \frac{da}{dt} = \frac{MI_P}{nF\rho} \tag{2.5}$$

where a is the pit radius, M is the molecular weight of the material; n is the valence; F = 96514 C/mol is Faraday's constant; ρ is the density, and I_P is the pitting current. Integrating Eq. (2.5) yields the pit depth a, up to the transition size a_{tr} at which a surface crack initiates:

$$a = \left(\frac{3MI_P}{2\pi nF\rho} t + a_o^3 \right)^{1/3} ; \quad a \le a_{tr} \tag{2.6}$$

where a_o is the initial pit radius, and t is the time required for a pit to develop to a depth of a. This pitting is a result of the potential difference between the alloy matrix and the constituent particles[17].

Work by M. C. Latham [15] showed that the pits are more elliptical in shape than they are hemispherical. Moreover, Latham showed that this improvement is of second-order. To keep the model simple, therefore, all damage is assumed to be hemispherical in shape.

2.3.3 Corrosion Fatigue Model

Harlow and Wei [16] have proposed two transition criteria that have been validated both empirically and statistically for the transition from pit formation to FCG. Pitting controls damage growth up until these transition criteria are met, at which point fatigue dominates damage growth.

$$\Delta K \geq \Delta K_{th} \quad and \quad (\frac{da}{dt})_{surface\ crack} \geq (\frac{da}{dt})_{pit} \tag{2.7}$$

The first transition criteria dictates that the stress intensity factor (SIF) of the crack must equal or exceed the threshold SIF for fatigue crack growth (FCG). The second transition criteria ensures the crack growth rate exceeds that of pit growth. A schematic of this process is shown in Figure 2.2.

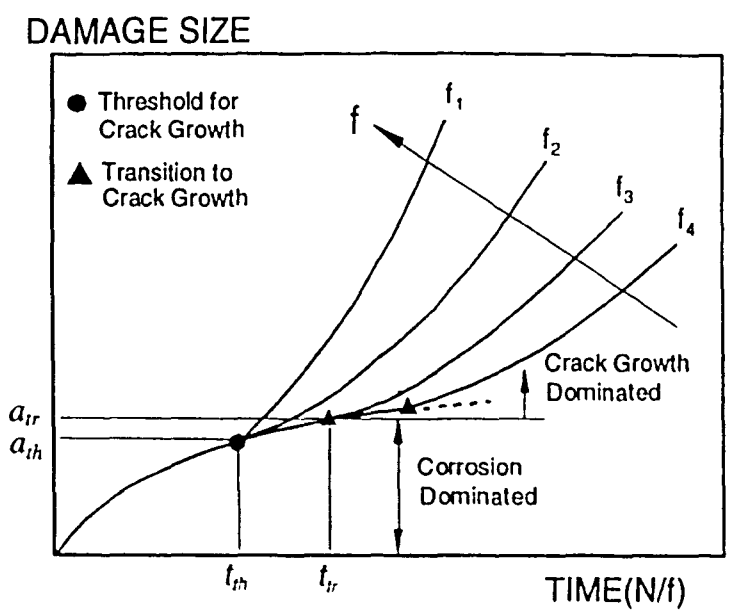

Figure 2.2: Schematic diagram of the development of corrosion and transition to corrosion fatigue crack growth [16].

For simplicity, the power-law representation for fatigue crack growth was adopted: [16]

$$\frac{da}{dN} = C_c \Delta K^{n_c} \tag{2.8}$$

except that:

1. n_c is taken to be a constant to ensure dimensional consistency and the appropriate dependence on ΔK, and
2. material and environmental dependency (including chemical and thermal) is attributed to the coefficient C_c which is taken as a random variable.

The crack driving force ΔK must be modified according to the type of crack. For a semicircular surface crack, the expression for ΔK is given as:

$$\Delta K_{SC} = \frac{2.2}{\pi} k_t \Delta\sigma \sqrt{\pi a} \tag{2.9}$$

where $\Delta\sigma$ is the far field stress range and the stress concentration factor k_t is 2.8 for a circular hole. The $2.2/\pi$ is the appropriate factor for a surface crack assuming the crack is semicircular and in an infinite plate in which linear elastic fracture mechanics (LEFM) are assumed.

For an infinite plate under uniaxial tension containing a circular hole with a single crack emanating from the hole in a direction transverse to the loading axis, ΔK is assumed to obey the following:

$$\Delta K_{tc} = F_{tc}(a/r_o)\Delta\sigma\sqrt{\pi a} \tag{2.10}$$

F_{tc} is a correction factor for the specified geometry and loading while r_o is the radius of the fastener holes. Numerical values for F_{tc} can be obtained empirically:

$$F_{tc}(a/r_o) = \frac{0.865}{(a/r_o)+0.324} + 0.681 \tag{2.11}$$

The crack length during the transition from a surface crack to at through thickness crack ($t_{tr} \le t \le t_{tc}$) is driven by the driving force ΔK_{sc}, and a is found to be:

$$\begin{aligned} a &= \left[a_{tr}^{b} + bfC_c\left(\frac{2.2k_t\Delta\sigma}{\sqrt{\pi}}\right)(t-t_{tr}) \right]^{1/b}; \\ b &= \frac{2-n_c}{2}; \quad n_c \neq 2 \end{aligned} \tag{2.12}$$

where $t \ge t_{tc}$ and a is implicitly obtained through numerical solution.

With the model thus developed what follows is a case study which investigated both size and special distributions for fatigue cracks as found in fastener holes of a

civilian aircraft. The purpose of this study is to provide justification for work of this thesis, namely both validation of the model heretofore discussed and justification for the reduction of variable-amplitude fatigue spectrum to an equivalent spectrum of constant-amplitude.

2.4 Case Study: Boeing 707

2.4.1 Introduction

Three different studies will be discussed. The first study was an initial study conducted by Boeing for the US Air Force (USAF) that used hand-held 20 X magnification to inspect a sampling of fastener holes as part of a plan to convert retired Boeing 707 aircraft into functional E-8C aircraft. The second study was conducted at Lehigh University as part of an MS thesis by Latham [15] with the goal of providing commensurate support for the Harlow-Wei simplified mechanistically-based probability model for fatigue crack growth. Latham used 150 X magnification to achieve a more reliable damage distribution. The third study was conducted as a component of this thesis by Adler at Lehigh University with the purpose being able to provide a rationale for the work to follow in the remaining chapters of his thesis. This was achieved by providing evidence of substantial fatigue cracks within the fastener holes of a civilian aircraft –therefore demonstrating that the fatigue crack phenomenon is important in both design and prognosis. It is clear, then, that there would be a

significant advantage to simplify the methodologies utilized to predict variable-amplitude fatigue since critical structures fail by this process.

Beginning with the initial study, as part of the USAF plan to convert retired Boeing 707 aircrafts into E-8C Joint Surveillance, Target and Attack Radar Systems (J-STARS) aircraft, wing panels from two retired aircraft were disassembled for analysis and inspection and were optically inspected at 20 X magnification by Boeing, which will be referred to as the J-STARS study[18]. Panels from the CZ-184 aircraft were later made available to Lehigh University for further analysis.

The aircraft under scrutiny was designated by Davis-Monthan AFB identification number CZ-184. This aircraft accumulated 57,382 flight hours and 22,533 flight cycles over a duration of approximately 24 years from delivery on 30 November 1966 to termination on 2 October 1990 [16]. This service life of 24 years was longer than its original design service objective (DSO) of 20 years.

Damage in the fastener holes of these panels was recorded and the data were utilized to construct probability of occurrence (PoO) plots for hole-wall damage in the lower left wing skins (2024-T3 aluminum alloy) of the CZ-184 aircraft. Data obtained in this inspection are represented in Fig. 2.3. As shown is a comparison of the PoO for all multiple-hole-wall-crack (MHWC) lengths reported by J-STARS and those measured during a earlier Lehigh University study. J-STARS only reported the largest damage length in any given hole while the data from the Lehigh University

study correspond to all observable cracks in each hole inspected at up to 150 x magnification with the use of a Hi-Scope[a] video imaging system.

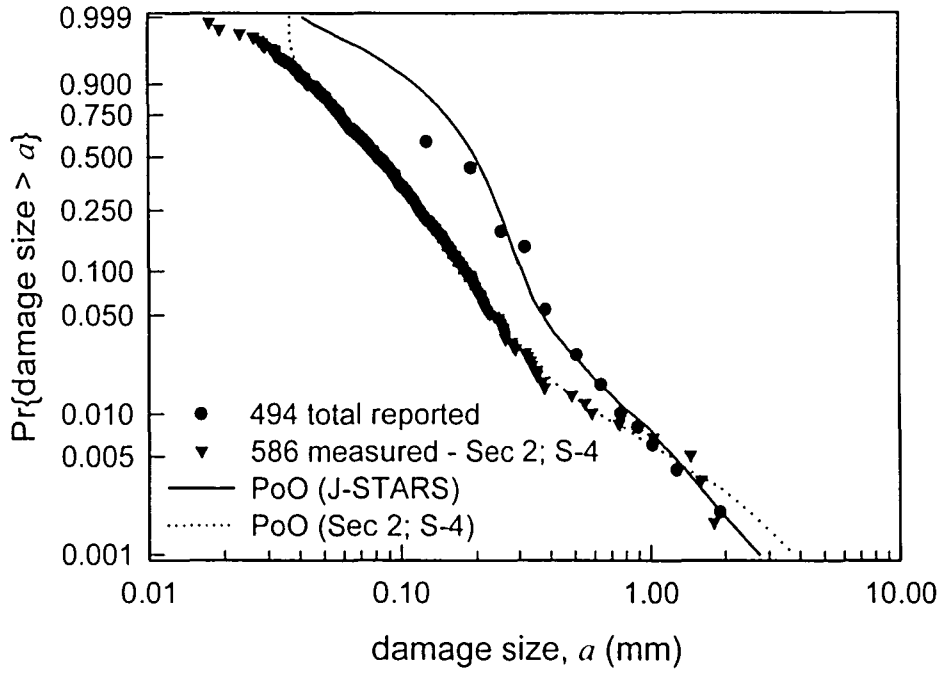

Figure 2.3: Comparison of the PoO for all MHWC lengths reported by J-STARS and all of those measured using video imaging microscopy for 110 holes from Section 2 along Stiffener 4 from the CZ-184 aircraft [16].

Furthermore, even though a large number of holes were inspected in the J-STARS report, the difference between the studies must be attributed to the resolution of the respective techniques. Despite the lack of resolution associated with the J-STARS study, the shape of the PoO curves for the maximum MHWC lengths reported by J-STARS and that reported by the Lehigh University study are similar. With limited resolution, the damage sizes were overestimated by the J-STARS study as data were

[a] Hi-Scope Systems Co, Closter, NJ, 07624

based on visual measurements made by means of a 20 X optical microscope with the largest observable damage size at 0.0635 mm. The minimum resolvable damage length was less than 0.01 mm for the previous Lehigh University study, which is over six times the resolution of the J-STARS study. One important point that should be made on the extent of damage for both studies is that some damage may have been hidden and, therefore, not detected.

In this study, additional data were obtained from the CZ-184 aircraft and show that FCG is of concern in aircraft components. Forty-six (46) fastener holes were inspected from Section 3, along Stiffeners 6-8 on the port side of the lower wing skin on this aircraft. This study compliments the earlier study of MHWCs from Section 2 along Stiffener 4 from the CZ-184 aircraft.

Harlow and Wei [16] considered the probability of occurrence (PoO) of damage size as a function of time according to the simplified mechanistically based probability model (see Fig 2.4.). Observe that the PoO is a cumulative probability plot where a given point on the curve indicates the probability that the damage size $\geq a$. The plot reflects the transition from localized corrosion to through-thickness crack growth [16].

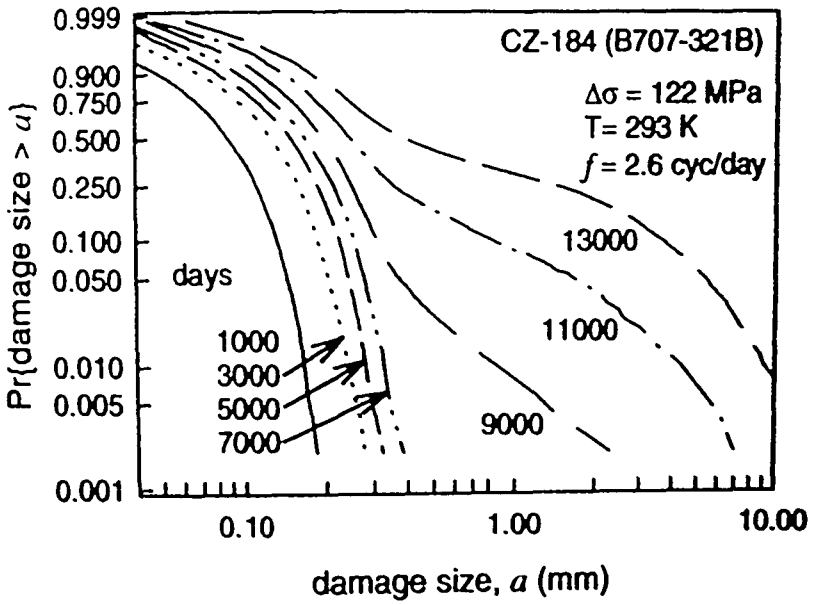

Figure 2.4: PoO of damage size as a function of time [16].

For the CZ-184 aircraft which accumulated an estimated 9000 days of service one predicts the cdf function obtained to be similar to the curve marked as 9000 on the plot. Additionally, one reasons that the damage be typified by a significant pitting period, as well as a noteworthy and influential transition to fatigue crack growth. Indeed, according to the statistical analysis of J-STARS tear-down data as well as that of the earlier Lehigh University study, this is the conclusion that was reached. Clearly, the J-STARS inspection was hampered by the lack of resolution, and so the sizes of the cracks were overestimated as well as grouped, which accounts for the seemingly few data points in Fig. 2.3. Nevertheless, even though the shapes of the curves are similar, it is obvious that higher resolution microscopy is needed to ascertain a more accurate determination of damage sizes.

2.4.2 Empirical Analysis of the Lower Left Wing Skin of CZ-184

The current investigation focused on fastener holes in the port lower wing skin, in Section 3, along Stiffeners 6-8. The portion of Section 3 along Stiffeners 6-8 which were analyzed in this study is shown in Fig. 2.5. The holes considered were all those shown in the diagram neglecting the top two rows. No damage was observed in the lower row, along Stiffener 6. Minimal damage was observed in the fourth and fifth rows, as measured from the bottom. Extensive damage was observed in the second and third rows. This finding matches well with the J-STARS study insofar as damage reported in that study is indicated in Figure 2.5 by a circle circumscribed around the damaged hole.

The data obtained in this study followed similar procedures as the earlier Lehigh University study. The same Hi-Scope ™ optical microscope was used, and all resolvable damage from 50-150 X magnification was recorded. It should be noted that for the measured data appearing in Fig. 2.6, multiple cracks were measured individually, and the individual crack lengths were measured rather than aggregate length. Additionally, repeated crack lengths were independently accounted for in this model, rather than being grouped, and so they appear as vertically aligned points. All cracks were recorded in this manner unless multiple cracks were so close together that they were assumed to be on the verge of linking, and therefore, would function, in essence, as a single, dominant crack [15]. In this case the effective total crack length of the linked cracks was used.

The cumulative distribution in observed damage is shown in Fig. 2.6 in comparison with that of the earlier Lehigh University study [15]. Indeed, the distributions are similar. One possible source for this difference, however, is simply that greater stresses are evident in Section 3 of the aircraft. The can be attributed to the aircraft construction, namely to the proximity to engine pylons, landing gears, flaps, etc. To support this hypothesis, the most multiple-hole-wall cracks (MHWCs) found within a single hole by the earlier Lehigh study was sixty-eight (68). In the current study, much more extensive damage was discovered. In a single hole, hole number 70, there was a total of 178 MHWCs For demonstration, an optical micrograph of a highly stressed region within hole number 27 is reproduced as Fig. 2.7 which displays extensive corrosion fatigue damage well beyond that which was discovered in the previous study. An important point is that a limited number of holes were analyzed in this study, most with significant to severe corrosion fatigue cracking (CFC). This implies that the greater damage prevalent in this region were attributed a greater influence than they would exude given collection of additional data. Regardless, the deviation is well within experimental error and the Harlow-Wei model [16] is supported. The obvious observation to be made is that stress corrosion assisted cracking is a powerful fatigue mechanism in the fastener holes of aircraft having aluminum wingskins. It is by variable-amplitude fatigue, of course, that produces this damage. This realization forms the basis for engaging in an investigation of the mechanisms of, and possible simplifications for, variable-amplitude fatigue crack growth.

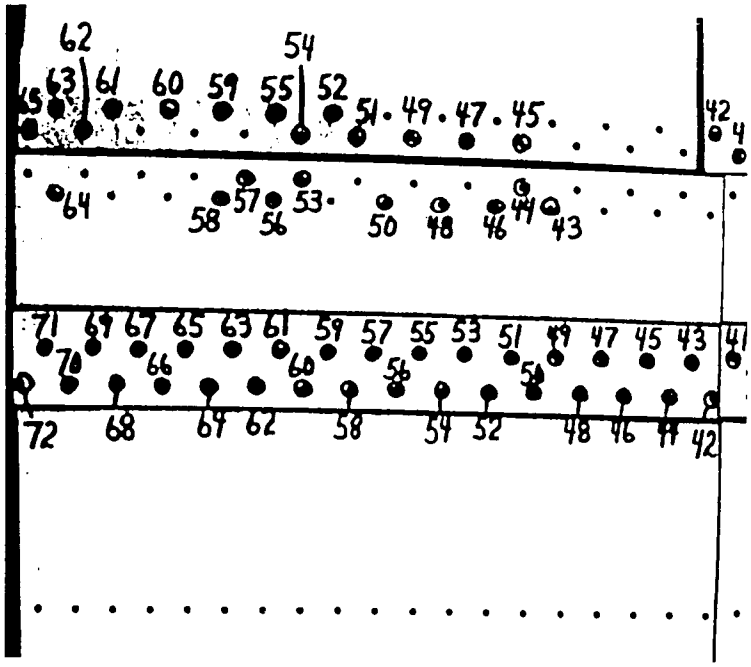

Figure 2.5: A portion of Section 3 along Stiffeners 6-8 from the CZ-184 aircraft for which microscopy and statistical analyses are made [18].

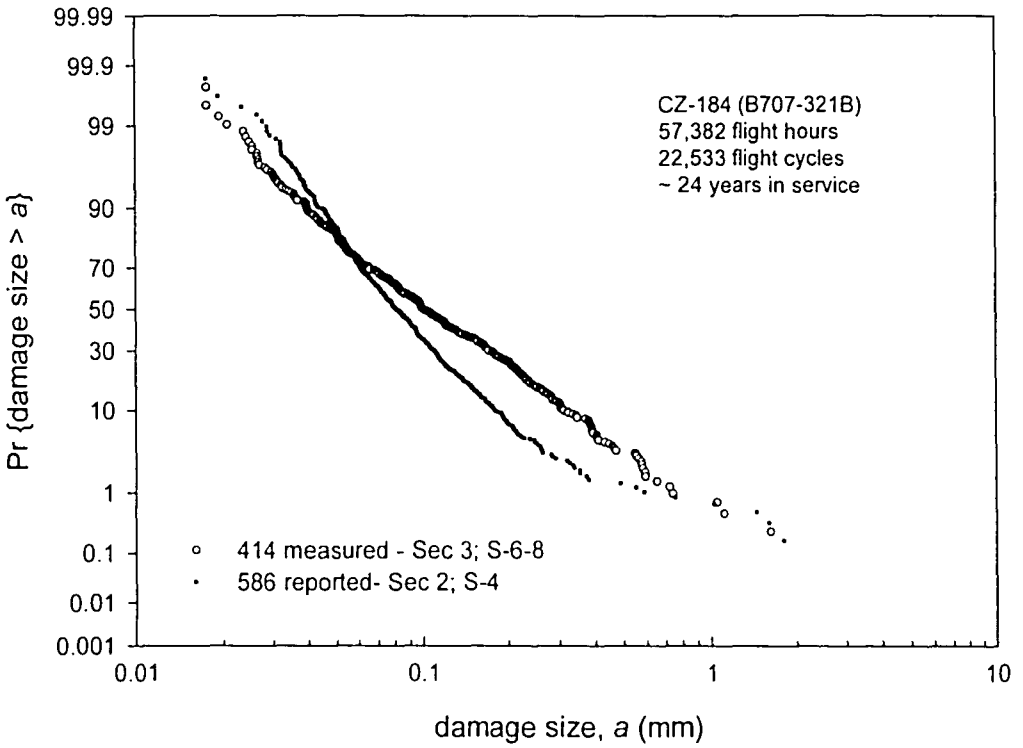

Figure 2.6: Comparison of the cumulative distribution function (cdf) for all MHWC lengths reported in 110 holes from Section 2 along Stiffener 4 and those measured using video imaging microscopy for 46 holes from Section 3 along Stiffeners 6-8 from the CZ-184 aircraft.

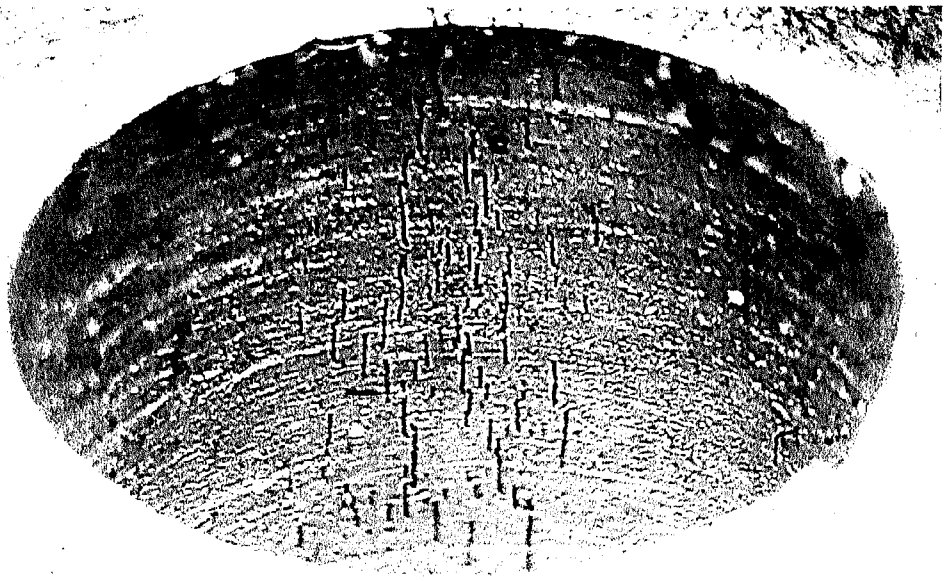

Figure 2.7: Optical micrograph of a highly stressed region of hole no. 27 in wing panel B3-9-2 of the CZ-184 aircraft showing extensive corrosion fatigue cracking.

2.5 Effect of Corrosion Protectants

It should not be overlooked that corrosion protectants, when appropriately applied to the surface of fastener holes may suppress corrosion and so render corrosion fatigue cracking as a non-issue. This argument fails to distinguish, however, that machining damage may be present a priori as congenital defects imparted before the component experiences its first service load, or that mechanical damage (such as fretting) may develop – in either case allowing significant areas of corrosion protectant to be removed. This would expose surfaces to the influence of corrosive environments.

3. UPGRADE OF MEASUREMENT EQUIPMENT FOR STUDYING CRACK NUCLEATION AND GROWTH – AC POTENTIAL DROP VERSUS DC POTENTIAL DROP SYSTEMS

3.1 Introduction to Potential Drop Methods

3.1.1 Summary

Two types of potential drop methods are available to the experimentalist, namely direct current (DC) and alternating current (AC). Electrical potential drop methods provide measurements of the average crack length through the thickness as opposed to visual measurements which give measurements of the crack length only at the surface. The general advantage of AC is that current is forced to the surface and thus the measured electrical potential drop at the surface is greater than for DC. This phenomenon is known as skin effect and depends on both material properties and frequency. Skin effect is explained in detail in Section 3.2.

DC systems, unfortunately, are influenced by thermal emf. AC systems typically allows for an order of magnitude reduction in applied current due to increased overall system gain. One significant detriment to AC systems, however, is impedance effects which compromise system repeability and reliability. Impedance effects occur mostly due to reactive components when the resistance of the material is highly sensitive to changes in test environment.

Here an evaluation is made of the relative sensitivity of the *ACPD* and *DCPD* (alternating current and direct current potential drop) methods. The comparison was made in detection of the onset of stress corrosion cracking (SCC) in Inconel 600 (IN

600) alloy with the specimen configuration as shown in Figure 3.8. The principal aim was to determine if there was enhanced sensitivity associated with the *ACPD* method by localization of current at the surface of the specimen and whether this is directly related to an increase in frequency.

Before the case study is discussed, however, some general background on potential drop methods with an emphasis on the skin effect which arises in a conductor carrying an AC current will be presented.

3.1.2 Introduction

Electrical potential drop methods rely on the phenomenon that there is a disturbance in the electrical potential field about any discontinuity in a current-carrying body[19]. To use the electrical potential drop to measure crack growth, a constant current is passed through a test specimen and the change in electrical potential for two points spanning the crack is measured across the crack as it propagates. This change in electrical potential reflects the increase in electrical resistance of the specimen as the remaining uncracked cross-section decreases. To quantify this change, an analytical or numerical expression needs to be developed to relate this potential increase across the crack length V_a to the crack length a.

As Aronson and Ritchie[20] illustrate, in practice, calibration curves are nondimensionalized and take the form of V_a/V_o versus a/W where V_o is a reference potential drop across the initial starter notch a_o and V_a is the instantaneous potential. By representing the relationship by use of nondimensionalized parameters the

calibration curve becomes independent of material properties, specimen thickness, and magnitude of applied, constant input-current. Calibration curves, therefore, become principally governed by both specimen and crack geometry, and by the location of the current and potential leads on the specimen.

For the middle-tension (MT) specimen shown in Figure 3.1 with a razor-thin slit of length *2a*, for instance, the following relationship was developed by Johnson [19] for the potential difference between two points placed symmetrically on the specimen centerline at a distance *y* above and below the slit:

$$\frac{V_a}{V_{a,o}} = \frac{\cosh^{-1}\left[\cosh(\pi y/2W)/\cos(\pi a/2W)\right]}{\cosh^{-1}\left[\cosh(\pi y/2W)/\cos(\pi a_o/2W)\right]} \tag{3.1}$$

where:

a = the crack size.

a_o = reference crack size

W = specimen width

V_a = the measured electrical potential drop (EPD) voltage

$V_{a,0}$ = the measured reference voltage corresponding to a_o

y = the voltage measurement lead spacing from the crack plane, i.e. one-half the gage length.

Theoretically, this relationship is valid only in cases where the current density is uniform and the voltage is measured on the centerline of the specimen across the crack

plane. Of course, by virtue of a crack the current density cannot be constant. A diagram of the standard geometry for the MT specimen is shown in Figure 3.1.

Li and Wei[21] confirmed that the Johnson equation can be used directly for crack length determination with good accuracy. This offers an advantage as otherwise a series of experimental calibration curves over a range of crack lengths must be determined.

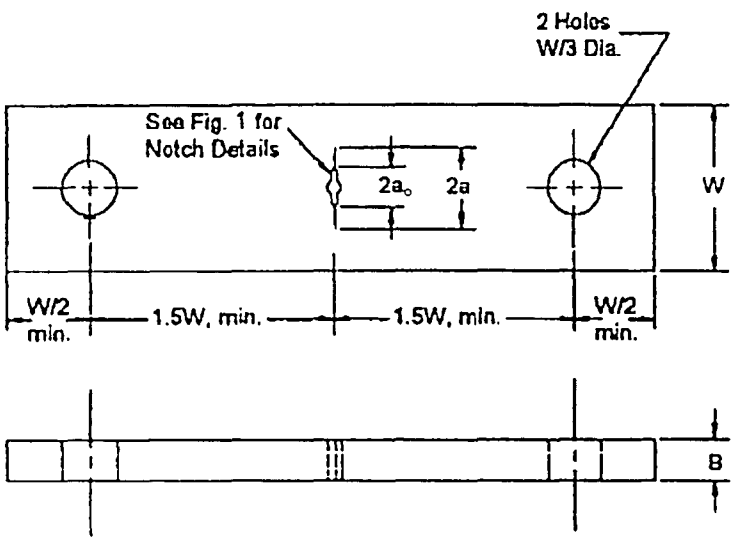

Figure 3.1: Standard Middle Tension MT Specimen for Fatigue Testing

K.-H. Schwalbe and D. Hellmann[22] demonstrated the applicability of Johnson's equation for the change in potential drop with crack length for the compact tension (CT) specimens. The CT specimen is desired since it has the property that its stress intensity factor changes rapidly with increasing crack length. Furthermore, Aronson and Ritchie [20] performed an optimization on the CT study by means of a finite element analysis which was based on four parameters: accuracy, sensitivity,

reproducibility, and measurability. Each of these terms is defined as follows: (i) accuracy is the capacity of the calibration curve to approach in its approximation the actual electrical potential versus crack length response, (ii) sensitivity is the ability to resolve small changes in crack length, or expressed mathematically, is the slope of the calibration curve dV/da where V is the potential drop and a is the crack length, (iii) reproducibility is a function of errors associated with positioning of current and potential leads, and (iv) measurability accounts for the magnitude of the output voltage signal as well as its signal-to-noise ratio. Based on their analysis, Aronson and Ritchie selected optimal locations for the current and potential leads. These locations were later slightly modified by K.-H Schwalbe and D. Hellmann [22], and are shown in Figure 3.2.

J. K. Donald[23] performed a calibration verification study of the CT geometry using Johnson's formula and the Schwalbe-Hellman lead spacing. Donald demonstrated that Johnson's formula holds to within a maximum error of 0.3% of W across an a/W ratio ranging from 0.30 to 0.90 when a linear post-test correction is applied to the calibration data.

The applicability of Johnson's formula to the CT geometry is shown by the plot of error versus the ratio of crack length a to specimen width W, shown as Figure 3.3 [23].

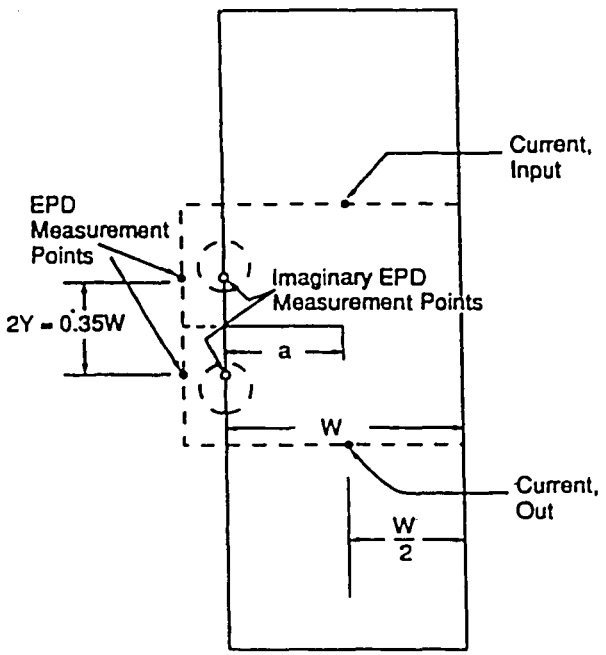

Figure 3.2: Representation of CT specimen using Johnson's formula [23].

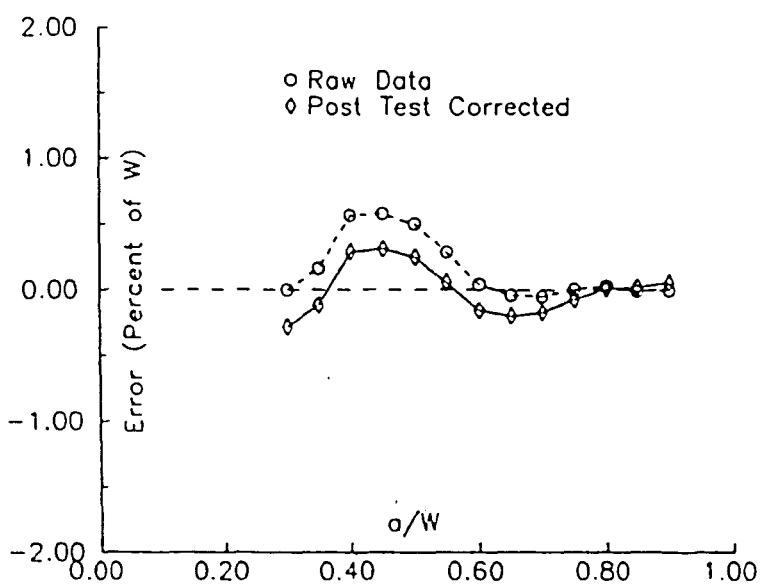

Figure 3.3: Error as a function of the ratio of crack length a to finite width W: calibration verification for the CT geometry using Johnson's formula, courtesy of J.K Donald [23].

It has been mentioned that two types of potential drop techniques exist, namely AC and DC. What follows is a case study which evaluates the efficacy of these methods in light of modern testing capabilities. The goal of the study was to qualify which is the better method, DC or AC, for the measurement of crack growth. In order to make such a comparison, however, some background must be introduced concerning the physical relationships which make potential drop methods possible.

3.2 Skin Effect in Cylindrical Conductors

The governing differential equation[24] for current density, *J(r)* in a cylindrical conductor carrying an *AC* current is given by:

$$r^2 \frac{d^2 J(r)}{dr^2} + r \frac{dJ(r)}{dr} + k^2 r^2 J(r) = 0 \tag{3.2}$$

This results in a solution of the form:

$$J(r) = a_0 J_0(kr) \tag{3.3}$$

Here, J_o is a Bessel function[25] of the first kind, order zero and the constant a_0 for a given frequency is computed by finding the magnitude of:

$$a_0 = \frac{k \cdot I}{\sqrt{2\pi a}} \frac{1}{J_1(ka)} \tag{3.4}$$

with

$$k = (1 - i)\sqrt{f\pi\sigma\mu} \tag{3.5}$$

where J_1 is a Bessel function of the first kind, order one [25]. *J(r)* is found by taking the magnitude of the resulting expression found upon substitution of the calculated value of a_o and Equation 3.5 into Equation 3.3

For the case of a rectangular cross section, *J(z)* is expressed as:

$$J(z) = J(a)_p \cdot e^{-z\cdot\sqrt{f\pi\mu\sigma}} \tag{3.6}$$

where *z* is the distance into the material from the surface and $J(a)_p$ is the current density at the plate surface [24]. The value of *z* that yields $J(z) = J(a)_p/e$ is traditionally known as "skin depth," which is explicitly defined as:

$$\delta = \frac{1}{\sqrt{f\pi\mu\sigma}} \tag{3.7}$$

The quantity $\mu\sigma$ typifies the vigor of the skin effect. Note that μ is found by multiplying the relative permeability, μ_r of a specific material by the permeability of free space. Ferromagnetic metals display a dramatic skin effect (large values of a/δ) even at relatively low frequencies due to their high magnetic permeability. Paramagnetic metals, such as nickel alloys, display less of an effect at the same frequency. Aluminum is nonmagnetic so its relative permeability is equal to one and

its permeability is the same as that of free space. *Thus, for aluminum there is no intrinsic benefit of skin effect and so testing with an AC source does not enhance resolution.* In fact, there is a serious concern when testing with AC to avoid impedance effects that it is imperative to use only shielded wire with a common ground as well as to avoid any great temperature fluctuation that, for aluminum, ACPD becomes more of a detriment than a benefit.

Equation 3.6 can be used to approximate *J(r)* in the cylindrical case by letting $z = a - r$ and imposing the restriction $a/\delta \geq 5$:

$$J(r) = J(a) \cdot e^{-\frac{r}{\delta}} \quad (a/\delta < 5) \tag{3.8}$$

There is, however, significant error associated with applying Equation (3.6) over the range $0 < a/\delta < 5$. In this range, the exponential decaying function is a poor approximation to the exact Bessel function (Equation 3.3), and yields a smaller value of *J(r)* than the exact solution and increases in divergence as *r* approaches zero.

Furthermore, an approximation [25] useful as an independent check of *J(a)* is:

$$J(a) = \frac{I}{\sqrt{2} \cdot r_0 \pi} \sqrt{f \pi \mu \sigma} \cdot \sqrt{r_0 / r} \qquad (a/\delta < 5) \tag{3.9}$$

With an understanding of the limitations of Equation 3.8, one can apply Equation 3.7 as an estimate of skin effect in cylindrical cross sections to determine if

there will be a significant increase in current density such that an improvement in flaw detection may be expected. A more precise method would be to plot Equation 3.3 for the material; however, this requires solving for the constant a_0 at several frequencies.

Once the current density at the surface *J(a)* is known, the voltage drop between two points on the surface is:

$$V(a) = \frac{L}{\sigma} J(a) \tag{3.10}$$

This expression shows that *V(a)* is linearly proportional to *J(a)*. This suggests that the signal-to-noise ratio will increase for increasing *J(a)*, thereby increasing the system resolution allowing for the detection of smaller flaw sizes.

To facilitate the estimation of increase in current density at the surface (improvement of signal to noise ratio) with increasing frequency, a plot of $J(a)/J(a)_0$ versus a/δ was constructed over the range of practical ACPD frequencies (Figure 3.4). This plot is specific to geometry (fixed radius = 0.00254m) but is independent of material. Here $J(a)_0$ is a constant equal to the convergent value of *J(a)* as a/δ approaches zero, which reduces to *I/A* or the constant DC current density:

$$V = \frac{L \cdot I}{\sigma \cdot A} \tag{3.11}$$

Observe that at a very low frequency, the current profile becomes evenly distributed and Equation 3.10 is equivalent to the DC case given by Equation 3.11.

Moreover, seeing that there is no increase in surface current density for a/δ less than unity, it is obvious that the minimum AC frequency required to achieve skin effect can be found by setting Equation 3.7 equal to the radius a and solving for frequency. For demonstration, Table 3.1 gives the minimum required frequency for IN 600 and a carbon steel.

Table 3.1: Material property data and minimum frequency at onset of skin effect.

Material	σ $(m\cdot\Omega)^{-1}$	μ_r	Freq (Hz) @ $a/\delta = 1$
IN 600	972,101	1.01	40,028
Carbon Steel	5,000,000	100	79

It is evident that much higher frequencies are required in IN 600 in order to generate skin depths on par with those found in a ferromagnetic material such as steel. For frequencies resulting in values of $a/\delta > 1$, the factor of increase in surface current density can be expressed by a linear model as shown in Figure 3.4 explicitly expressed as:

$$J(a)/J(a)_0 = 0.7049(a/\delta) + 0.2075 \qquad a/\delta > 1 \tag{3.12}$$

Using equations 3.7 and 3.12 predictions of the benefit of skin depth can be made in terms of improvement of signal to noise ratio. Note that Equations 3.10 and 3.12 assume that L is several times larger than the flaw depth; clearly once the probes are moved in very close to the flaw then this linear relationship becomes invalid.

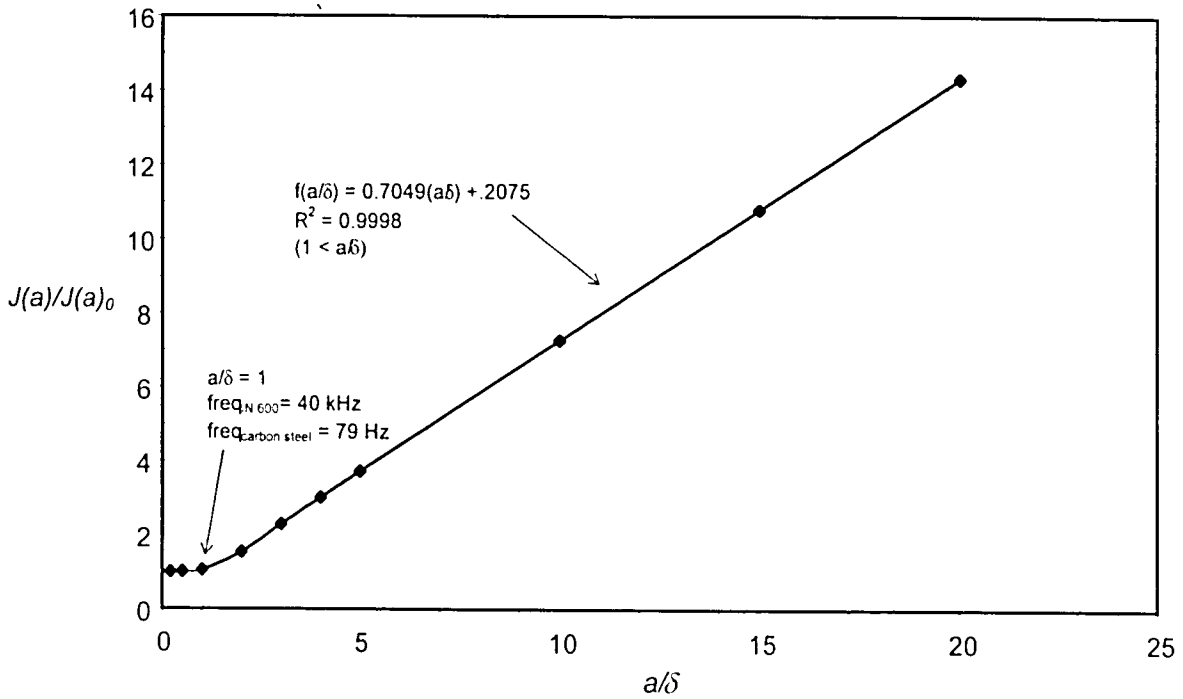

Figure 3.4: Factor of increase in $J(a)/J(a)_0$ with increasing a/δ where $J(a)_0$ is the constant value of current density that occurs below the frequency where $a/\delta \leq 1$ and a is the fixed outer radius of 2.54 mm.

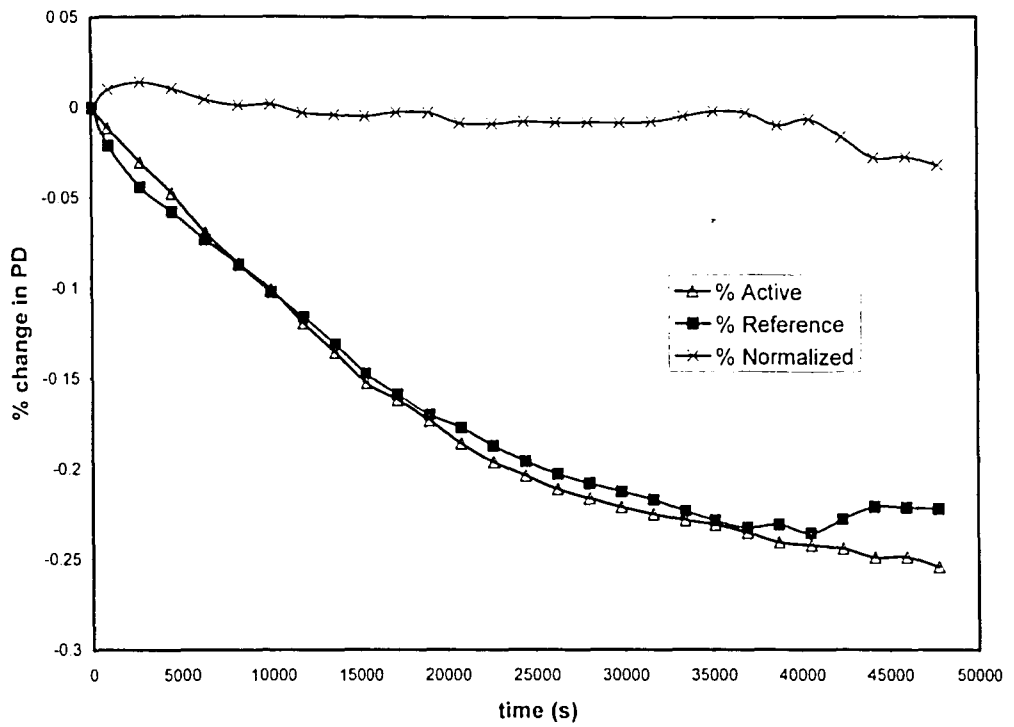

Figure 3.5: Stability check for potential drop system showing efficacy of the normalization procedure.

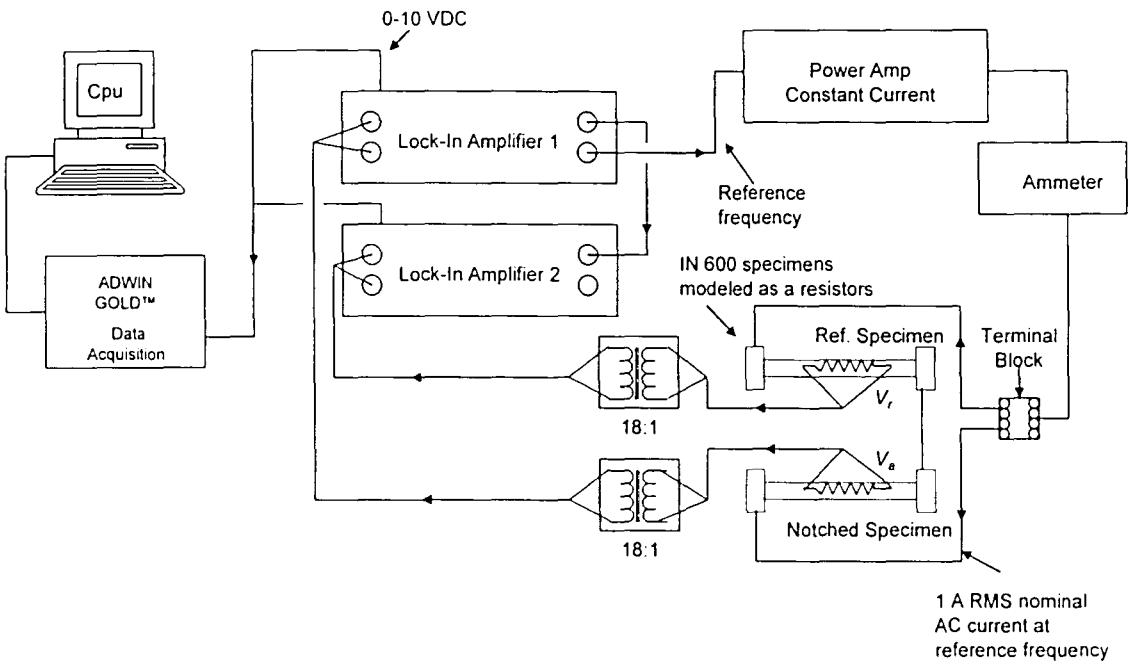

Figure 3.6: Schematic representation of the Lehigh University FTA Alternating Current Potential Drop (ACPD) system.

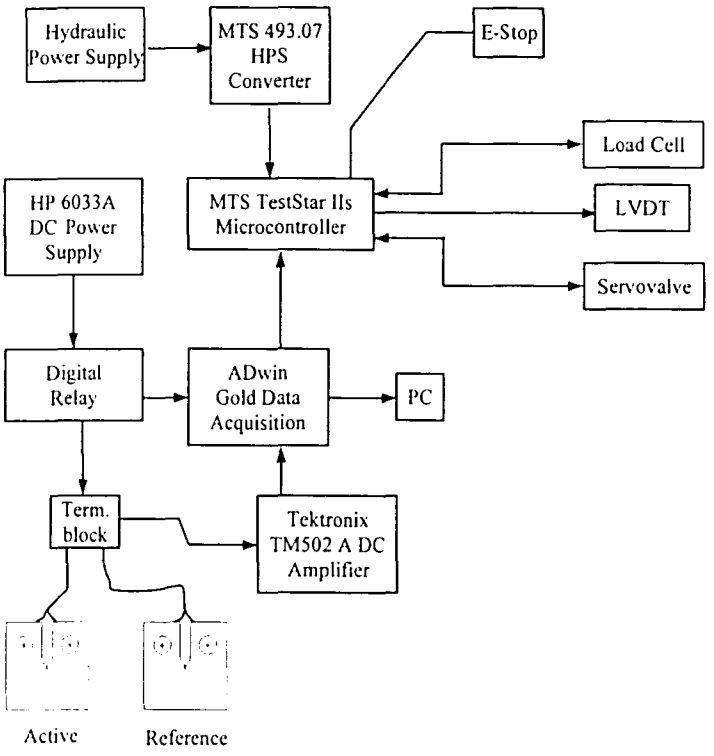

Figure 3.7: Schematic representation of the Lehigh University Direct Current Potential Drop (DCPD) system.

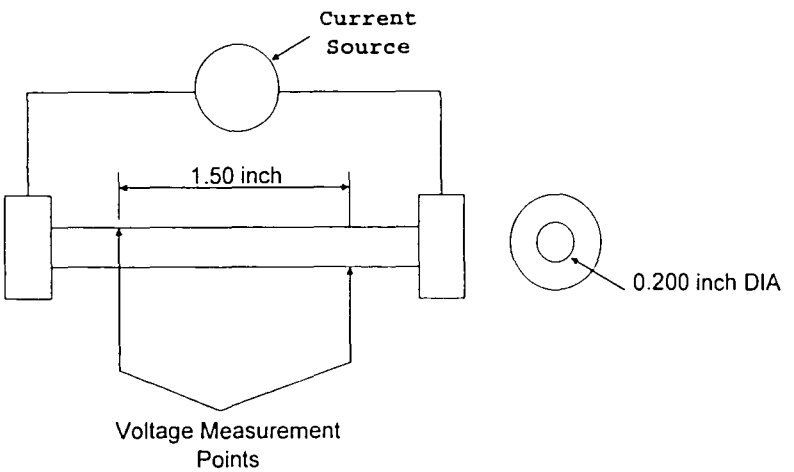

Figure 3.8: Schematic of IN 600 specimens.

3.3 Choice of Potential Drop Method: A Flaw Detection Study

A flaw detection study was conducted on crack nucleation sites in cylindrical specimens in order to reevaluate and modernize electrical potential drop systems in light of advances made since the last upgrade at Lehigh University. Smooth, cylindrical specimens were used considered since the physics is are easier to model for the cylindrical geometry than for fatigue specimens used for crack growth studies. The flaw detection study fits within the context of the fatigue crack growth studies (discussed in chapter 4 and chapter 5) because the conclusions drawn from this study are universal statements concerning potential drop techniques.

The geometry of the specimens used for this evaluation is schematically shown in Figure 3.8. For the initial assessments, cracking was simulated by cutting a small

notch in the specimen gage section in 0.0254 mm increments, to a total depth of 0.254 mm. Comparisons of the AC and DC systems were made at nominal working currents of 1.0 A RMS and 1 A DC respectively. The results show that the *ACPD* system (operated at 9 kHz) offered no distinct advantage over the *DCPD* system, with detection of damage for both between 0.0508 mm and 0.0762 mm. This was due to the fact that IN 600 is non-ferromagnetic and does not develop appreciable skin effect below 40 kHz. Aluminum is even less magnetic than nickel with an absolute permeability approximated by the permeability of free space. Accordingly, aluminum alloys will not see any enhancement by means of testing with alternating current.

3.3.1 Experimental Procedure

The *ACPD* system used at Lehigh University is shown in Figure 3.6. This system operates in constant current mode applying RMS current of up to 1 A for frequencies in the range of 50 Hz to 12 kHz. The current of this system decreases linearly with increasing frequency up to 12 kHz then rolls off dramatically. This reflects the frequency response of the power amplifier. The evaluation, therefore, was made at 9 kHz with a corresponding maximum current of 0.782 A RMS. Using Equation 3.3, theoretical current density profiles as a function of radial distance from the center were computed for the IN 600 specimens at 9 kHz and 160 kHz and are depicted in Figure 3.9. A frequency of 9 kHz was chosen to model the test frequency,

and 160 kHz corresponds to the frequency at which $a/\delta = 2$. For comparison, the response for carbon steel is also shown at 9 kHz.

For a basic system check, Equation 3.10 at 1 Hz and Equation 3.11 were used to find the theoretical DC voltage drop (Table 3.2). The actual measured value on the DC system at 1 A was 1.83 mV. The 6% difference between the measured and theoretical value was attributed to error in material constant σ. Also, Equations 3.10 and 3.11 assumes a large length to diameter aspect ratio, which may not have been completely satisfied over a gage length of 38.10 mm. This agreement, however, is reasonable for a system check. Numerical constants used in conjunction with Equation 3.4 are also given in Table 3.4.

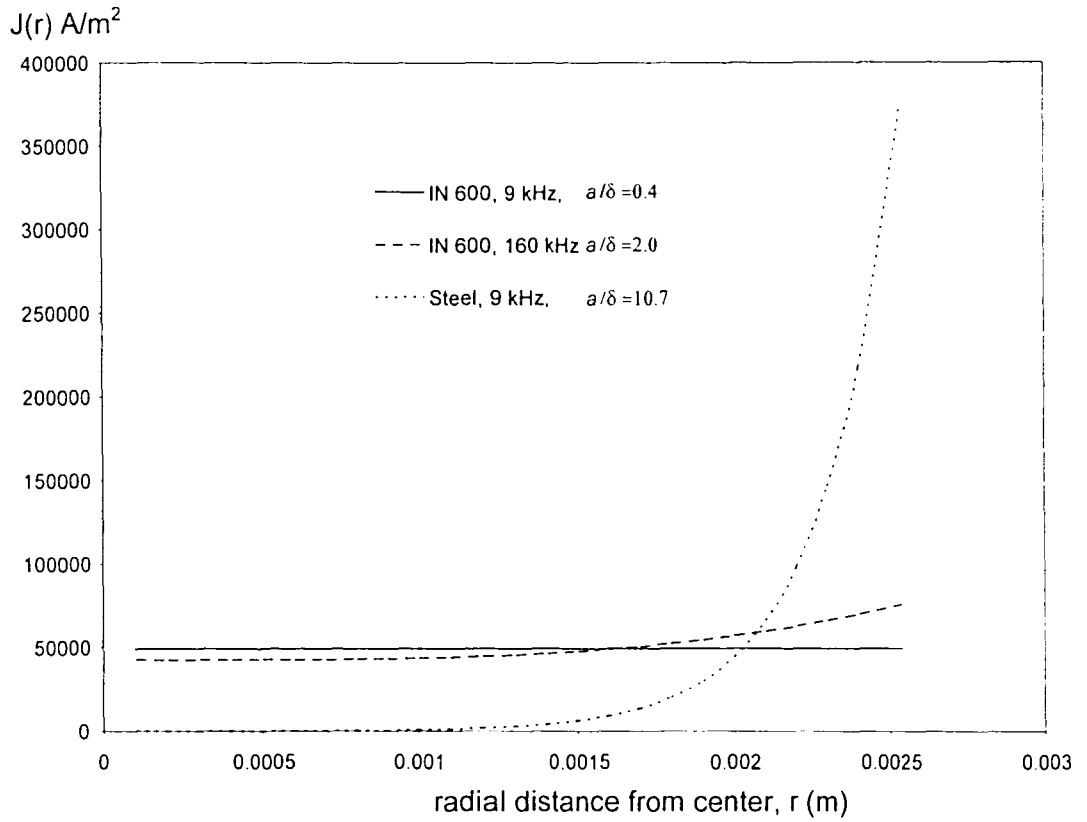

Figure 3.9: Theoretical current density profiles for IN 600, a paramagnetic material. Carbon steel, a ferromagnetic material, is provided as a comparison. Aluminum would have an even weaker current density response to skin effect than the nickel-based IN 600.

Inconel 600 specimens were thus configured with current leads and voltage leads attached in the configuration shown in Figure 3.8. To simulate the cracking process, a small groove was cut in the gage section between the leads using an abrasive cut-off disk with diameter and thickness of 19.05 mm and 0.2032 mm, respectfully. The disk was lowered onto the surface of the specimen in increments of 0.0254 mm to a final depth of 0.254 mm by means of an elevation jack with micrometer control. Measurements of the final notch indicate a deeper notch than anticipated and that the error in the depth for each increment may be on the order of

0.010 mm. A pause of 300 seconds was allowed at each depth for the system to stabilize. The active voltage V_a was measured across the notched specimen as well as a reference voltage V_r across an unnotched specimen. Data was collected at 10 points per second and at every 500 point interval, an average was stored for V_a and V_r.

Table 3.2: Material and numerical constants used in the mathematical analysis.

Material	σ 1/(m·Ω)	μ_r	f (kHz)	δ (mm)	a_0	J(a) A·m²	Predicted Voltage (mV)	Measured VDC (mV)
IN 600	972,101[a]	1.01	9	5.36	49,312	49,468	1.94	1.83
IN 600	972,101	1.01	160	1.27	42,550	75,747	--	--
Steel	5,000,000	100	9	0.24	82.981	382,350	--	--

The reference voltage was used to compensate for temperature and electronic fluctuations, and a corrected voltage referred to as the normalized voltage V_n was found by:

$$V_n = V_a \cdot \frac{V_{r,0}}{V_r} \qquad 3.13$$

[a] *Aerospace Structural Metals Handbook, 1974.*

Data were analyzed by two methods: 1) in terms of percent change in normalized potential, and 2) relative change in normalized potential as defined in Equation 3.14 and 3.15, respectively:

$$\%\Delta V_n = (V_n - V_{n,0})/V_{n,0} \cdot 100 \qquad 3.14$$

$$\Delta V_n = (V_n - V_{n,0}) \qquad 3.15$$

This procedure was independently repeated on three separate specimens for the *ACPD* and *DCPD* systems each. In an attempt to make an equitable comparison, the amperage of the *DCPD* system was set to 1 Amp. As stated earlier, the maximum value of RMS current of the *ACPD* system used was 1 Amp RMS, however, this values fades to 0.782 A with increasing frequency.

3.3.2 Summary of Results

An evaluation of *ACPD* and *DCPD* methods for automated crack length measurement was conducted to determine which method could detect the smallest increment of crack growth (initiation) from an arbitrary location on a smooth, round specimen. Of particular interest was to see if the skin effect[26] that arises in metals would provide an advantage in the *ACPD* method. The round specimen considered here was chosen due to its simplicity of geometry; the relevance of which in terms of

the 7075-T651 CT specimens as fatigue specimens is that any insights drawn from the IN 600 cylindrical geometry are so generic as to readily apply to the general class of all potential drop techniques.

It was the conclusion of this work that, for aluminum alloys, DCPD is preferred because: i) aluminum is nonmagnetic and so no appreciable skin effect develops at reasonable signal waveform frequencies, and ii) alternating current impedance effects are difficult to mitigate, therefore compromising signal reliability. It was observed this was not an issue of errors in wire placement but instead of system drift. This drift was caused by fluctuations in the total impedance of the system which in turn was caused by changes in the environment.

3.3.3 Detailed Results

Graphical representation of the empirical data follows directly from the procedure herein outlined and is represented in Figures. 3.10-3.13. These graphs demonstrate the absolute and percent change, respectfully, versus depth of cut, in specimen electrical potential for both the DC and AC potential drop systems. Figures 3.10 and 3.12 are represented by lines as drawn through the six data points (500 point averages) collected during each interval, while Figures 3.11 and 3.13 show the average voltage over the entire interval. Along the ordinate (depth of cut) axis each tick mark represents 0.0254 mm damage size as increasing from left to right. Perhaps it is best

seen in Figures 3.11 and 3.13 that a definitive rise in voltage is detected at notch depths greater than approximately 0.0508 mm.

It is evident from these figures that increased damage size correlates to greater electrical potential drop V_n. Figure 3.10 clearly represents this trend. The ordinate in Figure 3.10 represents the percentage in signal at the sample normalized to a reference value at a similar sample subject to the same conditions. The percentage change in normalized signal is considered to be zero at zero depth of cut. Figure 3.10 displays the trend for the signal to increase with increasing damage size with a greater percent increase at each damage size interval, indicative of the sensitivity of the system to damage evolution and propagation, which is a demonstration of the founding theory that propels both DC and AC potential drop methods as viable non-destructive techniques (NDT) for crack growth measurements.

Three duplicate tests were conducted for both the DC and the AC systems in which good agreement was obtained. Deviations are attributed to the variance in notch location and depth. Figures 3.12-3.13 are AC tests that display similar results. It is noted, however, that the change in specimen potential plotted along the ordinate in Figure. 3.13 is inclusive of the transformer gain. In order to obtain the true voltage drop at the specimen, therefore, the transformer gain must be divided out of the system. This boost in signal introduced by the transformers is an inherent benefit to the *ACPD* system, effectively increasing the sensitivity of the system while increasing the signal to noise ratio. The percentage change in normalized signal ratio is therefore greater in the AC system than the DC system, which is clearly observable in

juxtaposition of Figures 3.11 and 3.13. This is an intrinsic benefit of an AC system due to its higher overall system gain in comparison to an effective DC equivalent. AC transformer gain, however, is a function of frequency which presents a troublesome complication. The model transformers used in this application are designed to provide a nearly constant gain from 50 Hz to 15 kHz with an estimated gain of 18:1 at 9 kHz.

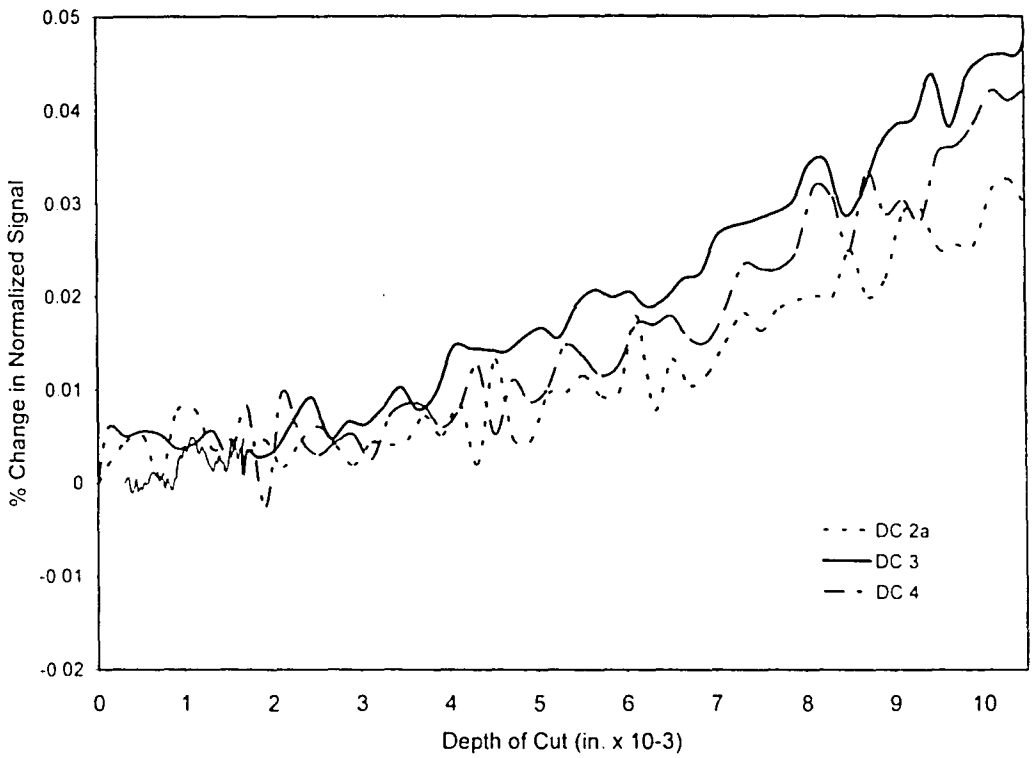

Figure 3.10: Percent change in specimen electrical potential as a function of cut depth for three direct current (DC) potential drop tests.

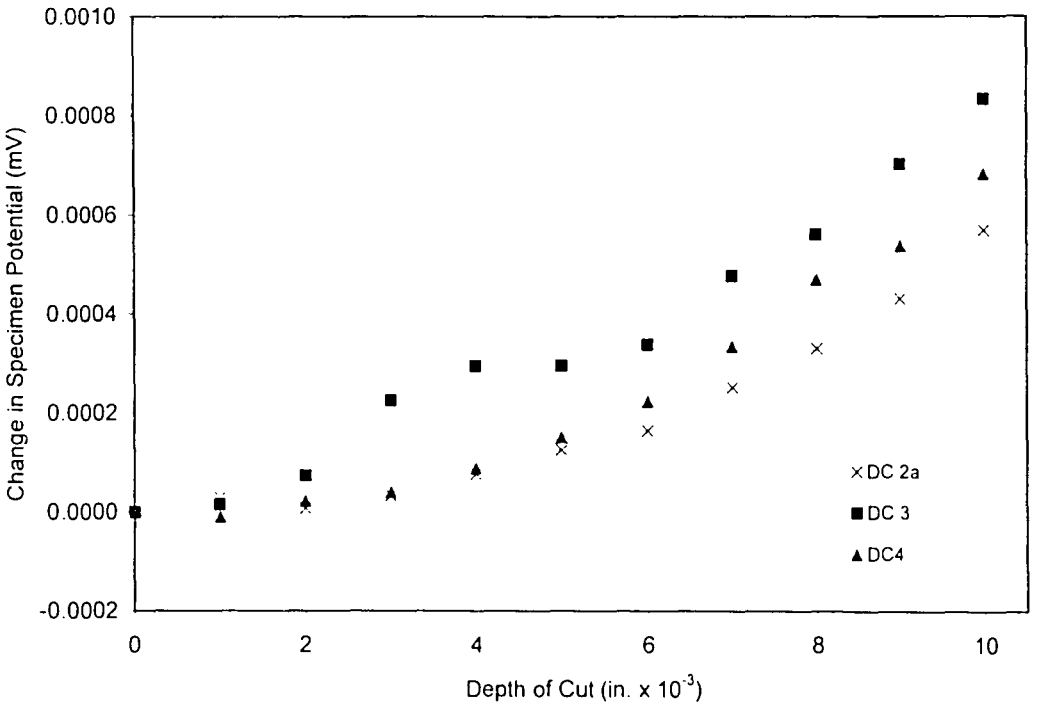

Figure 3.11: Absolute change in specimen electrical potential as a function of cut depth for three direct current (DC) potential drop tests.

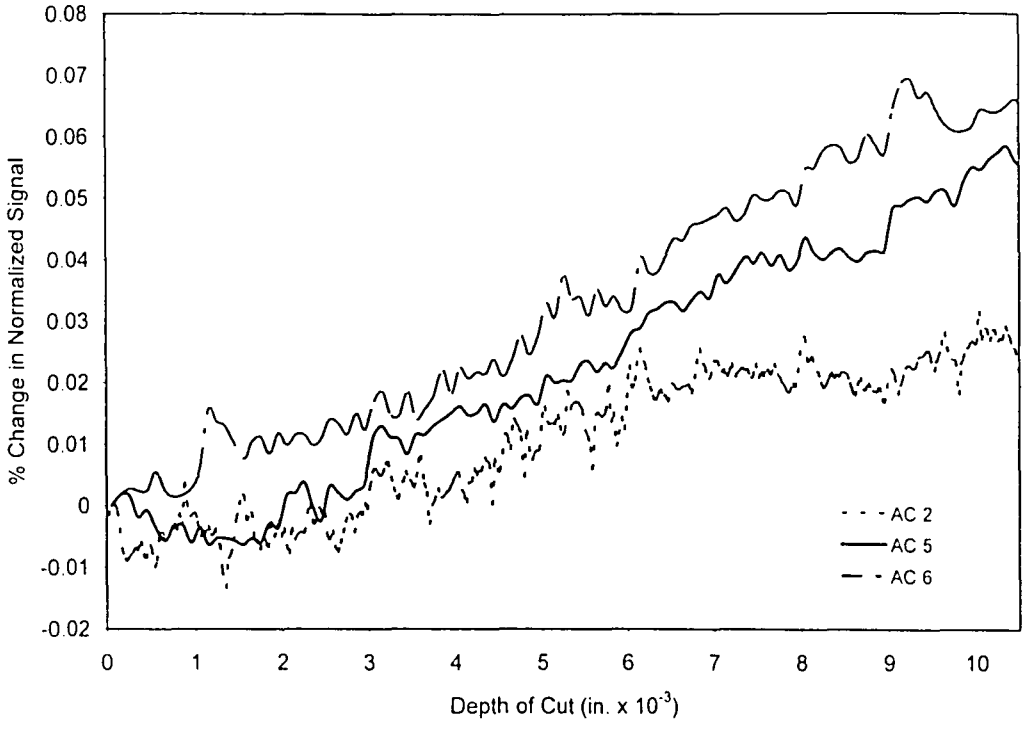

Figure 3.12: Percent change in specimen electrical potential as a function of cut depth for three alternating current (AC) potential drop tests.

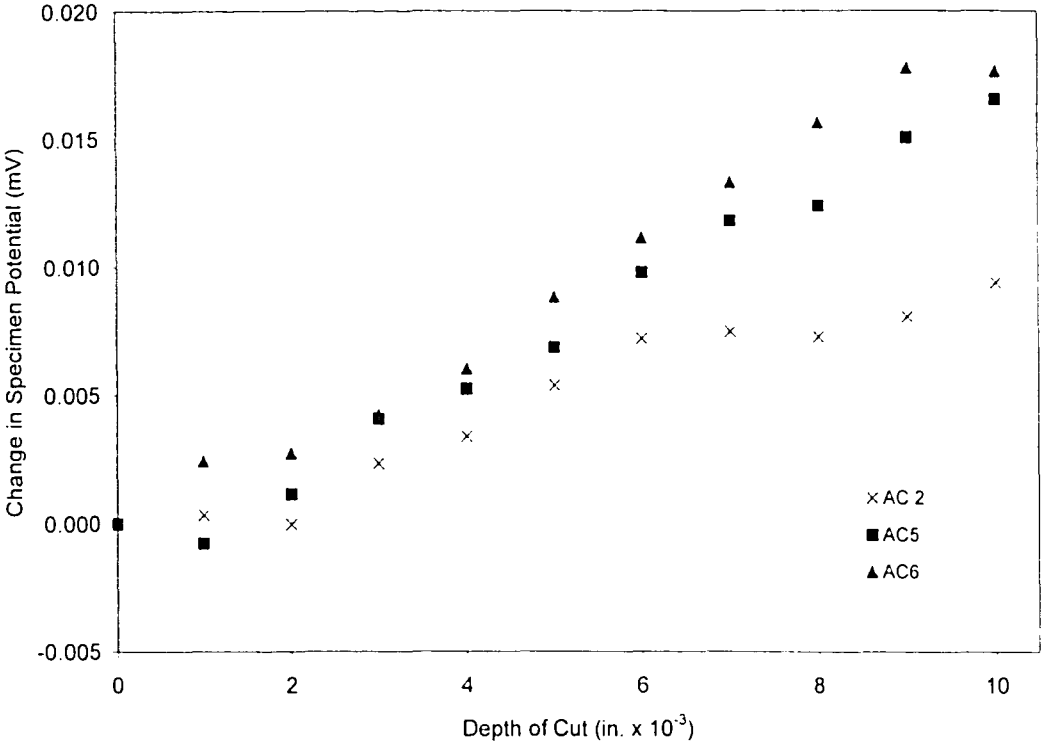

Figure 3.13: Absolute change in specimen electrical potential as a function of cut depth for three alternating current (AC) potential drop tests.

3.3.4 Discussion

To improve the resolution, one possibility is to increase the current which would reasonably have a beneficial effect for both systems for current quantities within the realm of practicality. If available current is limited, however, as was the case for the *ACPD* tests conducted herein, then this becomes infeasible.

For probes that are far enough away from the notch (more than several notch depths), the relative change associated with the notch, ΔV_n will be constant for all values of L and $J(a)$. Then, it can be seen that the percent change in signal with an increasing depth of the notch, $\%\Delta V_n$ will increase linearly as L is reduced:

$$\%\Delta V_n = \frac{\sigma}{L}\frac{(\Delta V_n)}{J(a)} \cdot 100 \tag{3.16}$$

Additionally, for IN 600, as described by Equation 3.3, higher frequencies above 40kHz correspond to an increase in $J(a)$ Systems of capable of higher frequencies do exist and are described in the literature[27]. For large dimensions of L compared to the notch depth, an increase in current density should improve system sensitivity and reduce scatter giving better agreement across repetitive experiments. This would be similar to raising the current. Once the probes are brought very close to the notch, of course, then non-linear effects of the local field perturbation must be considered.

3.3.5 Conclusions and Recommendations

At 9000 Hz, the *ACPD* and *DCPD* systems evaluated were similar in terms of the minimum depth of cut that could be resolved. This depth was approximately 0.0762 to 0.1016 mm. No improvement in the *ACPD* method was demonstrated at this frequency because skin effect in IN 600 does not occur below 40 kHz. An *ACPD* system capable of significantly higher *AC* frequency may improve resolution by increasing the surface current density, thereby improving signal to noise ratio and reducing scatter in the data.

To improve resolution with either the *ACPD* or the *DCPD* systems, a reduction in probe spacing is recommended so long as L >> flaw depth. ACPD uses much lower levels of operating current as well as having a superior overall system gain than DCPD. DCPD is preferred for aluminum, however, since no appreciable skin effect will develop in aluminum at modest operational waveform frequencies. DCPD is also unaffected by impedance or thermal emf.

4. EXPERIMENTAL PROCEDURE

4.1 Introduction

The motivation for this work is to develop a means of achieving accurate lifetime predictions of structures that are subjected to variable-amplitude fatigue. This will facilitate probabilistic analysis through numerical simulations that emulates in-flight spectrum loading. To achieve this objective this research is divided into (i) exploratory numerical simulations which provide a basis for the experimental approach, (ii) derivation of an appropriate constant-amplitude spectrum, (iii) experimental comparisons of these fatigue responses, and (iv) an investigation into the relative significance of the maximum and minimum loads in a generic spectrum.

4.2 Material

The material used in this study is a 50.8 mm thick plate of high-strength 7075-T651 aluminum alloy provided by ALCOA[a]. Chemical and mechanical properties of the plate are provided in Table 4.1 and Table 4.2, respectfully.

Table 4.1: Spectrographic chemical analysis on 7075-T651 test specimens.

Si %	*Fe %*	*Cu %*	*Mn %*	*Mg %*	*Cr %*	*Zn %*
0.050	0.297	1.52	0.024	2.25	0.185	5.36

[a] Aluminum Company of America, Pittsburgh, PA 15212

Table 4.2: Mechanical properties of the 7075-T651 plate

σ_y (MPa)	σ_{ut} (MPa)	σ_f (MPa)	E (GPa)
541	585	719	69

4.3 Specimen Design

The geometry for the specimens was chosen as compact tensions (CT) since the CT geometry has the desirable characteristic that the stress intensity factor changes rapidly with the ratio of crack length a to finite width distance W according to:

$$\Delta K = \frac{\Delta P}{B\sqrt{W}} \frac{(2+\alpha)}{(1-\alpha)^{3/2}} (0.886 + 4.64\alpha - 13.32\alpha^2 + 14.72\alpha^3 - 5.6\alpha^4) \qquad (3.1)$$

where B is the specimen thickness, W the specimen width, ΔP the range of load, and α the ratio of crack length a to W. The expression is valid for $\alpha \geq 0.2$.

50.8 mm wide compact-tension specimens (Figure 4.1), oriented in the long-transverse (LT) direction were used in fatigue crack growth studies. Specimens were fabricated so that the crack plane would be perpendicular to the rolling direction as well as the long-transverse (LT) surface since this orientation simulates the service conditions of material components in an outer wing panel (OWP). This orientation of material with respect to its final form is shown in Figure 4.4. A diagram of the specimen geometry[a] is shown in Figure 4.1. The initial starter notch, approximately 7.62 mm was made by electro-discharge machining (EDM) to minimize induced

[a] Metcut Research Inc., Cincinnati, OH 45209

residual stresses. The loading holes were parallel to within 0.0127 mm. The intersection of the tips of the machined notch (a_n) with the specimen faces was specified to be equidistant from the top and bottom edges of the specimen to within 0.005W.

The developed, operational precracking procedure was to provide fatigue cracks to a length of 1.524 mm by means of K control with R = 0.10, K = 5.494 MPa $\sqrt{m}$, and C = 0 where C is the normalized K gradient and R is the load ratio. These conditions were sufficient to ensure that the precrack conformed to ASTM guidelines which specify that crack growth rates for precracking must not exceed 1.0 E-08 m/cycle. The crack growth rate for the conditions expressed above were 6.02 E-9 m/cycle which complies with ASTM E647 specifications.

As a general statement, the purpose of precracking is to introduce an actual crack into a specimen for subsequent fracture toughness testing or crack growth testing. Ideally, the crack should have a sharp tip with minimal plastic zone surrounding the crack front to limit impact on its natural growth. For variable-amplitude testing, and in particular, for comparison of various fatigue tests, careful efforts were made to achieve equal starting precrack lengths as to minimize variability that might be introduced by either the starter notch geometry and residual stresses produced by EDM. Post fracture examinations showed that the variation in precrack lengths was on the order of 1E-6 m. Note that comparisons of a versus N should be made by picking identical initial crack lengths.

Samples were tested by Metcut Research for evidence of residual stress by measuring a distance on the TS surface spanning the base of the EDM notch both before and after removal of material by EDM. The results showed the as-manufactured residual stresses to be insignificant. An SEM of the end of an EDM notch and the beginning of the precrack is shown in Figure 4.2.

Orientation of specimens with respect to the original plate is shown in Figure 4.3. Observe that specimen was fabricated out of both faces. The specimen orientation was chosen in order to simulate the orientation of the material that is used in manufacture of wing skins, a schematic of which is shown in Fig. 4.4.

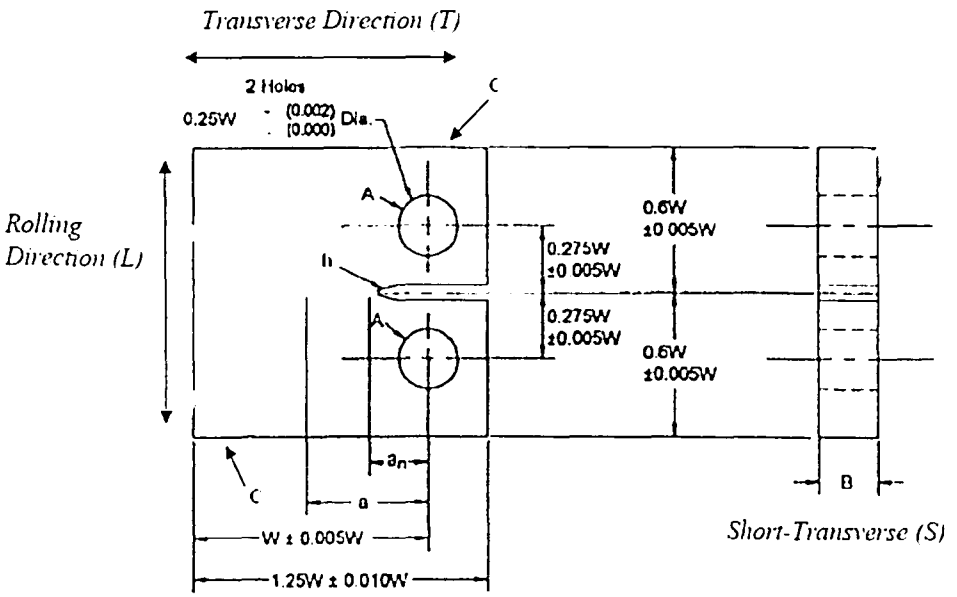

Figure 4.1: Compact tension (CT) specimen design used for testing.

$$B = 6.35 \pm 0.127 \text{ mm}$$

$$a = 15.24 \pm 0.051 \text{ mm}$$

$$W = 50.8 \pm 0.127 \text{ mm}$$

$$h = 0.254 + 0.051 \text{ mm}$$

ϕ = hole diameter = 0.25W + 0.002

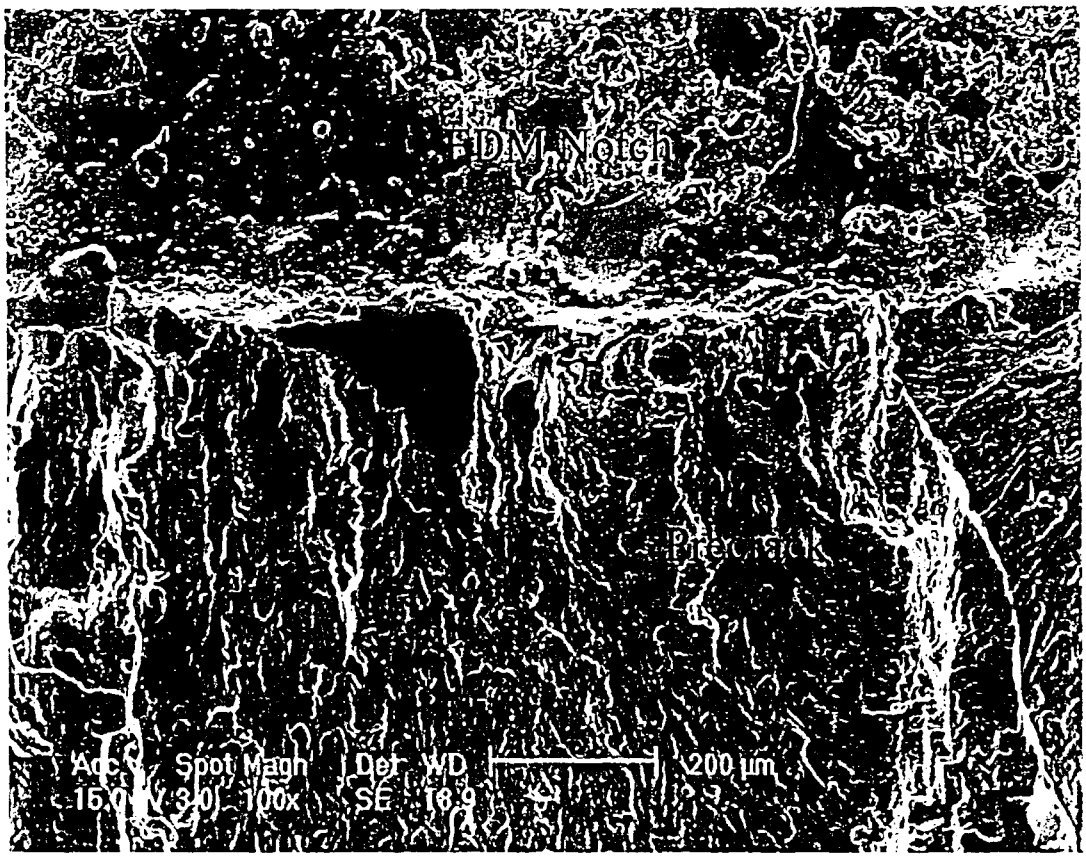

Figure 4.2: SEM micrograph of the end of the EDM notch and the beginning of the precrack.

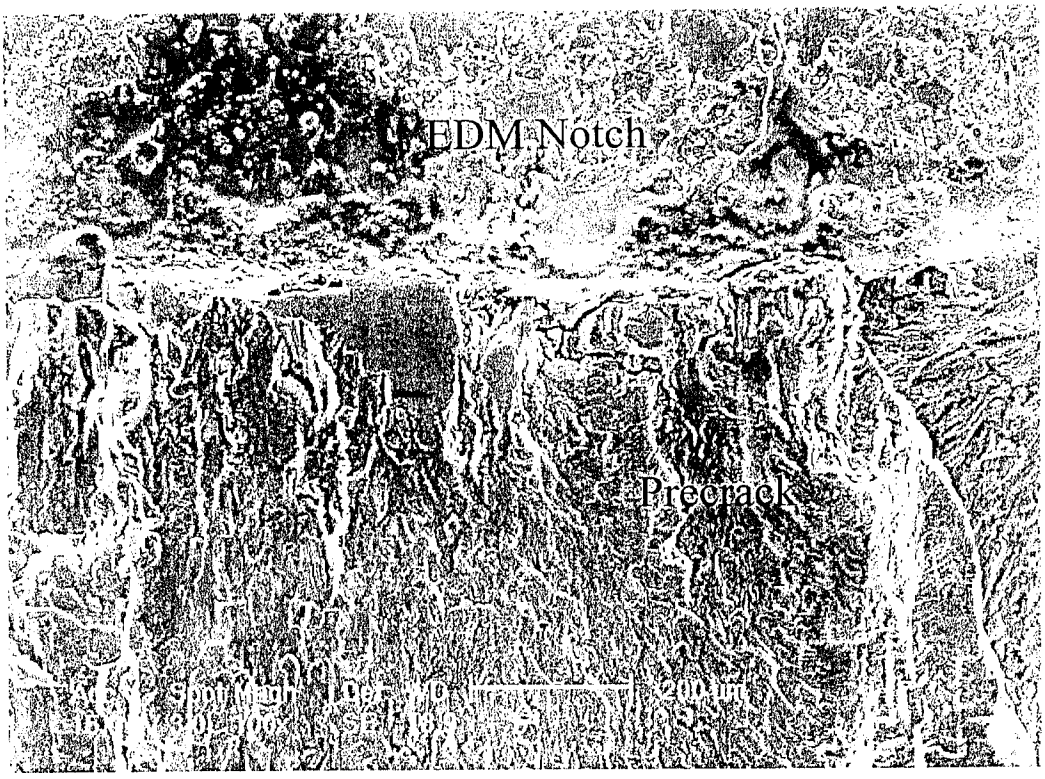

Figure 4.2: SEM micrograph of the end of the EDM notch and the beginning of the precrack.

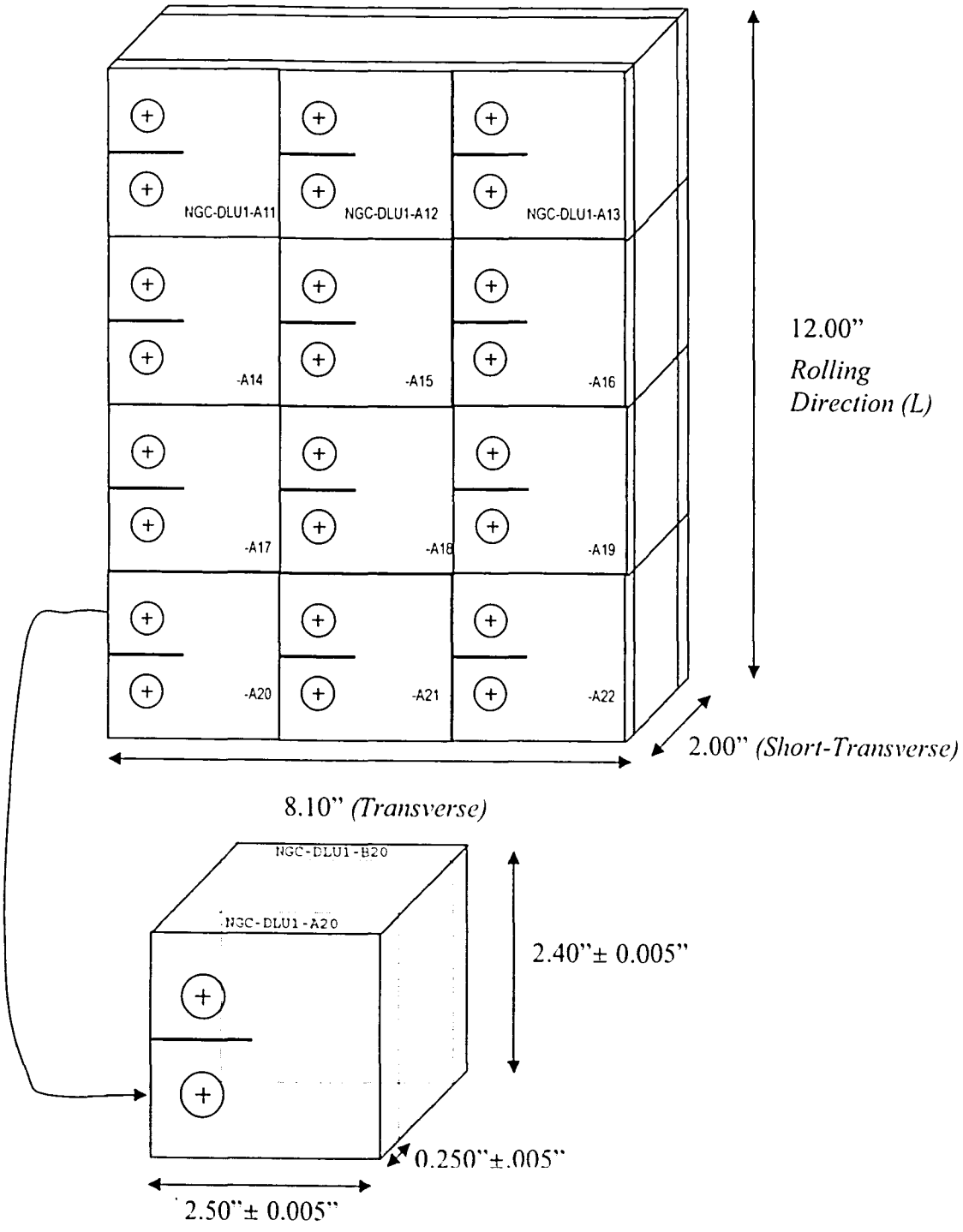

Figure 4.3: Orientation of specimen location with respect to original plate.

4.4 Specimen Preparation

Specimens were wet sanded by hand with 600 grit sandpaper along the projected crackfront in a motion orthogonal to the crack growth direction. The specimens were then polished with a Dremel™ tool and circular buffer pad and compound. A small amount of methanol was then applied to the specimen in order to clear the surface of any remaining debris or buffing compound with the result being a mirror-like shine on the specimen surface. Lastly, the specimen was cleaned with dry, compressed air in order to remove any moisture that would otherwise contribute to greater than expected crack growth rates[28].

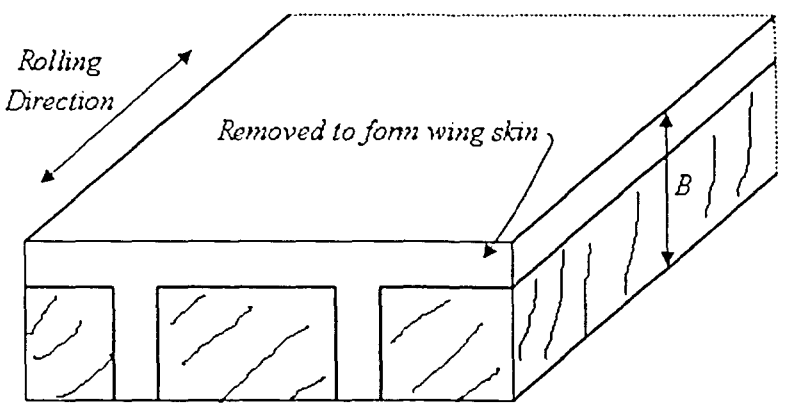

Figure 4.4: Specimen orientation reflecting wing surfaces. Specimens are fabricated from material near the surface.

4.5 Testing Equipment

Specimens were tested on either one of two frames, a 10 or 20 kip MTS[a] servohydraulic test frame at laboratory temperature and pressure. Each testing frame consisted of a closed-loop servohydraulic system including frame, linear actuator, axial load cell, and FTA[b] data-acquisition interface. This interface is an integrative package designed to work with any closed loop servohydraulic mechanical test system that is suitably configured for fatigue crack growth (FCGR) testing. Load control was estimated to be better than ±0.1 percent of target load for constant-amplitude loading and better than ±1 percent for variable-amplitude. Such high precision was obtained though the use of a damage parameter Γ concept[29] which is defined through:

$$\Gamma = \sum_{i}^{n} = \frac{(P_{i,act})^2}{(P_{i,tar})^2} = \sum \frac{(actual\ loads)^2}{(target\ loads)^2} \tag{3.3}$$

This parameter essentially sums the cumulative error between the actual and target loads. A damage parameter greater than one indicates that, on average, the target loads are being exceeded. Likewise, a damage parameter less than one indicates that the actual loads, in an average sense, are less than the target loads. The reader is referred to [29] for more details on this approach of waveform generation. The FTA software *FTA FCGR Testing* provides waveform signals to the servohydraulic machine via its internal function generator and is capable of operating in either the

[a] MTS Systems Corporation, Eden Prairie, MN 55344
[b] Fracture Technology Associates, Bethlehem, PA 18020

load or stress-intensity-factor K mode of control. Fatigue-rated clevises were used to pin-load the CT specimens and to ensure uniaxial tension-tension loading. This minimizes the moment that could be applied to the specimen as the crack propagates. Once the specimen was mounted, the parallelism of the grips pins was measured by means of a micrometer and ensured to be within 0.0254 mm (0.001 in.). A solid-state relay was implemented in order that reversing DCPD could be employed which has as a benefit the mitigation of thermally induced EMF.

In the absence of a current reversal there would be a presence of thermally induced EMF – induced when there are temperature differences at junctions of dissimilar metals. For a direct-current-potential-drop (DCPD) system, therefore, thermal EMF would be induced at the measurement junctions. These signals would be in addition to those due to the electrical field through the sample. This would, therefore, degrade both system stability and accuracy. J. K. Donald[23] suggests that compensation for thermally induced voltages is perhaps the most important consideration in the variability of crack length measurement. Minimizing the number of connections as well as establishing good control of test environment, clearly, will reduce variability in measurement. In this study, a reversing direct-current-potential-drop (DCPD) system was used to monitor crack growth. In addition, with reversing DCPD, measurements are taken at each current polarity and the corrected electrical potential drop is equal to one-half of the difference of the measured potential readings. This has as direct benefit a doubling of the potential difference for an equivalent magnitude of current input.

Each frame was equipped with an MTS TestStar II or TestStar IIs micro-controller which would send appropriate command to the servovalve based on the error between command and feedback. Analog to digital conversion was accomplished by means of a Keithley Instruments[a] ADwin-Gold real time control and data acquisition system, with 16-bit resolution for analog input and output and with time-dependent processes to run independent of the PC operating system. Function generation, data acquisition, as well as data processing required for crack length determination, and *K*-control are performed within the environment of the ADwin-Gold unit. A PC was used as an interface for the user as well as for final data storage.

Because of the high thermal-sensitivity of resistivity for aluminum, temperature was maintained at 295.37 °K ± 1°K. This is critical for the testing of aluminum, for as J. K. Donald[23] shows, a 3 °K change in an aluminum alloy can result in a 1% change in the resistivity of the material.

To compensate for these effects the measured potential difference is normalized by dividing this voltage by the voltage at some a remote location on the specimen. If a location does not exist that would be satisfactorily remote from the perturbed electric field passing around the crack, then the reference voltage must be measured on a reference specimen of the same material. For the CT specimen, due to its compact size, no such remote location exists. For this study, therefore, a reference specimen was connected in series with the active specimen with its current and potential drop spacings identically configured. The ratio of active voltage to

[a] Keithley Instruments, Inc. Cleveland, Ohio 44139

reference voltage is capable of accounting for changes in applied current, specimen temperature, as well as all material variability and some instrumental variations, e.g. stability of amplifier gain or current supply. The efficacy of this normalization approach has been empirically demonstrated by Donald[23] and is made apparent in Figure 3.5. This figure displays the results of a stability test on the ACPD system of Lehigh University. For the stability test, specimens were configured according to Figure 4.1 and the potential across the EDM notches were measured.

With the use of a reference specimen, a stable measurement system was achieved. In fact, an order of magnitude improvement in system sensitivity was achieved. For the DCPD system with a working current of 10.0 amperes, the system provided an average measurement sensitivity of about 0.025 mm in crack length a per tenth of microvolt (μv) change in potential . Resolution is better than 0.00254 mm.

5. EXPLORATORY STUDY OF SPECTRUM SIMPLIFICATION

5.1 Material Characterization

In order to provide baseline crack growth data for use in numerical packages FASTRAN or AFGROW, fatigue crack growth rate experiments were conducted on 7075-T651 specimens in the LT orientation in accordance with ASTM E-647: Standard Test Method for Measurement of Fatigue Crack Growth Rates [13]. Saxena et al[30] demonstrated that both decreasing and increasing crack growth rates can be obtained from the same specimen. The procedure involves conducting fatigue tests from near-threshold to unstable final fracture. For these tests, the K-decreasing portion was done first, followed by the K-increasing segment so as to avoid any overload effects[31].

The data corresponding to two load ratios, R = 0.10 and R = 0.50 are shown in figure 5.1. The desired K and crack growth rate gradients were achieved via computer control according to:

$$K_f = K_0 e^{C(a_f - a_0)} \tag{5.1}$$

where K_f = instantaneous K level
K_o = initial K level
C = normalized K gradient defined as $\frac{dK/da}{K}$
a_f = instantaneous crack length
a_o = initial crack length

For the fatigue experiments conducted, the normalized K gradient C was set to -4 and 4 for the decreasing and increasing experiments, respectfully. This value was chosen as a compromise between test duration and reproducibility of data. The testing rate is especially critical in the decreasing load tests in that if the load shedding is too fast then the crack may be stalled due to closure effects. Irrespective of the choice for the K gradient, however, the associated fatigue crack growth rates should fall along the same $da/dN - K$ curve [31]. The testing procedure was designed with some overlap between the increasing-K and decreasing-K data to confirm data coincidence. The K-increasing test procedure was thus initiated at a K_{max} value slightly less than the maximum of the decreasing-K portion of the test. To avoid fracture of the specimen, a real-time crack growth rate limit was set to terminate each test. For the results shown in Figure 5.1 this crack growth was set to 2.54 E-6 m/cycle.

Upon completion of each K-decreasing test a marker band was grown into the material that was 0.127 mm long before starting the K-increasing segment. This band facilitates post-test correction since the marker band is distinguishable from neighboring surfaces as being significantly darker. Once the experiment is completed the specimen was then fatigued to complete failure and actual measurements of crack lengths (using the marker bands as guides) were made with a microscope. A linear post test correction was then applied to mitigate the error between predicted and actual crack lengths.

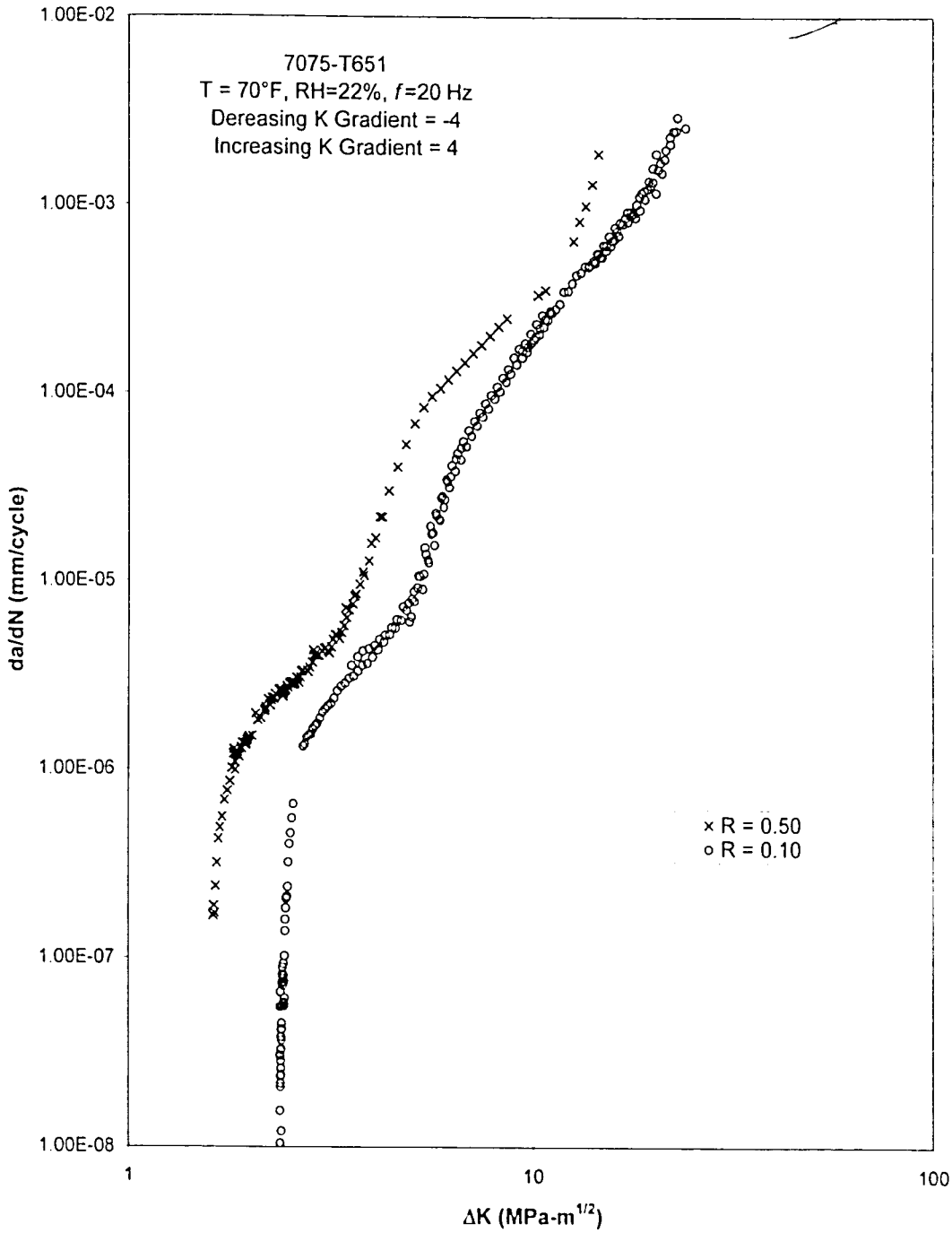

Figure 5.1: Aluminum 7075-T651 crack growth rate data for R = 0.10, 0.50.

5.2 Simulations in AFGROW

The exploratory study began with a numerical examination in AFGROW. The goal was to test the hypothesis that a VA spectrum can be replaced with an equivalent CA spectrum. These numerical comparisons would encourage and establish a basis for conducting expensive, time-consuming experiments. AFGROW was used to estimate the fatigue crack growth of a variable-amplitude spectrum as well as that of diverse constant-amplitude spectra. The CA spectra were created as modifications to the original VA spectrum by means of the Barsom RMS method as discussed in Section 1.3. Willenborg Retardation model was implemented with a shutoff overload ratio (SOLR) of 3.0, a typical value for aluminum. The generalized Willenborg model uses the shutoff overload ratio (SOLR) as a material property to control the effect of overload history on fatigue life.[32] It is a simple model that uses an effective stress intensity factor based on the size of the yielded zone in front of the crack tip. Four simulations were conducted:

1. SIPS Full Outer Wing Panel (OWP) VA spectrum with compression, Willenborg Retardation, OLR = 3.0
2. SIPS Full OWP VA – No Compression – Willenborg Retardation, OLR = 3.0
3. SIPS OWP Reduced – No Compression – Willenborg Retardation, OLR = 3.0
4. Constant Amplitude Reduction – Modified Barsom RMS Method

There were exactly 2640 load cycles in the original SIPS Full OWP VA spectrum, a spectrum provided by Northrop Grumman for use in the Structural Integrity

Prognosis Systems (SIPS) program. Each flight was either 7, 8, or 9 cycles not inclusive of the ground cycle in the compressive Ground-Air-Ground (GAG) spectrum with a mean number of cycles per flight of 8.32. Each flight was composed of two basic types of cycles: i) high P_{max}, low R, and ii) low P_{max}, high R. It has been consistently argued that for a given spectrum that it is the first type (as number one above) that is the dominant mode of damage and that, for simplistic spectra, the non-damaging cycles can be eliminated – thus simplifying the spectrum. For the present case, the spectrum was reduced to 1620 load cycles or a reduction of 38.64%. If these cycles truly contribute minimal overall damage then we expect that simulations of the SIPS Full OWP VA – No Compression spectrum and the SIPS OWP Reduced spectrum to yield nearly equivalent crack growth responses. Figure 5.2 shows that this expectation is verified numerically. As calculated by AFGROW the fatigue life for SIPS Full OWP VA – No Compression was 108,359 cycles. Therefore, according to the percent reduction in the reduced spectrum one would expect that 108,359 × 0.6136 = 66,489 cycles for the lifetime of the reduced spectrum. The actual number of cycles to failure for SIPS OWP Reduced was 66,435. Percent error between these predictions is 0.081%. Simulations suggest, therefore, that some cycles do not contribute to damage evolution. This is apparent in Figure 5.2.

Clearly there are different effective crack driving forces that govern crack growth during simple, constant-amplitude loading, when load interaction effects are absent, and between variable-amplitude loading histories. In the simplest case of a regular

sinusoidal waveform, superimposed with a peak overload, the crack growth is retarded through the overload plastic zone before resuming of the original crack growth rate[33].

Wei and Shih [33] have shown that this delay phenomenon is exceedingly complex and depends strongly on all of the loading variables: stress intensity range, stress ratio, number of cycles at high load, time at high load, etc. As yet, no consistent phenomenological model for estimating fatigue crack growth under variable-amplitude loading has been developed.

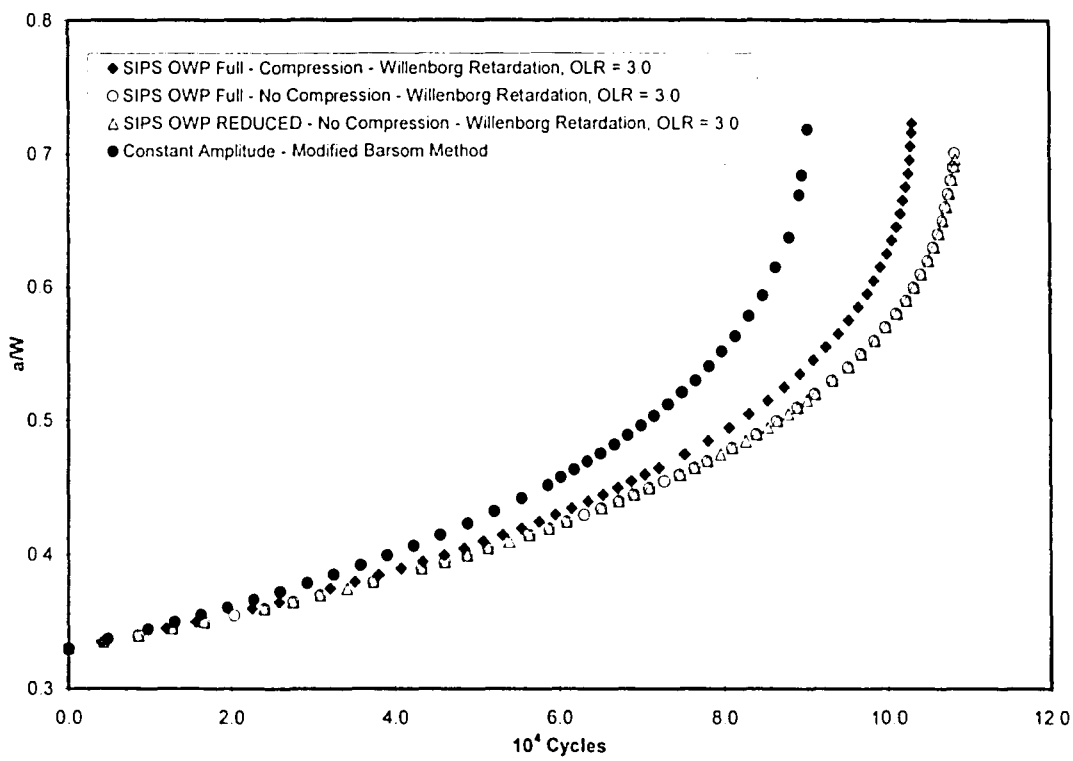

Figure 5.2: AFGROW simulations of crack growth behavior for 7075-T651with K_{max} = 16.48 MPa – $m^{1/2}$ as a justification for experimental reduction to the VA spectrum.

5.3 Reduction to Constant-Amplitude

With justification for an attempt at VA reduction having been achieved through simulation the next phase was to conduct fatigue experiments and compare the fatigue responses of the original VA and the reduced CA spectra. Fatigue experiments were conducted over a range of initial K_{max} levels to validate that this method of reduction is rational over a range of crack growth grate response. Experiments were thus conducted at three independent sets of initial K_{max}, namely 9.12, 10.99, and 16.48 MPa $\sqrt{m}$ (8.30, 10.0, and 15.0 ksi $\sqrt{in.}$). For each set of experiments corresponding to a particular value of initial K_{max} the original VA spectrum was first tested to establish the crack growth response associated with this original, unaltered spectrum. In most cases, a second VA test was conducted to ensure repeatability of testing.

Once the VA crack growth response was established the immediate endeavor was to develop a CA spectrum along the lines of the RMS approach proposed by J.M. Barsom as discussed in Section 1.3. To recapitulate, this entails removing the small load excursions from the spectrum and then independently calculating RMS values for both peak and valley loads. These *rms* values are then equated to the maximum and minimum CA spectrum loads, respectfully. For the variable-amplitude spectrum used throughout the testing, the load ratio was found to be 0.287 from this modified Barsom approach. Experiments demonstrated that this method failed to approximate the VA fatigue with a replacement CA spectrum. The Barsom method, therefore, was

modified in the following manner: the maximum loads were maintained at the RMS value, but the minimum loads were scaled by a constant. Since the maximum loads were maintained this thus had the effect of changing the load ratio. Generally, the Barsom approach resulted in fatigue that was too conservative and so the load ratio had to be decreased to promote a faster crack growth response. An additional CA experiment was conducted at this new load ratio and if this second fatigue response was not sufficiently close to the original VA response then the load ratio was adjusted again, indefinitely, until there was total convergence. The various spectra associated with this reduction are provided in Figs. 5.3-5.5.

Figs. 5.6-5.8 show that the VA spectrum can be replaced with a CA equivalent. Experiments were conducted at three values of initial K_{max}: 9.12, 10.99, and 16.48 MPa-m$^{1/2}$ with optimal load ratios R_{cq} of 0.24, 0.10, and 0.12, respectfully. Figure 5.9 is a comparison of the data of figure 5.7 with AFGROW which shows its inadequacy in predicting crack growth. Observe that the two VA experiments are highly coincident, yet the AFGROW prediction is overly conservative. In addition, this is not a function of poor baseline da/dN-ΔK data inherent to the AFGROW program since the 7075-T651 fatigue data from AFGROW was graphically compared to the data as obtained in this study and graphed in Figure 5.1 and was shown to be in agreement. Figures 5.6 and 5.9 show the inadequacy of AGROW in precting fatigue crack growth.

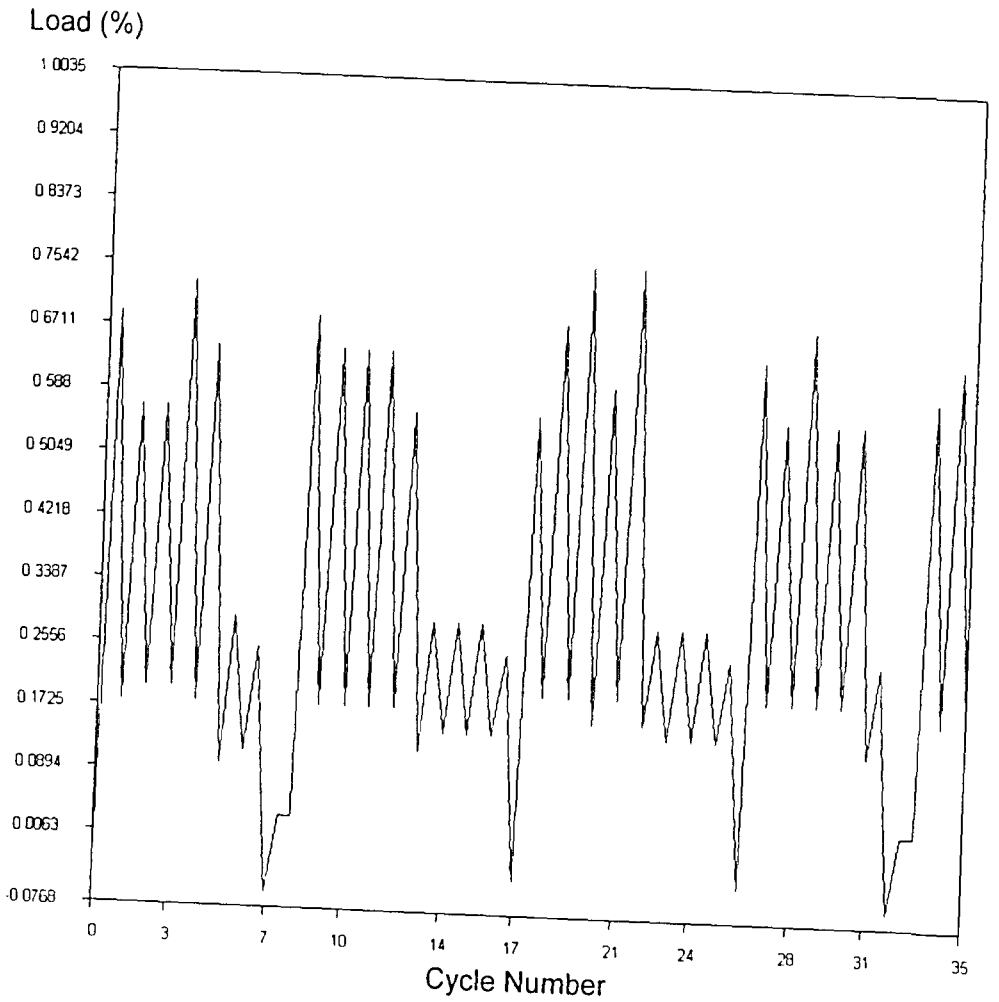

Figure 5.3: A sample from SIPS Outer Wing Panel (OWP) Full VA spectrum, a screenshot from AFGROW.

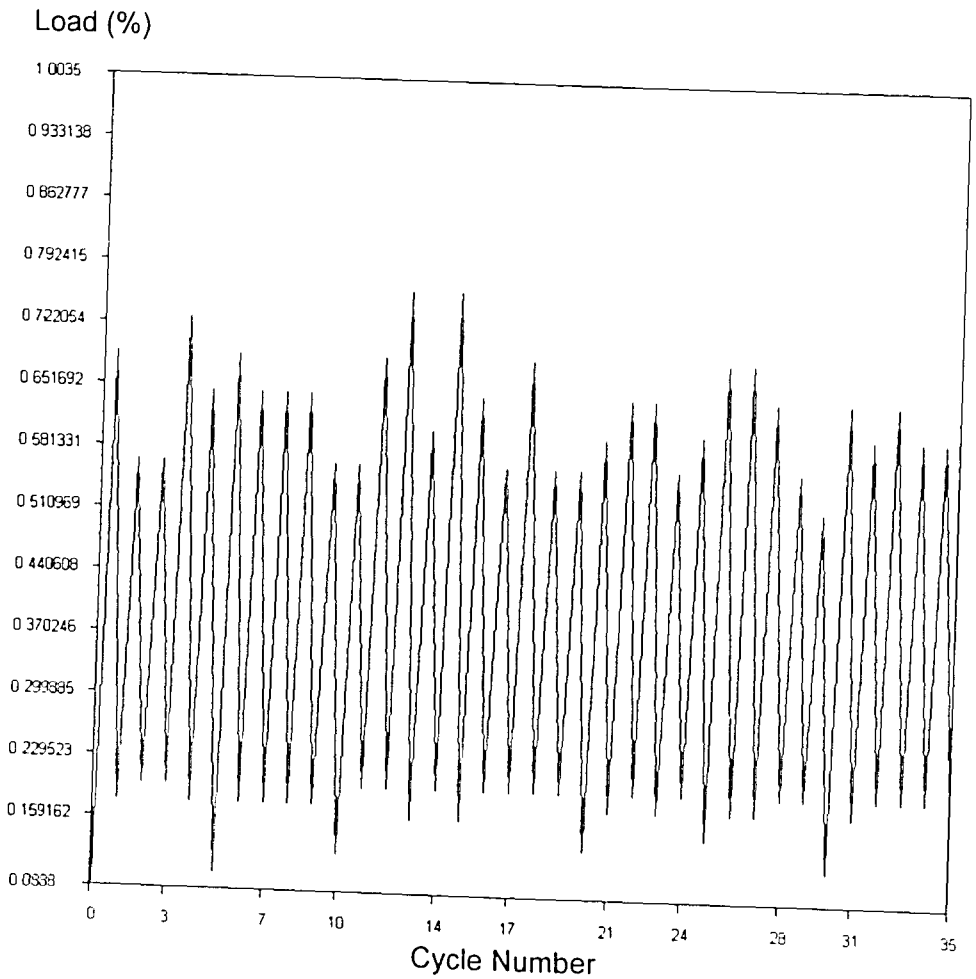

Figure 5.4: Sample segment from the SIPS Outer Wing Panel (OWP) Reduced VA spectrum with small load fluctuations removed, a screenshot from AFGROW.

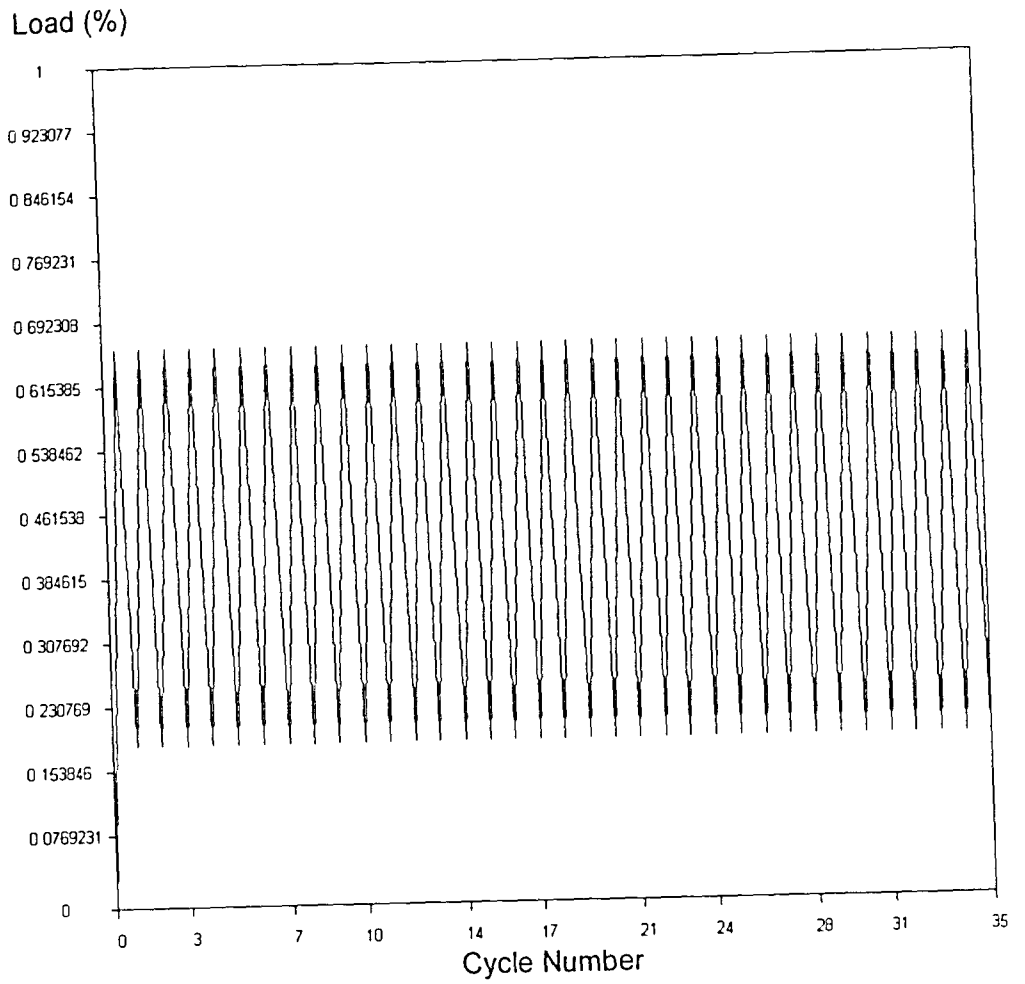

Figure 5.5: Sample segment from the CA spectrum derived from the Modified Barsom Method, $R = 0.287$, a screenshot from AFGROW.

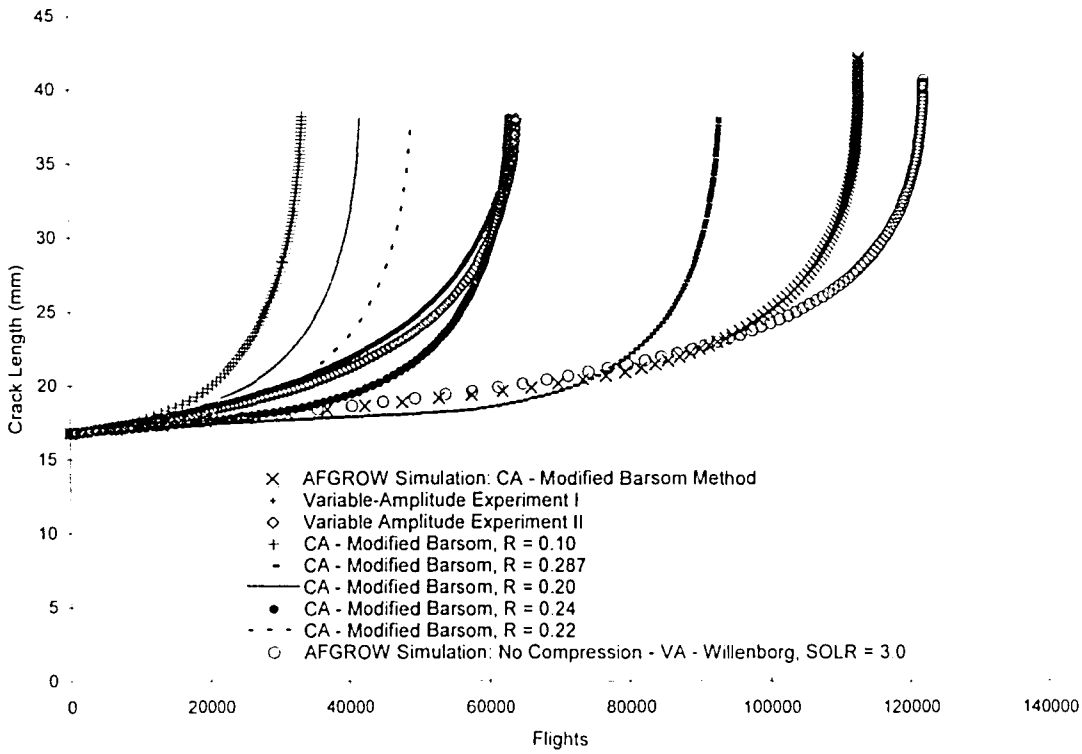

Figure 5.6: Collapse of constant-amplitude fatigue data onto experimental variable-amplitude curve for initial K_{max} = 9.12 MPa – $m^{1/2}$, R_{eq} = 0.24.

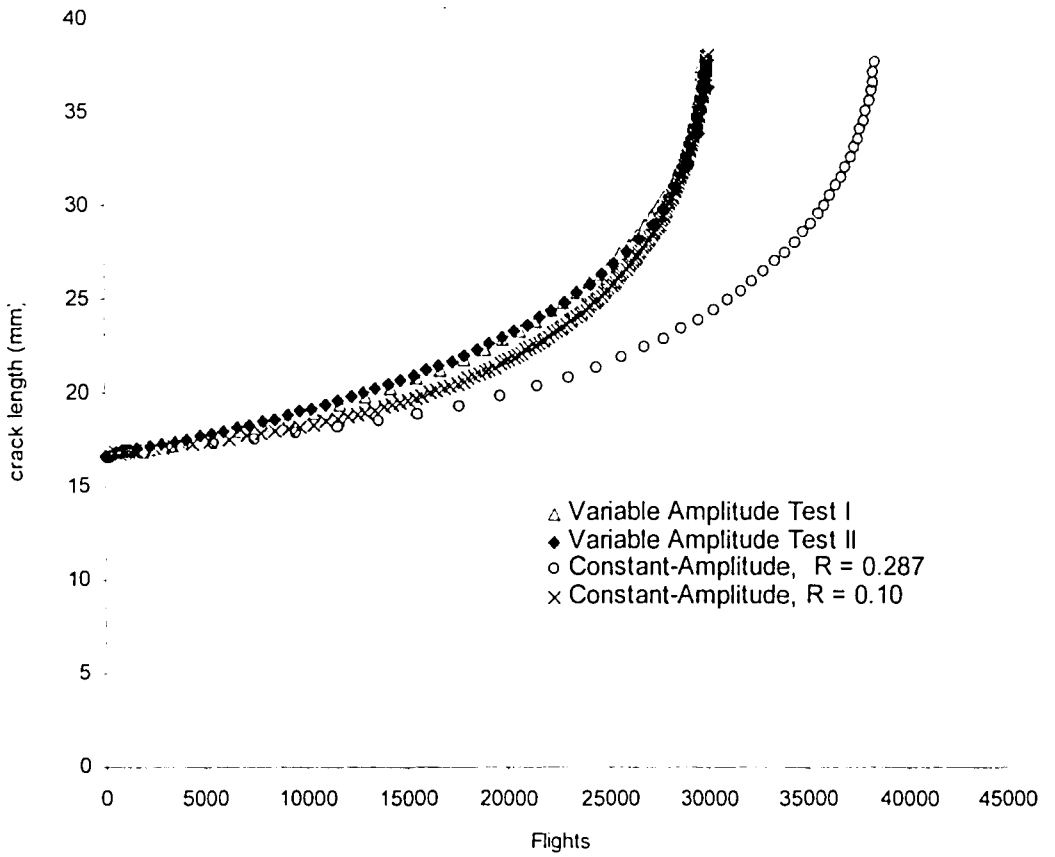

Figure 5.7: Collapse of constant-amplitude fatigue data onto experimental variable-amplitude curve for initial K_{max} = 10.99 MPa – $m^{1/2}$, R_{eq}= 0.10.

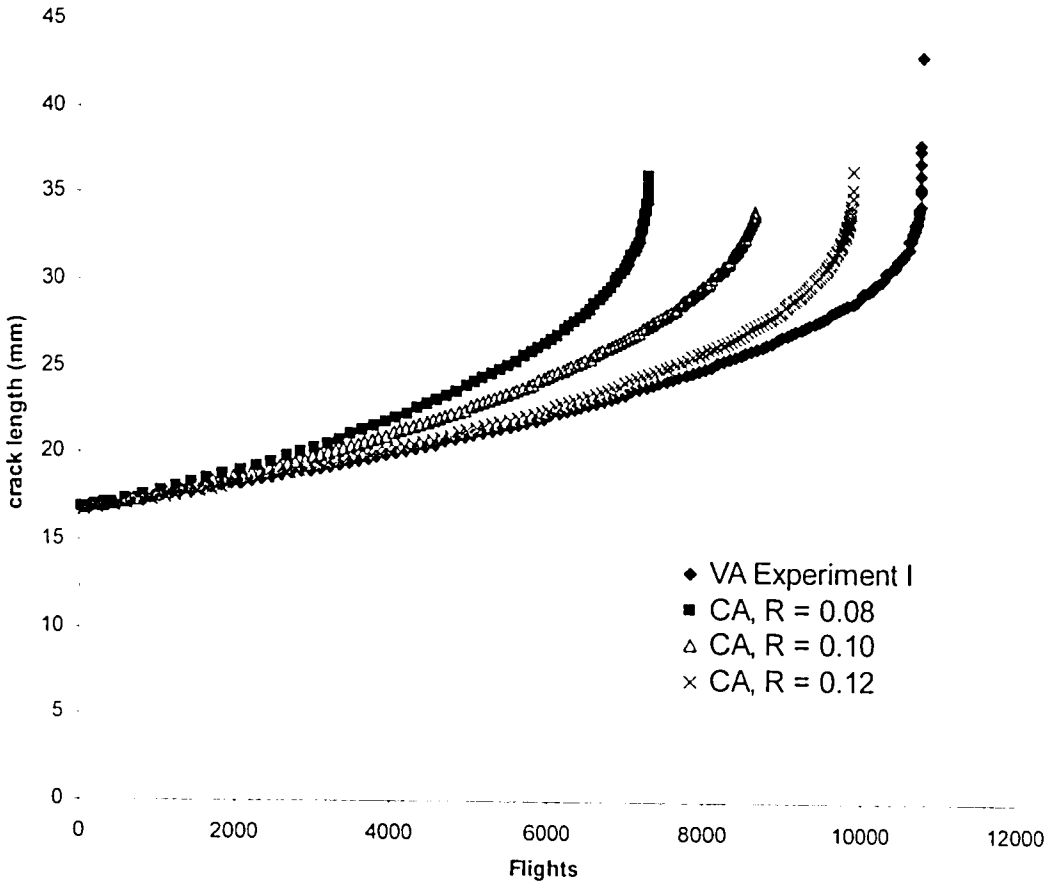

Figure 5.8: Collapse of constant-amplitude fatigue data onto experimental variable-amplitude curve for initial K_{max} = 16.48 MPa – $m^{1/2}$, R_{eq}= 0.12.

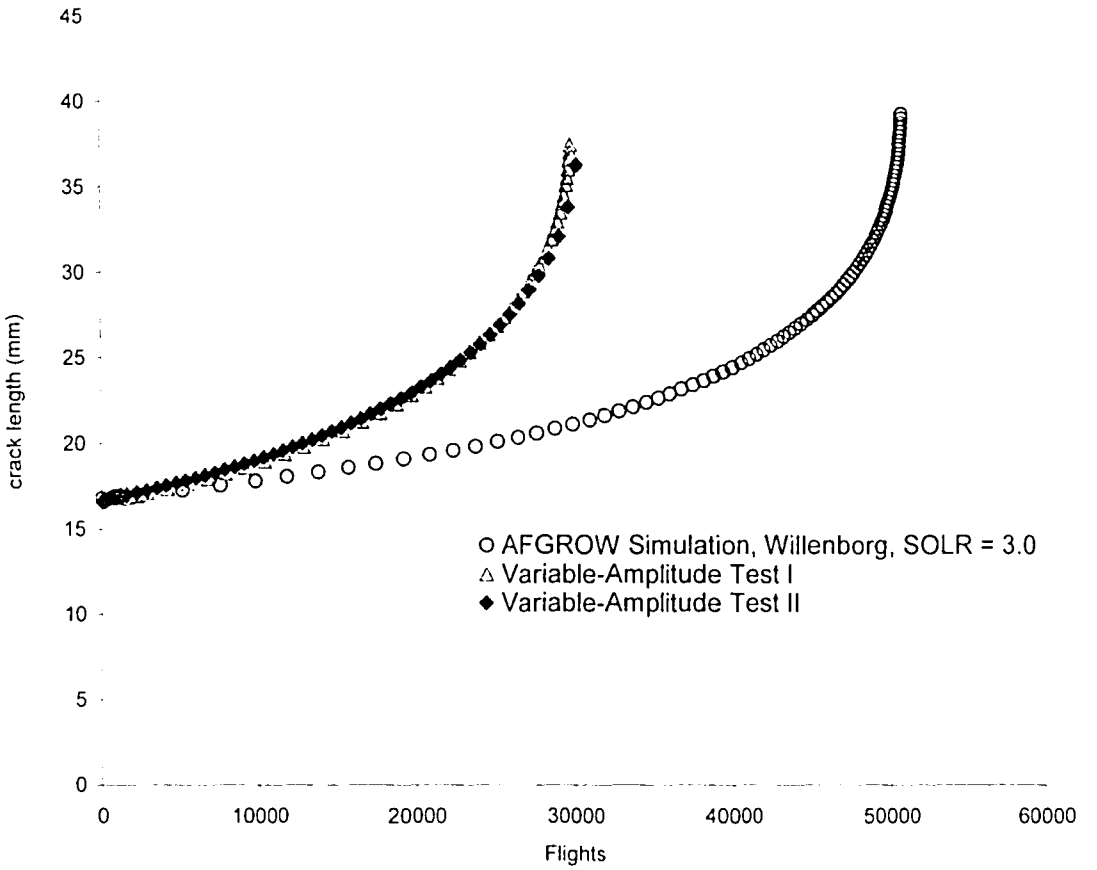

Figure 5.9: Comparison of AFGROW simulation to experiment.

5.4 Prediction of Optimal Load Ratio

Using the empirically obtained (K_{max}, R_{eq}) pairs, an attempt was made to predict the optimal load ratio for a new value of K_{max}. Accordingly, a curve was drawn through the available data points, and for the arbitrarily chosen K_{max} value of 9.89 MPa-$m^{1/2}$ the desired load ratio R_{eq} was estimated as 0.1744. A variable-amplitude experiment was conducted as well as the constant-amplitude test at this derived load. Theoretically, the fatigue responses should be coincident. Figure 5.10 indicates that this is nearly so, with a ratio of VA life: CA life = 1.15. This finding provides support for the RMS approach to variable-amplitude reduction.

5.5 Environmental Considerations

It was clear that the data suggested a strong influence of atmospheric moisture content. This is obvious when one compares the results when initial K_{max} was set to 10.99, and 16.48 MPa-$m^{1/2}$ with optimal load ratios R_{eq} 0.10 and 0.12, respectfully. for There is no physical basis that can predict, for the same environment, that the optimal load ratios required for equivalence should increase with increasing initial K_{max}.

Moreover, variations in lab environment no doubt affected the reliability of the data, since, as was previously mentioned, the resistivity of aluminum is highly

susceptible to changes in temperature, and as crack growth rates are affected by moisture content at the crack-tip. It is thus the variance in environment that is held accountable for the loss of repeatability [23].

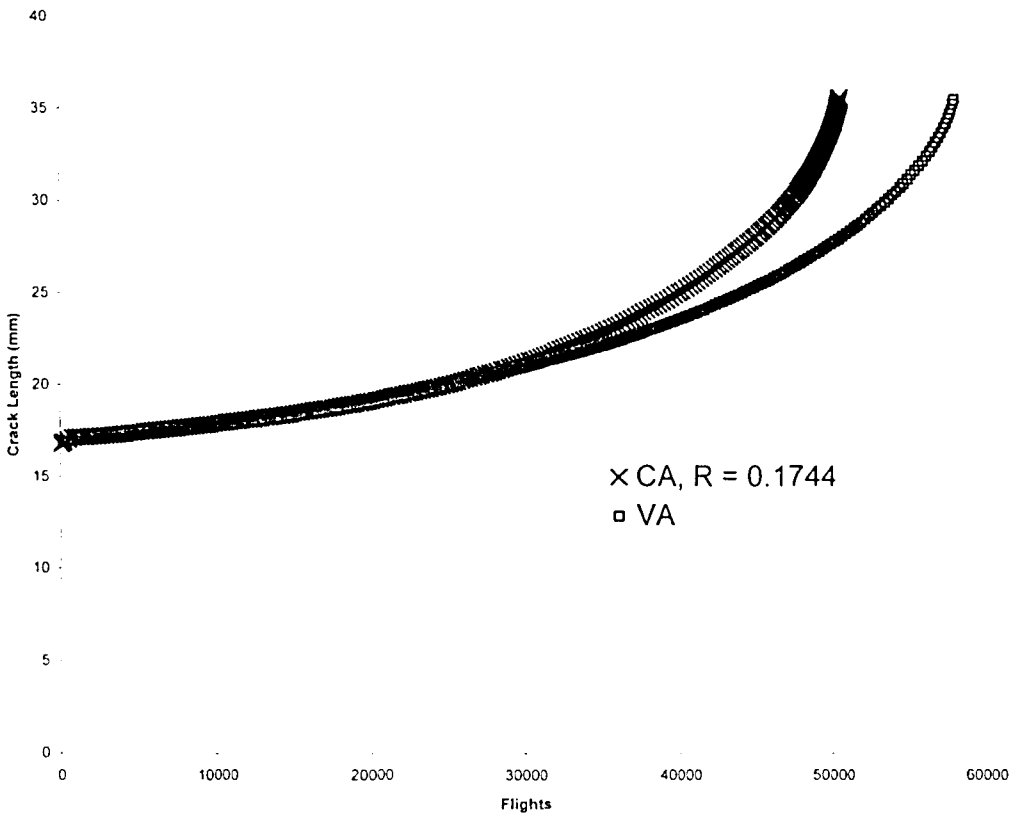

Figure 5.10: Experimental fatigue comparison of the constant-amplitude spectrum to the original variable-amplitude spectrum in which the optimal load ratio R_{eq} was predicted by the empirical relationship for an initial Kmax of 9.89 MPa – $m^{1/2}$.

The most noted peculiarity is that the optimal load ratio R_{eq} *increased* as the initial K_{max} was increased from 10.99 to 16.48 MPa-$m^{1/2}$. The cause for this contradiction is attributed to changes in humidity since it was later established that

fluctuations as great as ± 10% in relative humidity were observed whereas the temperature fluctuation was within ± 1%. It was clear, however, that both temperature and humidity needed to be well maintained.

Accordingly, an additional series of experiments were conducted in which the testing environment, specifically both temperature and relative humidity, was rigorously maintained at the specimen. These conditions were regulated by flowing pre-purified gaseous nitrogen through a chilled water bath which was maintained at 32.1 °F and then reheated to 72 °F to achieve a controlled relative humidity of 22 percent. Since the temperature at each phase of the system can be easily maintained by means of an appropriate heater or chiller coupled with a thermoregulator, a favorable means of obtaining repeatability in testing conditions is established. A schematic of this environmental control system is shown in Figure 5.11. It is noted that the calculation above is confirmed[a] with reference to a standard psychometric chart[34]. Accordingly, experiments were conducted with the newfound control of testing environment on four unique spectra:

A. VA Full SIPS (Figure 5.3)

B. CA Reduced as produced by the modified Barsom method, R = 0.287 (Figure 5.5)

C. VA with minimum loads = *rms* of peaks, minimum loads = unchanged

[a] For saturated air, the dry-bulb, wet-bulb, and dew-point temperatures can be obtained from the psychometric chart by drawing a horizontal line from any point on a line of constant relative humidity. The temperature at the intersection point is the dew-point temperature.

(Figure 5.13)

D. VA with maximum loads = *rms* of peaks, maximum loads = unchanged

(Figure 5.14)

5.6 Results and Discussion.

The motivation for these experiments was to deduce which cycles are the dominant driving force for damage accumulation. The results of this series of tests are shown in Figure 5.12. As an observation, it is clear that the large load excursions are dominant in the fatigue process. It is also clear that the small load excursions do contribute to damage accumulation.

A numerical finite difference code was written to differentiate the data in Figure 5.12 so that the relationship between *da/df* and crack length *a* could be observed. This relationship is provided in Figure 5.15. The crack growth rates for two cases are highly congruent well the full variable-amplitude SIPS spectrum and the variable-amplitude spectrum generated when the minimum loads are set equal to the *rms* of all the minimum loads. The crack growth rates for the spectrum with the maximum loads set equivalent to the *rms* of all the maximum loads is vertically shifted indicating greater crack growth rates across the full range of *a/W*. This makes sense when one compares Figure 5.13 to Figure 5.14 and observes that the mean load ratio is much greater for the case when the maximum loads are set equal to their *rms* value than when the minimum loads are set equal to their *rms* value.

In addition, some delay is expected in variable-amplitude fatigue. Here delay refers to the period of abnormally low rate, or zero rate, of fatigue crack growth between a decrease in load level following an overload. Delay is usually measured in the number of cycles required for the original rate of crack growth to resume. Moreover, much less delay is anticipated for the spectrum shown in Figure 5.14 than for that shown in Figure 5.13. This because delay will occur when a spike overload is introduced and the crack must grow through the induced plastic zone before crack growth can resume. The crack growth rate corresponding to the modified Barsom method spectrum is the lowest of the four spectra tested and was unaffected by delay since it was a constant-amplitude spectrum (see Fig. 5.5). Since the modified Barsom method entails setting both the maximum and minimum loads equal to their respective *rms* values it is logical that this spectrum would have the slowest crack growth since the spectrum is effectively being "averaged" at both ends and the effective load ratio is decreased.

Wei and Shih[35] conducted a systematic examination of the effects of various loading variables on delay. They showed that delay increases with the number of high load excursions, reaches a maximum, then decreases. This relationship is shown in Figure 5.16 [35]. This in agreement with the results obtained from the experiments of this thesis. By setting the minimum loads equivalent to their *rms* value (Fig. 5.13) the effect was to increase the delay. Delay effects were annihilated when the maximum loads were set equivalent to their respective *rms* value (Fig. 5.14). This is in agreement with Figure 5.17 which shows that for fixed values of K_1 and K_2 that delay

decreases with increasing R_2 and also with increasing values of K_{2max}/K_{1max} [35]. Moreover, when K_{2max} is equal to K_{1max} then no delay will be experienced.

It is also noted that the fatigue crack growth rate data in Figure 5.15 demonstrate starting transient effects, that is the crack growth rate at the onset of fatigue cracking has not reached steady-state and may be discontinuous. In addition, at the later stages of the fatigue tests the cracks are exceedingly long (on the order of $a/W = 0.7$) and so out of plane cracking is expected. This accounts for the high variability in fatigue cracking at the later stages of the experiments.

It is reiterated, however, that the VA Full SIPS and the VA RMS Min have crack growth rates are highly coincident over the full range of a/W. This suggests that modifying a variable-amplitude spectrum in such a way will not alter its fatigue crack growth response, and so is therefore at least a first step towards even greater spectrum reduction.

For the same experiments from Figure 5.15, Figure 5.18 plots the relationship of da/df versus flight where da/df is the rate of crack growth per flight. The interesting aspect of this plot is that the crack growth rate demonstrates an obvious periodicity with flight. It is not believed that this periodicity reflects any short-term fluctuation in testing waveform signal since the period is on the order of 2000-3000 flights which corresponds to a period in time of approximately 15-20 minutes in testing time. It is reasoned that this periodicity is therefore also not a function of random fluctuations in environment since it is not realistic that such fluctuations would be so periodic. It is suggested that this periodicity reflects the delay experienced by the material within

each pass of the spectrum since only a few peak overloads are experienced with each spectrum pass. The modified Barsom constant-amplitude experiment did not exhibit periodic relationship in *da/df* versus *flight*.

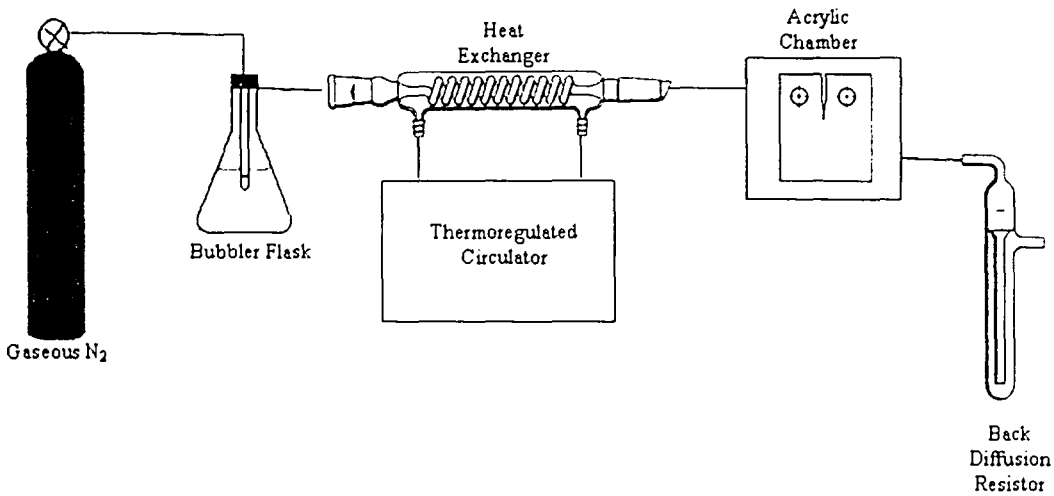

5.11: System for control of environment.

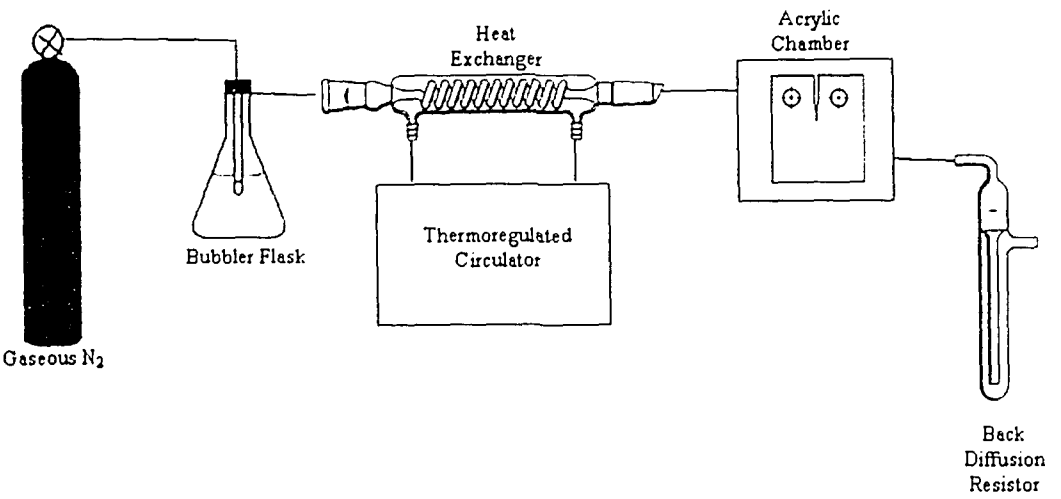

5.11: System for control of environment.

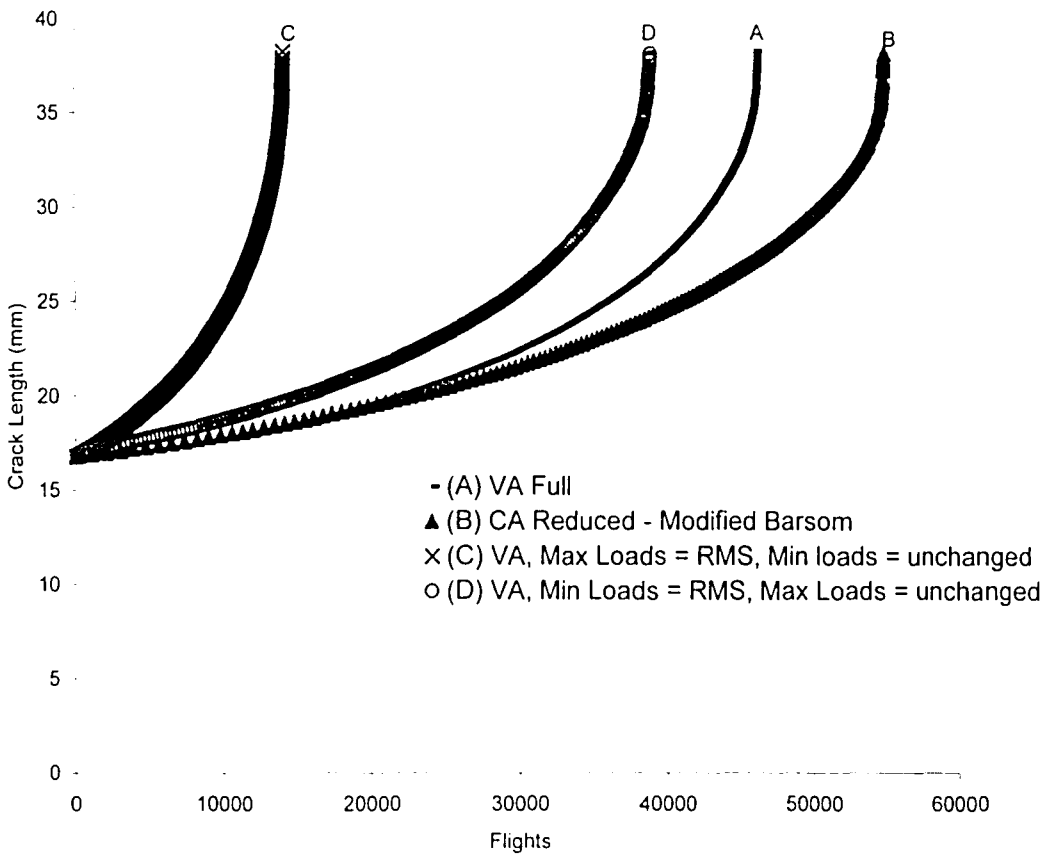

Figure 5.12: Demonstration of the relative significance of the max and min loads in variable-amplitude fatigue. Data corresponds to an initial K_{max} of 10.99 MPa – $m^{1/2}$.

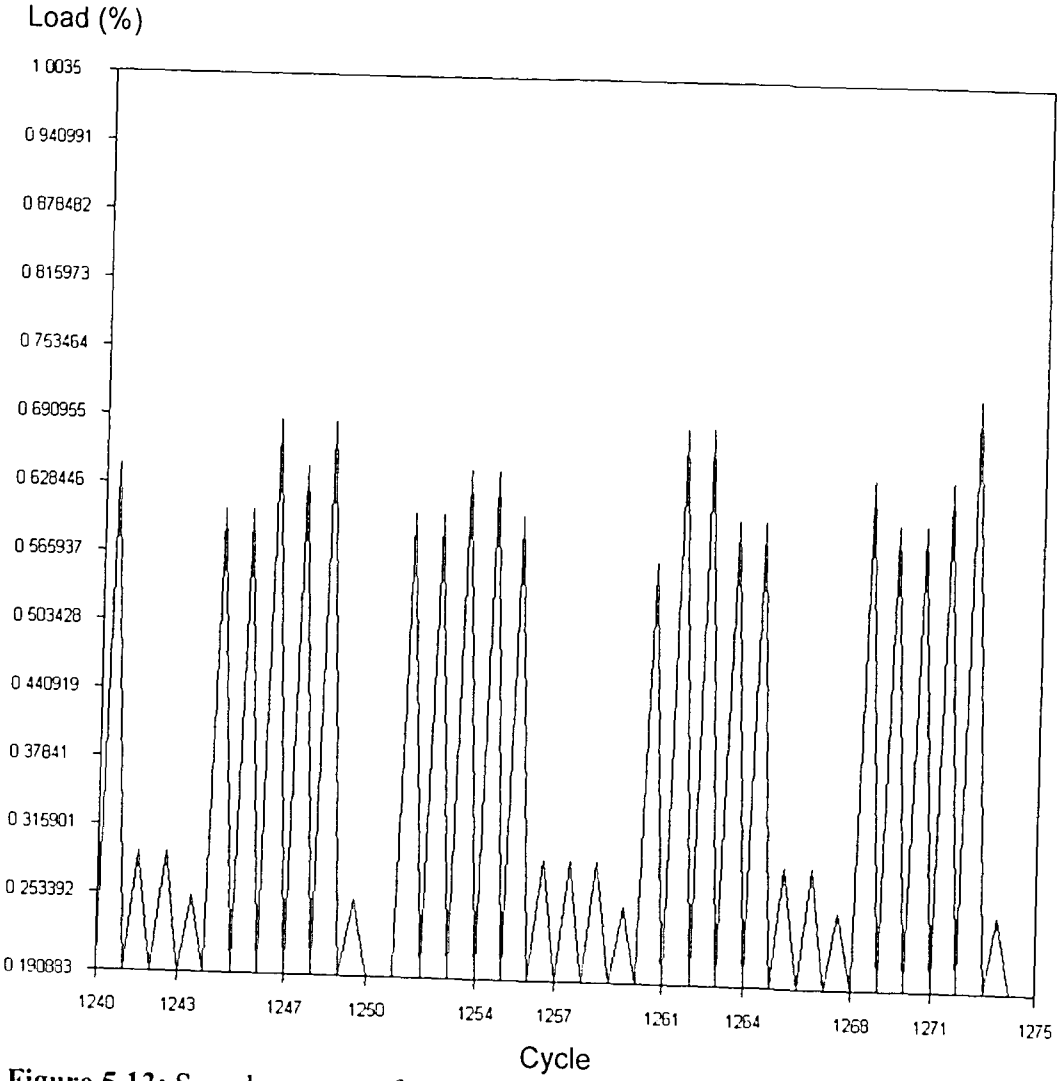

Figure 5.13: Sample segment from VA spectrum with minimum loads equal to the *rms* of the peaks and the maximum loads unchanged, a screenshot from AFGROW.

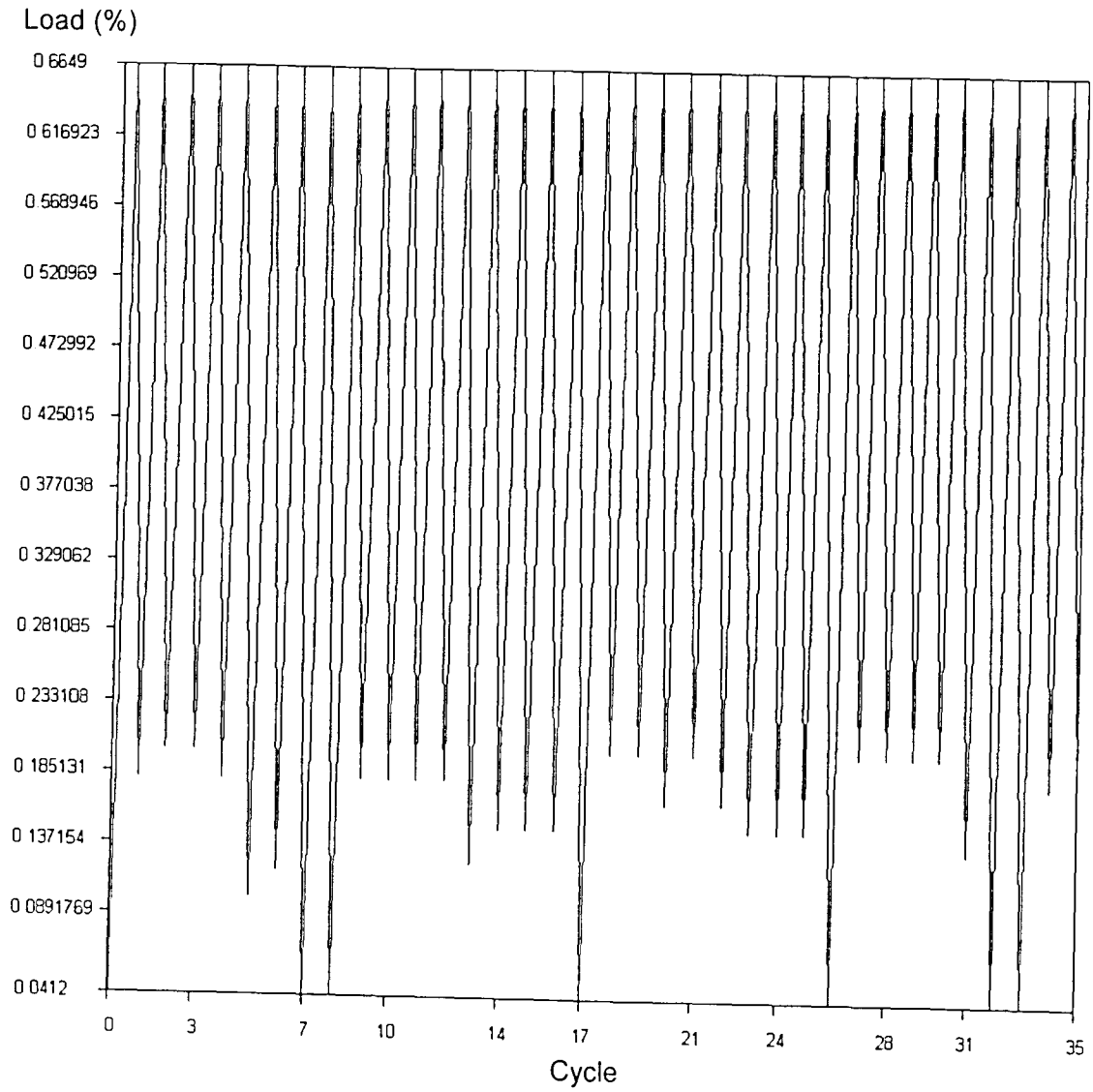

Figure 5.14: Sample segment from VA spectrum with maximum loads equal to the rms of the peaks and the minimum loads unchanged, a screenshot from AFGROW.

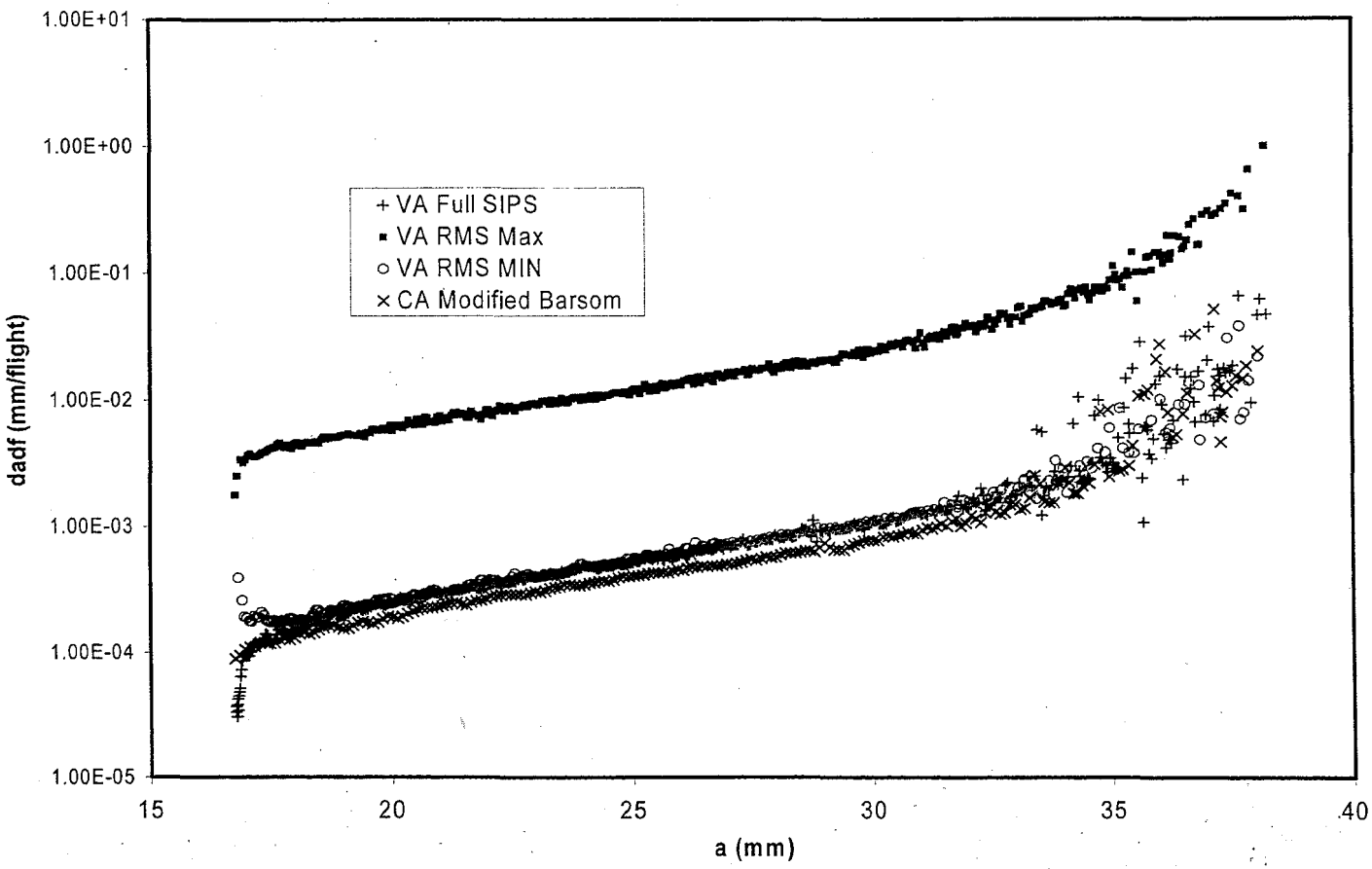

Figure 5.15: Rate of change of crack length with flight versus crack length.

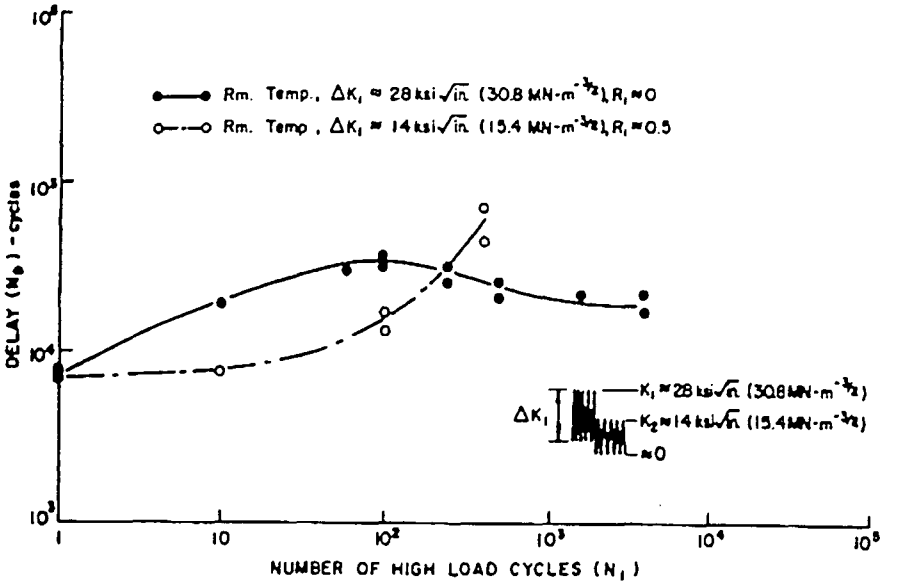

Figure 5.16: Effect of multiple high load excursions on delay [35].

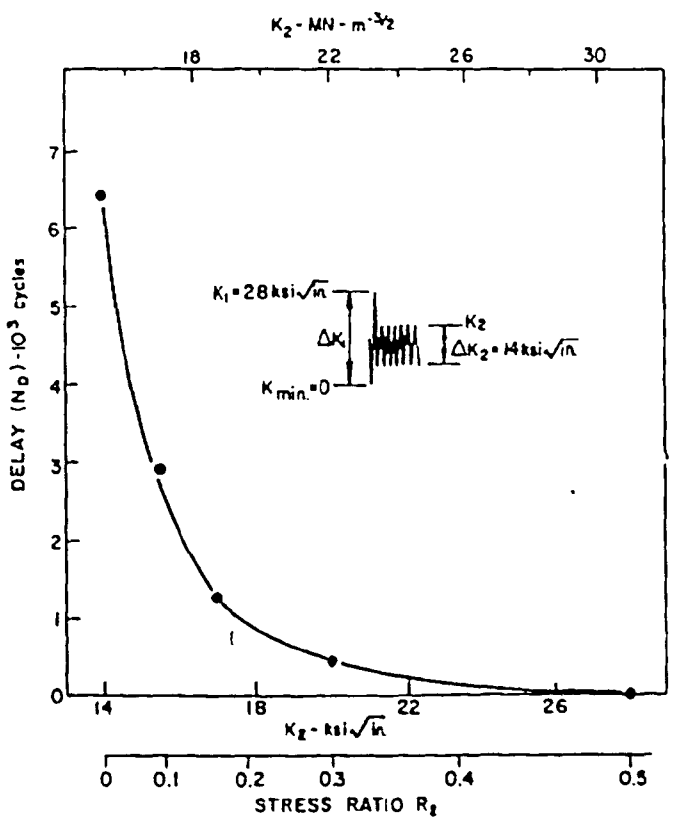

Figure 5.17: Effect of R_2 or K_2 on delay [35].

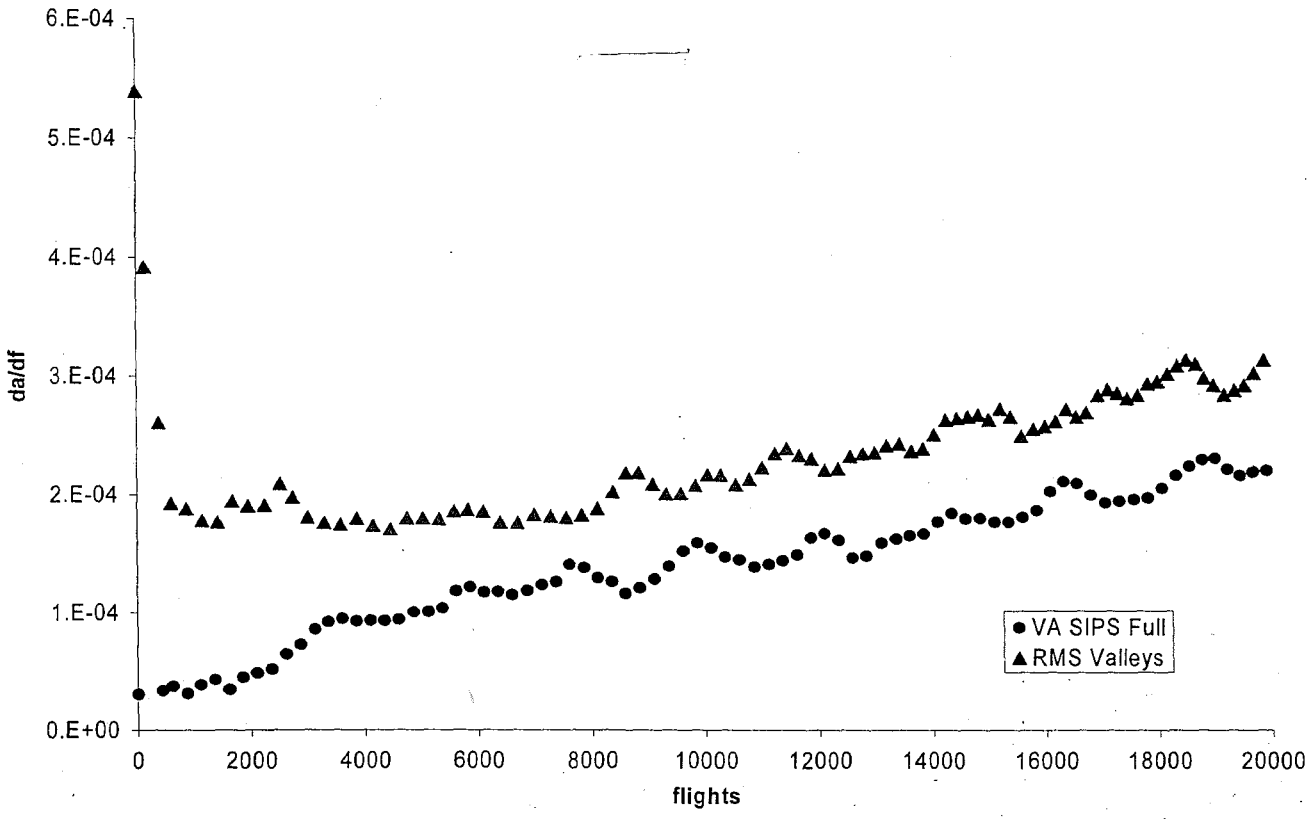

Figure 5.18: Rate of change in crack length per flight versus flight which is characterized by an obvious periodicity.

6. CONCLUSIONS AND FUTURE WORK

6.1 Conclusions

The overall goal was spectrum simplification to facilitate real-time management of engineered systems, e.g., fleet of aircraft. The explicit goal was to reduce a variable-amplitude fatigue spectrum to a spectrum in constant-amplitude go gauge the feasibility of replacing current numerically based procedures for variable-amplitude fatigue crack growth in order to facilitate probabilistic analyses. This thesis has shown that there is promise in such a reduction. Additional conclusions are discussed:

First, it is clear that fatigue damage is prevalent in the fastener holes of aircraft. Moreover, support for the Harlow-Wei model for pitting and transition to FCG has been developed since the MHWC data obtained coincide with model prediction.

Second, reversing DCPD is preferred over ACPD, since it avoids the effects of capacitive and inductive impedances which otherwise decrease measurement reliability. In addition, since aluminum develops no skin effect at reasonable operational excitation frequencies, ACPD offers no intrinsic benefit over DCPD. It is also realized that the phenomenon of skin effect is a complex solution to the wave equation. The concept that skin depth is the depth at which the current density decays to 1/e times the current density at the surface is simply untrue, despite its widespread acceptance as such.

Third, a method for replacing a generic variable-amplitude fatigue spectrum has been presented. This method calls for the VA spectrum to be replaced with a CA spectrum with its loads set equal to the *rms* value of the maximum and minimum loads. This *rms* approach to variable-amplitude reduction is promising and would prove useful; nevertheless, it is clear that any attempt to do so must be attempted with firm control of testing environment as the environment has a direct, potent influence on crack growth rates.

Fourth, analytic models which comprehensively account for crack closure, overload, and load-history effects that permit the rapid prediction of crack growth as a basis for life estimation have yet to be developed. Comparison between experiment and AFGROW predictions has consistently rebuked the efficacy of that model.

Next, the high load, low R cycles contribute greatly to damage accumulation. It is also apparent, however, that the low max load, high R cycles have been shown, indeed, to exude a modicum of influence on overall crack propagation. This is despite the fact that they were numerically demonstrated to have no influence on crack growth.

Last, it has been shown that crack growth rates under variable-amplitude fatigue reflect some form of periodicity. As discussed, this may either be a function of the deterministic nature of variable-amplitude fatigue tests themselves or else a function of the delay in crack growth encountered when the material is subjected to a peak overload.

6.2 Future Work

Accurate, mechanistic-based probability models for crack growth that permit the rapid simulation of crack growth characterization, eventually establishing a basis for life estimation have yet to be developed. This is especially true for the variable amplitude loading histories for which load interaction effects quantify a significant margin of crack development.

A new paradigm must be engendered that embodies the influence of key internal and external variables. There is a great inability, however, to invoke a joint distribution of the multiple features affecting the fatigue process[36].

Clearly, comprehension of the variable amplitude load interaction phenomenon is far from complete. In order to simplify a variable-amplitude spectrum, one approach to reduce the spectrum to constant-amplitude has been shown to have promise. This work has merit and should be continued.

Specifically, the model should be evaluated on additional spectra as well as across a greater range of initial load levels. Since there is a high degree of variation between individual variable-amplitude spectra additional tests must be conducted on other spectra to determine how general the approach is to variable-amplitude spectrum reduction. The hypothesis must also be tested against tension-compression variable-amplitude spectra but this should be considered only after a constant-amplitude equivalent is achieved for the tension-tension case since the latter is considered to be an easier problem.

Lastly, it is suggested that a novel approach towards a phenomenological understanding of the variable-amplitude fatigue process may be to derive the Buckingham Pi nondimensionalized constants as the driving force for crack growth, which would be capable of providing similitude between the two 'testing environments' of CA and VA. This would be much like an equal value for the Reynolds number in fluid dynamics allows testing in a wind tunnel to be applicable to the full-scale problem. It is postulated that such constants would be functions of the key internal and external variables of crack growth and would reduce the number of independent variables of the problem.

References

[1] R. Sunder, "Compilation of Procedures for Fatigue Crack Propagation Testing Under Complex Load Sequences", *Development of Fatigue Loading Spectra, ASTM STP 1006,* J.M. Potter and R.T. Watanabe, Eds., American Society for Testing and Materials, Philadelphia, 1989, pp. 211-230.

[2] Chitang Li, Probabilistic Modeling for Corrosion Fatigue Crack Growth. PhD Dissertation, Lehigh University, Bethlehem, PA, 1996.

[3] J.M. Barsom, "Fatigue Crack Growth Under Variable-Amplitude Loading in Various Bridge Steels," Fatigue *Crack Growth Under Spectrum Loads,* ASTM STP 595, American Society for Testing and Materials, 1976, pp. 217-235.

[4] C.M. Hudson, C.M., "A Root-Mean-Square Approach for Predicting Fatigue Crack Growth under Random Loading," *Methods and Models for Predicting Fatigue Crack Growth under Random Loading, ASTM STP 747,* J.B. Chang and C.M. Hudson, Eds., American Society for Testing and Materials, 1981, pp. 41-52.

[5] L.P. Pook, Analysis *and Application of Fatigue Crack Growth Data,* A General Introduction to Fracture Mechanics, Burlington Press, 1978, pp. 130-133.

[6] R. Sunder, "Compilation of Procedures for Fatigue Crack Propagation Testing Under Complex Load Sequences," *Development of Fatigue Loading Spectra, ASTM STP 1006,* J.M. Potter and R.T. Watanabe, Eds., American Society for Testing and Materials, Philadelphia, 1989, pp. 211-230.

[7] D. G Harlow, and R. P. Wei., "Linkage Between Safe-Life and Crack-Growth Approaches for Fatigue Life Prediction," *Materials Lifetime Science & Engineering,* 2003. 3-8.

[8] J.C. Newman, Jr., X.R. Wu, S.L. Venneri, and C.G. Li, "Small-Crack Effects in High-Strength Aluminum Alloys", NASA Reference Publication 1309, National Aeronautics and Space Administration., Langley Research Center, 1994.

[9] J.A. Harter, *AFGROW Users Guide and Technical Manual,*. AFRL-VA-WP-TR-2006-XXXX, Air Vehicles Directorate, Air Force Research Laboratory, WPAFB OH, 2006.

[10] David Broek, Elementary Engineering Fracture Mechanics, Kluwer Academic Publishers, The Netherlands, 1986.

[11] R.P. Wei, Introduction to Fracture Mechanics, unpublished work.

[12] P.C. Paris, M.P. Gomez, and W.E. Anderson, "A rational analytic theory of fatigue", *Trend in Engineering,* 13, 1961, pp. 9-14.

[13] ASTM E 647 – 00. Standard Test Method for Measurement of Fatigue Crack Growth Rates

[14] R. H. Jones Ed., "*Preface,"* Stress Corrosion Cracking: Materials Performance and Evaluation, ASM International, 1992, pp. v-vi.

[15] M.C. Latham, "Characterization of corrosion fatigue damage in the fastener holes of a Boeing 707,". Masters Thesis, Lehigh University, Bethlehem, PA, USA, 2001.

[16] D.G. Harlow, and R.P. Wei, "Probability modeling and statistical analysis of damage in the lower wing skins of two retired B-707 aircraft". *Fatigue Fract. Engng Mater. Struct. Vol.* 24, 2001, pp. 523-535.

[17] R. H. Jones and R.E. Ricker. "Mechanisms of Stress-Corrosion Cracking," Stress Corrosion Cracking: Materials Performance and Evaluation, ASM International, 1992, pp. 8-9.

[18] A. J. Hug, "Laboratory Inspection of Wing Lower Surface Structure from 707 Aircraft for the J-STARS Program," Boeing FSCM No. 81205, Document No. D500-12947-1, Boeing Company, Wichita, Kansas, USA, 1996.

[19] H. H. Johnson, "Calibrating the Electrical Potential Method for Studying Slow Crack Growth," *Materials Research and Standards,* Vol. 5, No. 9, September 1965, pp. 442-445.

[20] G. H. Aronson, and R. O. Ritchie, "Optimization of the Electrical Potential Technique for Crack Growth Monitoring in Compact Test Pieces Using Finite Element Analysis," *Journal of Testing and Evaluation,* JTEVA, Vol. 7, No. 4, July 1979, pp. 208-215.

[21] C.Y Li and R.P. Wei, "Calibrating the Electrical Potential Method for Studying Slow Crack Growth," *Materials Research and Standards, Vol. 6, No. 8.* American Society for Testing and Materials, pp. 392-394.

[22] K.-H. Schwalbe, and Dieter Hellman, "Application of the Electrical Potential Method to Crack Length Measurements Using Johnson's Formula," *Journal of Testing and Evaluation, JTEVA.* Vol. 9, No. 3, May 1981, pp.218-221.

[23] J. K. Donald and J. Ruschau, "Direct Current Potential Difference Fatigue Crack Measurement Techniques," *Fatigue Crack Measurement: Techniques and Applications,* 2001, pp. 11-36.

[24] W.C. Johnson, Transmission Lines and Networks, McGraw-Hill, New York, 1950, p.58.

[25] Verpoest et al., "An Improved AC Potential Drop Method for Detecting Surface Microcracks during Fatigue Tests of Unnotched Specimens," Fatigue of Engineering Material Structures, Vol. 3, 1981, pp. 203-217.

[26] R. P Wei, and R. L Brazill, "An Assessment of AC and DC Potential Systems for Monitoring Fatigue Crack Growth", Fatigue Crack Growth, ASTM STP 738, Philadelphia, Pennsylvania, 1979.

[27] U. Eai, N. J. Marchand, and M. Hongoh, "Fatigue Crack Growth Measurements in TMF Testing in Titanium Alloys Using an ACPD Technique," Special Applications and Advanced Techniques for Crack Size Determination, ASTM STP 1251, J.J. Ruchau and J. K. Donald, Eds., American Society for Testing and Materials, Philadelphia, 1995, pp. 17-32.

[28] R. P. Wei, "The Effects of Temperature and Environment on Subcritical Crack Growth," *Institute of Fracture and Solid Mechanics*, 1972, p. 4.

[29] J. K. Donald, K. George , "Variable Amplitude Fatigue Crack Growth using Digital Signal Processing Technology", Symposium of Fatigue Testing and Analysis under Variable Amplitude Loading Conditions: ASTM STP 1439, P.C. McKeighan and N. Ranganathan, Eds., ASTM International, West Conshohocken, PA, 2004, pp 53-66.

[30] A. Saxena, S.J. Hudak, Jr., J. K. Donald, and D. W. Schmidt, *J. Test Eval.,* Vol. 6, 1978, p. 167.

[31] R. W. Hertzberg. Deformation and Fracture Mechanics of Engineering Materials. John. Wiley & Sons, Inc. 1996. pp 634-635.

[32] J. P. Gallagher, "A Generalized Development of Yield-Zone Models," AFFDL-TM-74-28, Air Force Flight Dynamics Laboratory, Wright-Patterson Air Force Base, Ohio, 1974.

[33] R. P. Wei and T. T. Shih, "Delay in Fatigue Crack Growth," *Institute of Fracture and Solid Mechanics*, 1972, p. 8.

[34] A. Yunus, A. Cengel, M.A. Boles, Thermodynamics: An Engineering Approach. McGraw Hill. 2002, p. 672.

[35] R.P. Wei and T.T. Shih, "Delay in Fatigue Crack Growth", International Journal of Fracture, Vol. 10, No. 1, March 1974, pp. 77-85.

[36] M. Liao. "Probabilistic Modeling of Fatigue Related Microstructural Parameters in Aluminum Alloys, 2007," Symposium on Materials Damage Prognosis and Life Cycle Engineering, Snowmass, CO, 26 July, 2006.

Appendix A: Procedure for Fatigue Experiments

This account of experimental procedure is provided to reduce the strain on future researchers. It is not an exhaustive checklist, but almost.

Preparation of Specimen & System:

1. Wetsand specimen surface along projected crackfront with a motion orthogonal to direction of crack growth, then polish with Dremel tool and circular buffer pad and compound.
2. Mark specimen with a fine razor at a/W = 0.360.
3. Blow compressed air into crack as this will remove moisture before loading in grips and using as test specimen. Moisture in the crack will drastically affect crack growth rates.
4. Open the MTS Testware software and load the configuration file, FTA.ACPD.cfg. This is the config file used for ACPD testing. A similar config file will be used for DCPD.
5. *Turn on hydraulics*: Initiate at low pressure. This is critical when there is a service manifold. Hold for a few seconds and then ramp up to high pressure Turn on hydraulics before loading specimen. Never turn on hydraulics while a specimen is loaded and the system is being activated from an unknown, idle state as the hydraulics seeks to reach the last point in memory which may occur rapidly with unsafe
6. Set span to 0% until you are ready to start, ultimately setting *span* to 100%, i.e., 10V in corresponds to 10V out.
7. Start FTA FCGR Testing Software.
8. Choose *DC Potential Drop* as the testing type.
9. Choose Unit Type as English.
10. Choose Application type as Steady-State Constant Amplitude.
11. Click *New Test*.
12. From the main menu, select *Input*, then *Data*, and load the user-supplied *Test Parameter file*.
13. Enter a Test ID.
14. Select the *Data Storage Path* by pressing the *Start Log File* button.
15. In *Stress Parameters* tab change Control Type to *Constant Load*.
16. From main menu select *Input*, then *Options*.
17. Enable *Reference Probe Active*.
18. For ACPD: *Enable Non-Reversing DCPD* (this way an AC lock-in amp can be used as the signal generator).
19. SEND TO DSP.

1. From main menu, select *Control*, then *Function Generator (full)*.
2. From main menu, select *Display*, *then Status*.
3. Verify that the DCPD channels are reading correctly.
4. Static Load System Check (make sure FTA software has control of hydraulics):
    a. *Fine Adjustment*, ramp to Hold level.

b. Click *Raise Hold* button.
c. *Dimensions* Tab: Load Cell Calibration = 1000 lb/volt (for a 10kip load cell with 10V span)
d. *Bug Alert:* If actual load does not respond to command signal, cycle the external command signal on and off. *(Be sure to release the specimen from the grips before doing so!)*
e. Command signal and actual load should be the same
f. If they are the same, cancel Ramp to Hold Level.

5. From *Initialize Tab,* Enable *Cal Type,* Under *K-Calibration Type* choose *Polynomial,* Under *PD Calibration Type* choose *Johnson's,*
6. In Data Input screen, update all parameters in *Dimensions Tab.*
   a. *Specimen Thickness = .250*
   b. *Net Specimen Thickness = .250*
   c. *Specimen Width = 2.00*
   d. *Load Cell Calibration = 1000lb/volt*
   e. *PD Gage Length = 0.70 in*
   f. *Initial Crack Length = 0.60 in.*
   g. *PD Gain* = 20,000.

PD gain = full scale voltage/sensitivity – this is important in ACPD when using lock-in amplifiers.

Note that to manually move the grips with the *Remote Station Controller*, counterclockwise is compression.

Transfer control to FTA before loading specimen in load control. When transferring over to FTA be sure to ***RESET FNG*** from the ***Function Generator Control***. Failure to RESET FNG will command the software to pick-up the sine wave from the last point stored in the ADwin box, which can be any value. It will do this regardless of the specified ***target load***. The software does not know that you may be working with a different specimen and therefore that you will want to begin at low loads, it will simply begin exactly where it had left off previously. Fail to RESET FNG and you are in serious jeopardy of overloading the specimen. A simple check is to examine the multi-colored balls in the right-hand side of the ***Function Generator Window;*** they should all be close to zero. Also make sure that the ***limit detectors*** in the MTS software to reasonable values. Enable External Command (The green play button from the external command tab): this transfers control to FTA.

Once transfer has been realized and FTA has taken control, there is no need to keep the MTS window open, this window can be minimized, but not closed.

Load Sample:

1. Attach current leads to specimen with 4-40 hex-screws ensuring to use insulative spacers between specimen and wire.
2. Maneuver grips close together using fine ramp to hold from *Function Generator* window of FTA with slight tension.
3. When the grips are close enough insert the pins and apply a small tensile load.
4. Use a caliper to measure parallelism of the grips. Pins should be parallel to within 0.001 in.
5. Instrument the Active voltage leads with 4-40 hex-screws, again insulating with spacers.
6. Power on the HP6033A Power supply.
7. Set Over-Voltage Protection (OVP) to 8.00 Volts (should remain intact after power down).
8. Set Desired Voltage to 5.00 Volts.
9. Set Desired Current to 10.00 Amps.
10. Ensure that the PD measurements for both Active and Reference samples are approximate in magnitude and of same sign.
11. DCPD values should be positive, else there is a problem with polarity. If DCPD is negative switch polarity from power supply to solid-state relay. Another option is to change the gain setting from within FTA FCGR software to a negative value.

Grow Precrack:

The purpose of precracking is to introduce a defect into a specimen for subsequent fracture toughness testing or crack growth monitoring. Ideally, the crack should have a sharp crack tip with minimal plastic zone surrounding the crack front as any plasticity in the crackfront will increase resistance to crack growth.

To achieve a precrack:

1. Test ID # should be SpecimenID-pc, e.g. NGC-DLU1-###-pc. (pc for precrack).
2. Change *Control Type* to *K-Control* and set $K_{max} = 5.0$, $R = 0.10$. These values have been empirically shown to provide crack growth rates below the maximum recommended ASTM precrack growth-rate of 3.94E-7 in/cycle.
3. Update initial DCPD readings.
4. Set *final crack length* to .660 in.
5. Set *Cycle Count Increment* = 10,000
6. Enable *FNG Shutdown.*
7. PRINT TO LOG.
8. RUN *(from function generator).*

9. When precrack is achieved, load in Constant Load, a few hundred pounds, to open up crack and make it visible for visual inspection with magnifying glass. Make a visual measurement, ensure it is close to razor mark.
10. Change R to high value (R = 0.6) and grow crack 5 additional mils to generate a dark marker band. Grow in either constant load or K-control modes. Can bump frequency up to 30 Hz during the growth of this marker band since there is a high R and therefore small displacement of specimen.
11. PRINT TO LOG.
12. Receive from DSP.
13. Reset FNG.
14. Manually record the DCPD level and crack length on the data-chart.

To Begin K-Decreasing Test after completion of precrack:

0. Grow a 5 mil marker band at a high R value. (See above).
1. Change Test ID # suffix to –a (use 'pc' for precrack, 'a' for decreasing-K, 'b' for increasing-K)
2. Clear-out *Storage Buffer* → this clears out data on the *da/dN vs. ΔK* plot as soon as you SEND TO DSP.
3. Move to the *Initialize Tab* of the Data Input screen and enable the Initialize radio button.
4. *Coefficient Tab* remains unchanged.
5. *Dimension Tab* remains unchanged.
6. *Stress Parameters Tab:* Change load ratio R to desired level for the decreasing-K test.
7. *Stress Parameters Tab:* Update K Control Parameters including *initial crack length a.*
8. Set frequency to desired level.
9. Leave *Control Type* in K-Control.
10. Set *K-gradient* = 0.00 (*da/dN* should remain constant before changing this setting)
11. In the Stress Parameters tab update the initial *a* (under *K* Control Parameters).
12. In *Data Acquisition Tab* set *number of PD cycles* = 50 → ensures adequate data-intervals for data-averaging.
13. Move to the *Data Storage window* and back-up initial *a/W* behind calculated *a/W* from the Status Window. This will force acquisition of a data point.
14. Open up *Final a/W* to 0.800, crack length should never reach this far for a decreasing-*K* test so test will run continuously with no premature shutdown.
15. Set *a/W* increment to approximately 0.0040 for sufficient data acquisition.
16. SEND TO DSP.
17. PRINT TO LOG.
18. RUN. (from *Function Generator)*

19. Observe *da/dN* vs. ΔK plot for stability of *da/dN* (data points should converge to a single point).
20. When *da/dN* is stable, Clear *Storage Buffer.*
21. *Initialize.*
22. Update *initial crack length* in *Stress Parameters tab.*
23. Verify that *da/dN* has stabilized and is constant before changing *K-gradient* to a non-zero, negative value. Change *K-gradient* to -4.00
24. SEND to DSP.
25. Receive from DSP.
26. Print to Log.

To go from K-decreasing to K-increasing:

When running a K-increasing, after a K-decreasing test, use the same magnitude K-gradient but opposite in sign.

Under *K* ***Control Parameters tab* make sure to adjust the ***initial a***, not adjusting this to current crack length will lead to erroneous calculation of K_f as:

$$K_f = K_0 e^{C(a_f - a_0)}$$

Obviously, with an erroneous value for a_0 the calculation will be flawed. Not adjusting this value to the current crack length may result in damage of specimen, exceedingly large loads, as well as complete compromise of testing efficacy.

Ideally, you want some overlap between the increasing-K and decreasing-K data, so start with K_{max} at a value slightly *less than the maximum of the decreasing-K* portion of the test to allow for some overlap.

Get a stable da/dN rate before switching on *crack growth rate storage limit* in case spurious or otherwise eccentric (transient) change in da/dN put you out of limit range and shut down the test.

1. Go to *Stress Parameters Window* and change *initial a* to current *a.*
2. Change *K-Gradient to 0.00.*
3. Wait until da/dN becomes constant.
4. Enable *crack growth rate storage limit* and set this to a reasonable value, say 1.0 x 10E-4 so that the test will cease before fast-fracture of specimen.
5. Change *K*-gradient to positive value with the same magnitude as used for the K-decreasing test.
6. Change suffix of Test ID # to: -b.
7. PRINT TO LOG.

VA Testing:

The procedure for VA is the same as for CA except for a few noted peculiarities:

First line of data file for a End Point File must have:
A,B,C,

A = Type of file: 0 for End Point File
B = Full Scale Max value in spectrum
C = offset value. Normally, negative endpoints are compressive loading and positive endpoints are tension and the value of C is zero.

Read in the End Point file – then SEND to DSP and cycle through a few points to ensure it has been read. End Point file should be in *.DAT format.

Start up with span = 0% so only command signal, no feedback

Command Control enables correction but a signal will still be sent out even if command control is not checked. Target and Command will be the same until *Command Control* is activated. With *Command Control* activated, the command will compensate for a poor damage parameter.

Damage Parameter Γ should be close to 1.000, 1.000 is optimum. Less than 1.000 and the Actual Loads are undershooting Target Loads, with $\Gamma > 1.000$ then Actual Loads exceed Target Loads.

Firm setting for Command Control enables quicker compensation of loads in terms of a larger percentage shift in error with each iteration. This is the suggested mode of operation.

Save Correction File from dummy specimen then use this file to load after precrack – then the spectrum test can be started immediately after precrack.

Full Scale – Set equal to the maximum load in the spectrum, then this value will correspond to the value for *Max Load* found in the Stress Parameters tab of the Data Input Window. So the Max Load will be correlated with this value.

For running a new spectrum test read in correction file from stored file after completion of precrack. Assuming the material, geometry, and testing conditions are the same – this correction file should provide a reasonable starting point for the spectrum test so that the spectrum test can be initiated at the immediate conclusion of

the precrack. This will ensure that all spectrum tests are initiated at the same point and thus comparison of alternate tests will prove useful.

Vita

Matthew Adam Adler was born as the youngest of five children on August 16, 1982 to Neal and Waltraud Adler in Englewood, NJ and benefited from an adolescence in Middletown, NJ. Mr. Adler graduated from Christian Brothers Academy, a private, all-boys Catholic high school, in Lincroft, NJ in 2000 where he was captain of the wrestling team during his senior year. Mr. Adler matriculated to Lehigh University where he was awarded an Army ROTC scholarship and earned a Bachelors of Science in Mechanical Engineering and Mechanics in May 2004.

It was at Lehigh University that Mr. Adler met Professor Robert P. Wei and was encouraged to remain at Lehigh in pursuant of a graduate degree in Mechanical Engineering & Mechanics. His thesis topic is on the reduction of a variable-amplitude fatigue spectrum to an equivalent constant-amplitude spectrum. He was awarded a National Science Foundation (NSF) Integrative Graduate Education and Research Traineeship (IGERT) Fellowship which supported Mr. Adler during the tenure of his research for the Master's degree. Mr. Adler will receive his Master's of Science in Mechanical Engineering and Mechanics from Lehigh University on May 21 2007 and anticipates graduating with a PhD in Spring, 2008.

Mr. Adler aspires to work for NASA.

END OF TITLE